THE GENERAL MILLS ELECTRONICS GROUP

Mills ELECTRONICS DIVISION

15 December 1962

COMMUNICATION VIA ARTIFICIAL SCATTERERS

PHASE II

Prepared for:

Department of the Navy
Office of Naval Research
Washington 25, D. C.

Prepared by:

W. Grosz
L. Flink
T. O'Malley
W. Parsons
R. Schindler
G. Wales

Submitted by: H. P. Raabe
H. P. Raabe,
Senior Technical Specialist

Approved by: M. J. Harpole
Murray Harpole, Manager,
Development Operations

Report No. 2353
Contract NONR 1589(24)

Engineering and Research
2003 East Hennepin Avenue
Minneapolis 13, Minnesota

TABLE OF CONTENTS

TABLE OF CONTENTS (Continued)

LIST OF ILLUSTRATIONS

LIST OF ILLUSTRATIONS (Continued)

LIST OF ILLUSTRATIONS (Continued)

SECTION I

INTRODUCTION AND SUMMARY

I. INTRODUCTION AND SUMMARY

The feasibility of establishing an effective scatter propagation communication path below the ionosphere has been further examined by General Mills, Inc. This communication path would be free from interruption due to ionospheric storms.

This report describes the investigations performed in Phase II of a continuation study coordinated by Dr. William J. Thaler formerly of the Office of Naval Research. Efficient scattering elements are to be placed within radio line-of-sight of two stations wishing to communicate. Additionally, studies were made of the potential use of active repeaters deployed on the ocean surface between two terminals. The investigations covered in this report are limited to a frequency range of 1 mc/s to 20 gc/s and an altitude of the artificial scatterers which is below the ionosphere.

Three major approaches to the general communication problem were studied in Phase II:

1) Scattering by coherent grating arrays deployed in the atmosphere.

2) Active repeaters placed on the ocean surface.

3) Scattering by a cloud of randomly oriented artificial scatterers in the atmosphere.

The coherent array as an efficient scattering system was discussed in the Phase I report. These ideas were extended from the notion of an array of tuned dipoles to that of a non-resonant conductive-sheet grating array. The theory of the grating array is presented. Path efficiency for a signal bounded off the grating may be determined for specific design purposes. The maneuverability limits of the grating are also determined wherein an acceptable signal will be received. An experiment was performed over a 272-mile path at VHF using a grating suported by a helium balloon. The experiment verified the grating theory to the extent that all quantities that were measured compared favorably with the theory. During the experiment,

the grating scattered signal was not significantly greater than the tropospheric scattered signal. Subsequent path loss measurements indicated that the marginal results can be attributed to excessive path loss and not to deviations from theory. Empirical data are available for realistic predictions of signal path losses to be expected over all types of communication systems contemplated for a near standard atmosphere. These data are to be used together with a satisfactory engineering margin to provide the desired communication channel.

The experiment that was performed was typical of only one of a larger class of grating scatterer applications. The experiment was designed for:

1) Specific terminal separation.

2) Grating located midway between terminals.

3) A chosen frequency.

4) A balloon-borne grating.

It is apparent that many variations are possible.

Theoretical investigations only were made on the other two approaches, namely active ocean surface repeaters and airborne noncoherent scatterers.

An introductory look at possible applications of active ocean surface repeaters is presented. Two general approaches are discussed—the serial repeater and the "patch". The serial repeater or "chain" system uses a number of repeaters deployed generally in a line between two terminals. In the patch system, a number of transponders are grouped on the ocean surface. When illuminated with a sufficiently strong pulse of r-f energy, each transponder repeats a coherent burst of amplified r-f energy. A beam is formed in the continuing direction of propagation to extend the communication range. Various theoretical descriptions of capabilities and constraints of either approach are presented. It is not known how practical either of the ocean surface systems could become. Their feasibility would depend on technical and operational factors.

Various types of efficient scattering elements were studied with the conclusion that a conductive dipole is the most effective scatterer available. A slight effort was spend studying a modified bubble concept and studying some mechanisms to retard settling. Studies were made to select a suitable frequency range for long distance (approximately 1000 mile) paths. The bistatic scattering area or the number of scatterers required over a given path are presented.

SECTION II

GRATED ARRAYS (GRATAR)

TABLE OF SYMBOLS – SECTION II

a	lateral width of equivalent grating window
α	general angle in horizontal plane
A_a	effective intercepting area of grating = nas
A_r	effective area of receiving antenna
b	height of equivalent grating window
β	general angle in vertical plane
B	bandwidth
d	distance between transmitter and receiver
δ_h	horizontal half power beamwidth
δ_v	vertical half power beamwidth
e	transmission efficiency = $\frac{P_r}{P_t}$
e_m	transmission efficiency with scatterer at midpoint
e_o	transmission efficiency for free space loss
E_1	maximum of distant field strength for first diffraction lobe
$E(\beta)$	distant field variation with β
f	frequency
γ	deflection angle of first order of diffraction lobe = $\beta_t + \beta_r$
γ'	desired deflection angle = $\beta_t' + \beta_r'$
G_{s1}	gain of beam formed by one grating window
G_{s1m}	maximum value of gain from one grating window
G_r	gain of receiving antenna (relative to isotropic)
G_t	gain of transmitting antenna (relative to isotropic)
h	height of grating above smooth earth
h_d	apparent height above horizon
h_{om}	minimum height to obtain horizon clearance
h_{ox}	height of scatterer for horizon limited case
h_{ro}	that altitude for scatterer to be at the radio horizon for the nearer (receiver) terminal
i_s	radiant intensity from grating
i_{s0}	peak value of radiant intensity from grating
i_{s1}	radiant intensity from one grating window
k	index number for order of diffraction lobe
K	a propagation constant, or Boltzmann's constant
l_r	lateral range of receiver to be within horizontal beamwidth
l_s	lateral range of scatterer for receiver to be within horizontal beamwidth
λ	wavelength
L_{bf}	basic transmission loss for free space condition
msl	mean sea level
n	number of equivalent grating windows
η	desired signal-to-noise ratio
p_s	irradiance or power density at scatterer
ϕ	a depression angle as viewed from scatterer
ϕ_r	depression angle of peak of first order diffraction lobe
ϕ_r'	depression angle of direct ray to receiver
ϕ_t	depression angle of direct ray from transmitter
ϕ_t'	depression angle of direct ray from transmitter
P_r	signal power available to receiver
P_{s1}	power intercepted by one window
P_t	signal power delivered to transmitting antenna
r_m	range from one terminal to scatterer when at midpoint
r_r	range from receiver to scatterer
r_t	range from transmitter to scatterer
r_x	range from one terminal to scatterer for horizon limited case
ρ	modified (4/3) earth radius taken as 8500 km
s	spacing between corresponding points on adjacent windows
sinc x	$\frac{\sin x}{x}$
Σ	bistatic scatter cross-section
θ	elevation angle of scatterer above radio horizon as viewed from nearer terminal
T_c	peak cosmic noise temperature
T_c'	average cosmic noise temperature
v_s	vertical range of scatterer for receiver to be within vertical beamwidth
x	distance of scatterer offset from midpoint
x_1	longitudinal range for horizon clearance
x_2	longitudinal range for receiver to be within vertical beamwidth

II. GRATED ARRAYS (GRATAR)

A. Introduction

A coherent scattering system consisting of a dipole array painted on or suspended from a balloon was described in the Phase I report. This section of the Phase II report discusses a system utilizing a nonresonant grated array. Both systems have the advantage of providing a coherent communication path with a relatively constant amplitude and phase character, and are free of scintillation. However, the nonresonant grated array offers the additional advantage of being less sensitive to frequency.

A general theory of the grated array is developed including maneuverability limits for the grating with respect to the terminal locations. A grating was built and field tested by being carried aloft by a free floating helium balloon. The grating was in the form of a hollow cylinder suspended vertically. The cylinder had alternate bands of conductive and dielectric plastic material. In this configuration, its effectiveness is relatively insensitive to rotational orientation as it is symmetrical, and it is also insensitive to small angular excursions from the vertical.

B. Conductive Sheet Grated Arrays

Resonant scatterers (dipoles) are of advantage only if a weight saving for the entire array can be realized and if one can make use of special properties, such as polarization and phase shifts. If one arranges dipoles as densely as possible and has to support them with a continuous sheet, it would be more advantageous to metallize the entire area occupied by the scatterers so that a nonresonant diffraction grating results.

1. Theory of Nonresonant Diffraction Gratings

a. Use of Babinet's Principle

To analyze the forward scattering from such gratings, we assume an idealized configuration which consists of rectangular conductive sheets suspended vertically and spaced in such a way that each sheet is centered at the level of an isophase ellipsoid (see Figure 2-2 of the Phase I report). The plane of the grating should be normal to the plane through the communicating terminals and the center of the earth. Such a grating is shown in Figure 2-1(a).

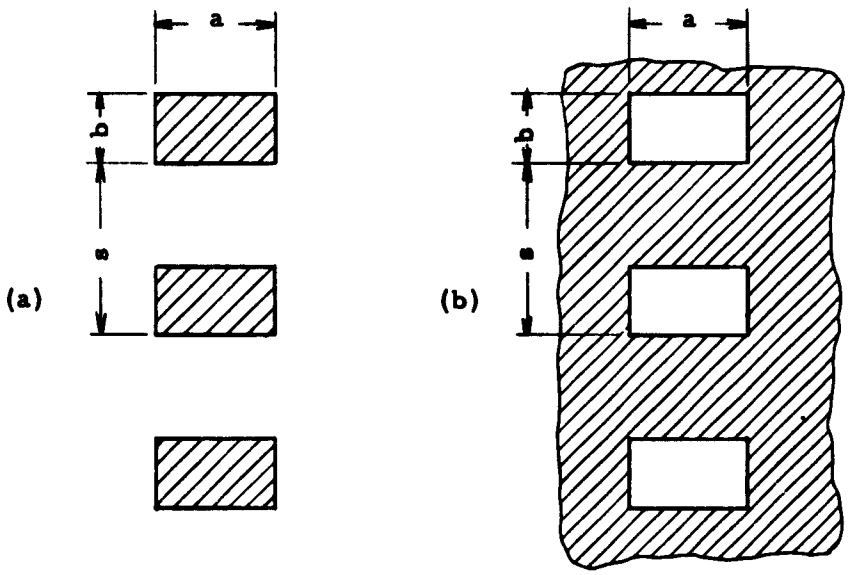

Figure 2-1. Array of Reflective Sheets and the Complimentary Array of Windows in a Sheet of Infinite Permeability

The grating is defined by the dimensions a and b of the individual sheet, the spacing s and the number of sheets n. The analysis of the forward scatter propagation can be greatly simplified if we apply Babinet's principle and introduce a complimentary screen which has open spaces or windows where the conductive areas of the grating are and which has infinite permeability

outside of these areas. Then, according to Babinet's principle, the sum of the field strengths due to the two complimentary screens for any point behind the screens equals the field strength if there were no screen at all. Now we may assume that at the receiving terminal the field strength is negligible in absence of any screen, hence the two complimentary screens are actually equivalent except for a phase shift of π. Since the phase of the signal is of no interest to us and since the dimensions of the area a and b are much larger than the wavelength, we can substitute a highly conductive screen for the highly permeable screen without affecting the field pattern in the vicinity of the receiver. Thus, a set of windows in a highly conductive screen as shown in Figure 2-1(b) is an acceptable substitute to describe the interesting portion of the forward radiation pattern.

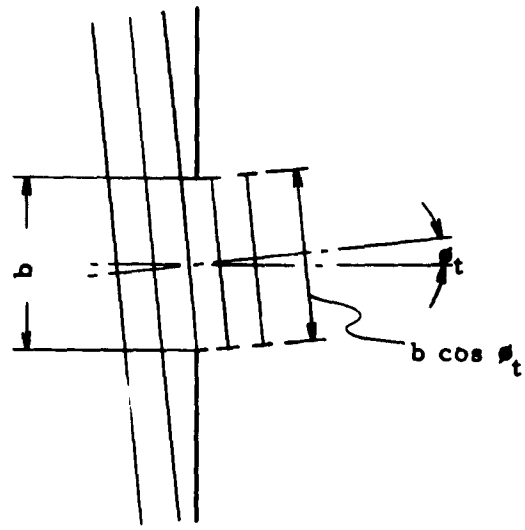

Figure 2-2. Illumination of a Window

b. Pattern of a Single Window

If we have an irradiance of p_s at the grating and a slight inclination of the wave front ϕ_t as explained by Figure 2-2, the intercepted power for one window becomes

$$P_{s1} = p_s \, ab \cos \phi_t \quad . \tag{2-1}$$

Actually, ϕ_t is always small if the grating is just above the horizon as seen from the transmitter. Therefore, we can set $\cos \phi_t = 1$ and

$$P_{s1} = p_s \, ab \quad . \tag{2-2}$$

The radiation field strength pattern of a rectangular, uniformly illuminated window has been derived in Appendix A, therefore we can write for the gain pattern, as illustrated in Figure 2-3

$$G_{s1} = G_{s1m} \, \text{sinc}^2 \left[\frac{a\pi}{\lambda} \sin \alpha \right] \cdot \text{sinc}^2 \left[\frac{b\pi}{\lambda} (\sin \beta + \sin \phi_t) \right] \quad . \tag{2-3}$$

Hereby, G_{s1m}, the peak gain of the rectangular aperture, is

$$G_{s1m} = \frac{4\pi \, ab}{\lambda^2} \quad . \tag{2-4}$$

The radiant intensity i of a source is defined by its power and gain pattern so that

$$i_{s1} = \frac{P_{s1} \cdot G_{s1}}{4\pi} \quad . \tag{2-5}$$

With the expression (2-2) and (2-3) we obtain

$$i_{s1} = p_s \left(\frac{ab}{\lambda} \right)^2 \text{sinc}^2 \left[\frac{a\pi}{\lambda} \sin \alpha \right] \cdot \text{sinc}^2 \left[\frac{b\pi}{\lambda} (\sin \beta + \sin \phi_t) \right] \quad . \tag{2-6}$$

c. Pattern of an Array of Windows

If the array consisted of an infinite number of elements at regular spacing, the pattern would take the form of a set of discrete rays along the directions where wave components are in phase. Figure 2-4 illustrates

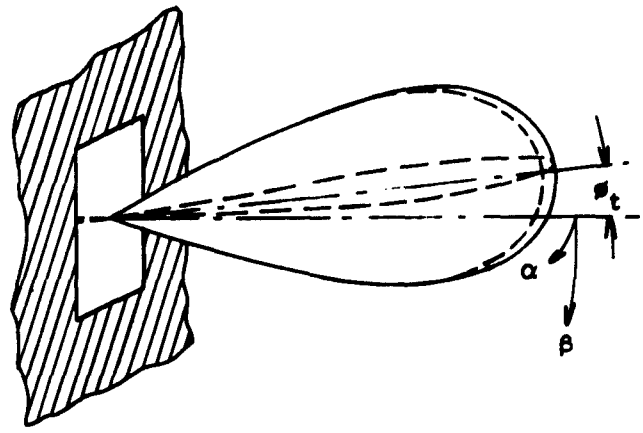

Figure 2-3. Radiation Pattern of a Window

this condition. A wave front which has just arrived at the center P_1 of the lower window has to advance the distance AP_2 to reach the center of the next higher window. To form a wave front in the depressed direction ϕ_r, the wave propagating through the upper window must advance the distance P_2B so that the total delay due to the distance AP_2B equals an integer number of cycles, or

$$s(\sin \phi_t + \sin \phi_r) = k\lambda, \; k = 0, 1, 2 \ldots . \qquad (2\text{-}7)$$

While k = 0 refers to the straight through propagation, k = 1 is the really interesting case for propagation to a ground station. Hence

$$s = \frac{\lambda}{\sin \phi_t + \sin \phi_r} \qquad (2\text{-}8)$$

A finite array of uniformly illuminated windows can be treated as an infinite array with a rectangular illumination function as shown in Figure 2-5. Thus, the pattern consists of a set of narrow beams in the direction of the discrete rays of the infinite array. The individual beam shape is that of a uniformly illuminated aperture extending over the actual number of windows,

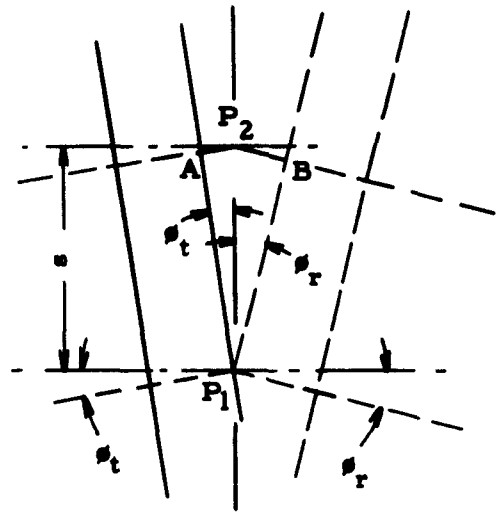

Figure 2-4. Ray Geometry for the Beam of Interest

whereby the illumination function is phased in such a way that the wave propagates in the direction of the discrete rays. Hence, if there are n windows the field strength pattern of the first secondary beam pointing in the direction of ϕ_r would be defined by the function

$$E(\beta) = E_1 \operatorname{sinc} \left[\frac{ns\pi}{\lambda} (\sin\beta - \sin\phi_r) \right] . \qquad (2\text{-}9)$$

The nulls of the beam pattern occur at

$$\frac{ns\pi}{\lambda} (\sin\beta - \sin\phi_r) = \pm\pi \qquad (2\text{-}10)$$

so that

$$\beta = \arcsin \left[\sin\phi_r \pm \frac{\lambda}{ns} \right] . \qquad (2\text{-}11)$$

Since $\frac{\lambda}{ns} \ll 1$ in most cases and since the beam width δ_v is approximately half as wide as the separation of the nulls, we can write

$$\delta_v = \tfrac{1}{2} \left[\arcsin (\sin\phi_r + \tfrac{\lambda}{ns}) - \arcsin (\sin\phi_r - \tfrac{\lambda}{ns}) \right] \qquad (2\text{-}12)$$

and

$$\delta_v = \frac{\lambda}{ns} \frac{d\,[\arcsin(\sin\beta)]}{d(\sin\beta)} \quad , \text{ for } \beta = \beta_r \quad . \tag{2-13}$$

This leads to

$$\delta_v = \frac{\lambda}{ns\cos\beta_r} \quad . \tag{2-14}$$

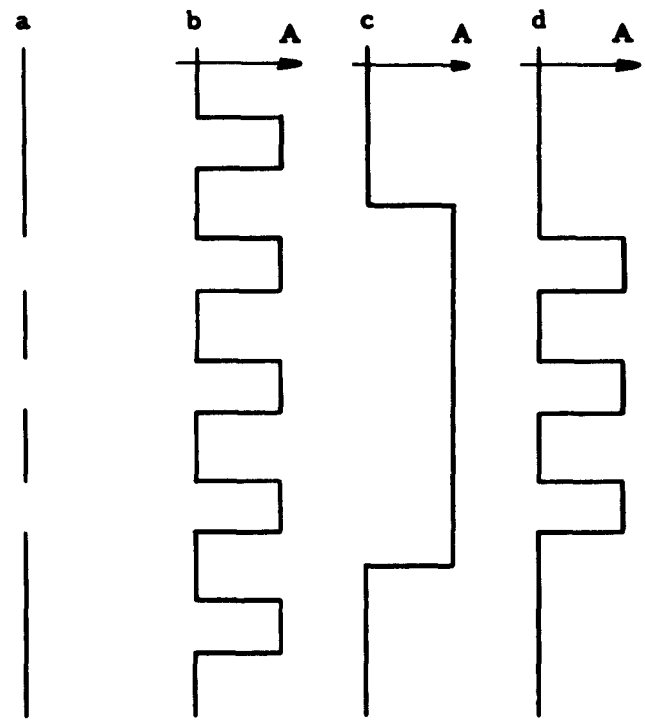

Figure 2-5. Amplitude of the Illumination Function d of the Vertical Aperture of a Grated Array a is Defined as the Product of an Infinite Periodic Illumination Function b and a Rectangular Function c Extending over the Aperture

To obtain the radiant intensity pattern for the beam in the ϕ_r direction, we realize that the peak intensity increases as the square of the number of windows, and that the beam takes the shape of the sinc^2 function so that from (2-6) and (2-9) we derive

$$i_s = p_s \left(\frac{nab}{\lambda}\right)^2 \text{sinc}^2 \left[\frac{b\pi}{\lambda}(\sin\phi_t + \sin\phi_r)\right] \text{sinc}^2 \left[\frac{ns\pi}{\lambda}(\sin\beta - \sin\phi_r)\right] \text{sinc}^2 \left[\frac{a\pi}{\lambda}\sin\alpha\right] . \tag{2-15}$$

If we substitute λ as defined by (2-8) for λ in the first sinc^2 function, (2-15) takes the simpler form

$$i_s = p_s \left(\frac{nab}{\lambda}\right)^2 \text{sinc}^2 \left[\frac{b\pi}{s}\right] \text{sinc}^2 \left[\frac{ns\pi}{\lambda}(\sin\beta - \sin\phi_r)\right] \text{sinc}^2 \left[\frac{a\pi}{\lambda}\sin\alpha\right] . \tag{2-16}$$

This equation shows that the window width a causes the peak intensity

$$i_{s0} = p_s \left(\frac{nab}{\lambda}\right)^2 \text{sinc}^2 \left[\frac{b\pi}{s}\right] \tag{2-17}$$

to increase as the square of a. This is due to the fact that not only the intercepting area increases proportionally with a but also the gain of the reradiated beam as indicated by the narrowing horizontal beam width. Therefore, a is limited by the desired horizontal characteristic.

The effect of b is more complex. While the first factor indicated symmetry with a, the sinc^2 function severely limits the intensity gain with b. Thus, (2-17) has a maximum value in b. To determine the b/s ratio for extreme values of the intensity, we set the first derivative

$$\frac{di_{s0}}{db} = 0. \tag{2-18}$$

Now we expand (2-17)

$$i_{s0} = p_s \left(\frac{nas}{\pi\lambda}\right)^2 \sin^2\left(\frac{b\pi}{s}\right) . \tag{2-19}$$

Then we derive

$$\frac{di_{s0}}{db} = p_s \left(\frac{na}{\lambda}\right)^2 \frac{s}{\pi} \sin\left(\frac{2b\pi}{s}\right) \quad . \tag{2-20}$$

This equation becomes zero when the argument of the sine either becomes zero or multiples of π. The first condition is trivial and describes the minimum $i_{s0} = 0$. If we set the argument equal to π, we obtain the first maximum under the condition

$$b = \frac{s}{2} \quad . \tag{2-21}$$

Hence,

$$\operatorname{sinc}^2\left[\frac{b\pi}{s}\right] = \frac{\sin^2\left(\frac{\pi}{2}\right)}{\left(\frac{\pi}{2}\right)^2} = \left(\frac{2}{\pi}\right)^2 \quad . \tag{2-22}$$

Now we substitute (2-21) and (2-22) in (2-16) and obtain

$$i_s = p_s \left(\frac{nas}{\pi\lambda}\right)^2 \operatorname{sinc}^2\left[\frac{ns\pi}{\lambda}(\sin\beta - \sin\varphi_r)\right] \operatorname{sinc}^2\left[\frac{a\pi}{\lambda}\sin\alpha\right] \quad . \tag{2-23}$$

d. Derivation of the Transmission Formula

To design a communication link between two ground terminals via a diffraction grating, we have to define the signal which we want to receive. Then a compromise must be made between the size and directional characteristics of the scatterer and the power of the transmitter, and the directional characteristics of the two terminals. As long as no specific data are available, the transmission efficiency

$$e = \frac{P_r}{P_t} \tag{2-24}$$

should be of greatest interest.

If the transmitting antenna has a gain G_t, the power density or irradiance at the scatterer location is

$$p_s = \frac{P_t G_t}{4\pi r_t^2} \quad . \tag{2-25}$$

With a radiant intensity i_s of the scatterer and a receiving cross section A_r of an antenna the power intercepted by the antenna becomes

$$P_r = \frac{i_s A_r}{r_r^2} \quad . \tag{2-26}$$

The antenna gain G_r is related to the receiving cross section as

$$A_r = \frac{G_r \lambda^2}{4\pi} \quad , \tag{2-27}$$

so that (2-26) takes the form

$$P_r = \frac{i_s G_r \lambda^2}{4\pi r_r^2} \quad . \tag{2-28}$$

Now we can form the expression for (2-24) with (2-25) and (2-28) and using the peak level i_{s0} from (2-23). Thus,

$$e = \left(\frac{nas}{4\pi^2 r_t r_r}\right)^2 G_t G_r \quad . \tag{2-29}$$

For the sake of convenience we may express (2-29) in the form

$$A_s = nas = 4\pi^2 r_t r_r \sqrt{\frac{e}{G_t G_r}} \quad . \tag{2-30}$$

where A_s is over-all cross section of the grating. If the scatterer is in the center between the terminals, (2-30) becomes

$$A_s = \pi^2 d^2 \sqrt{\frac{e}{G_t G_r}} \quad . \tag{2-31}$$

An interesting and useful parameter is the bistatic scattering cross section of the grated array. This cross section is defined as the equivalent area Σ having an isotropic scattering characteristic and generating the same signal strength as the grated array in the direction of the receiver. Thus, the radiant intensity can be expressed by

$$i_s = p_s \frac{\Sigma}{4\pi} \quad . \tag{2-32}$$

With p_s as in (2-25) and i_s as in (2-28) we derive

$$\Sigma = \frac{4^3 \pi^3 r_t^2 r_r^2 P_r}{G_t G_r \lambda^2 P_t} \quad . \tag{2-33}$$

For P_r/P_t we set e as in (2-29) and (2-30) and obtain

$$\Sigma = \frac{4(nas)^2}{\pi \lambda^2} = \frac{4A_s^2}{\pi\lambda^2} \quad . \tag{2-34}$$

The scattering cross section according to this expression implies a substantial gain. Otherwise, the effort would not be justified. If we set the physical cross section equal to A_s, thus including the open spaces between the reflective sheets, the peak gain of the scatterer would be defined as

$$G_s = \frac{\Sigma}{A_s} = \frac{4A_s}{\pi\lambda^2} \quad . \tag{2-35}$$

In comparison with the peak gain of an antenna of rectangular aperture as shown in (2-4) the gain of the scatterer is one order of magnitude ($1/\pi^2$) lower. This can be explained by the fact that the grating has some other strong lobes, transmissive as well as reflective, besides the one which is utilized.

2. Maneuverability Limits of Gratar

a. Lateral Maneuverability

To have a useful scatterer the requirement for the accuracy of the positioning should not be too stringent. In general, one can control the altitude of a balloon more precisely than the lateral position. Figure 2-6 shows that the positional tolerance depends on the width of the forward scatter beam.

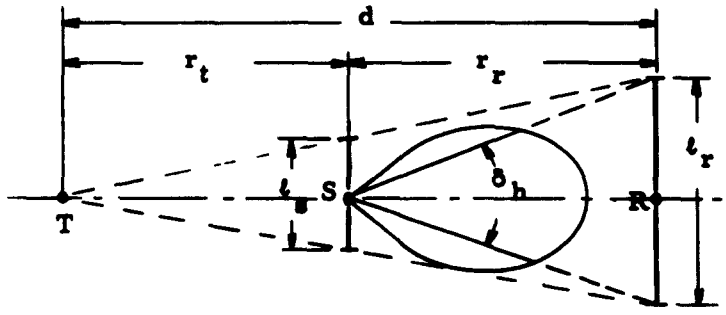

Figure 2-6. Lateral Positional Tolerance Due to Horizontal Beamwidth

Obviously, the receiver can occupy any position over a lateral range of

$$\ell_r = 2r_r \tan\frac{\delta_h}{2} \approx r_r \tan\delta_h \approx r_r \delta_h \ . \qquad (2\text{-}36)$$

If we consider R fixed and S can move laterally the relation applies

$$\frac{\ell_r}{\ell_s} = \frac{d}{r_t} = \frac{r_r \delta_h}{\ell_s} \qquad (2\text{-}37)$$

$$\ell_s = \frac{r_t r_r \delta_h}{d} \ . \qquad (2\text{-}38)$$

This equation shows that the widest lateral tolerance is obtained in the central position, namely

$$\ell_s = \frac{d}{4}\delta_h . \tag{2-39}$$

For the vertical positional tolerance we have a similar expression:

$$v_s = \frac{d}{4}\delta_v . \tag{2-40}$$

Since δ_h and δ_v are determined by the width and length of the scatterer by the relations from Appendix A and Equation (2-14)

$$\delta_h = \frac{\lambda}{a} \text{ and } \delta_v = \frac{\lambda}{ns} , \tag{2-41}$$

we can write

$$\ell_s = \frac{d\lambda}{4a} \tag{2-42}$$

and

$$v_s = \frac{d\lambda}{4ns} . \tag{2-43}$$

The cross section of this maneuverable space is approximately the shape of an ellipse whose major axes are ℓ_s and v_s.

In general terms

$$v_s = \frac{r_t r_r \delta_v}{d} \tag{2-44}$$

then

$$\ell_s = \frac{r_t r_r \lambda}{a d} \tag{2-45}$$

and

$$v_s = \frac{r_t r_r \lambda}{ns d} . \tag{2-46}$$

b. Longitudinal Maneuverability

For the longitudinal maneuverability, two conditions limit the range: The horizon and the beam orientation. For the horizon limited case, refer to Figure 2-7.

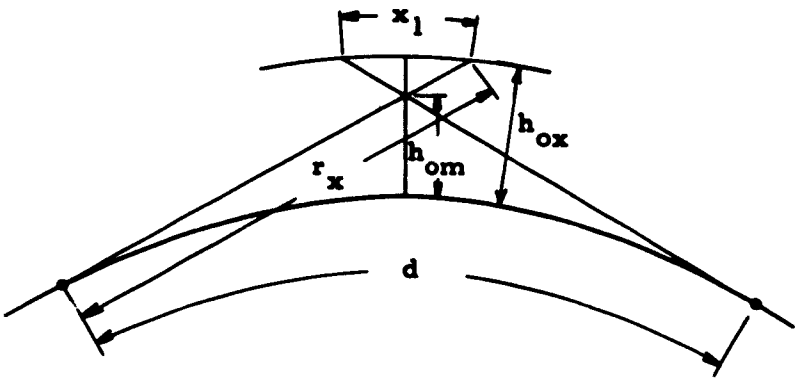

Figure 2-7. Geometry to Describe Longitudinal Maneuverability for Horizon Limited Case

From equation 2-2 of the Phase I report, $r_x = \sqrt{2\rho h_{ox}}$, we have

$$d = r_x - x_1 + r_x = 2r_x - x_1 , \tag{2-47}$$

$$x_1 = 2r_x - d = 2\sqrt{2r\ h_{ox}} - d . \tag{2-48}$$

Next consider the case where beam orientation is the limit. The actual beam deflection by Equation (2-8) is

$$\gamma \approx \phi_t + \phi_r \approx \frac{\lambda}{s} . \tag{2-49}$$

Desired beam deflection for the near horizon case is from Appendix B

$$\gamma' = \phi'_t + \phi'_r \approx \frac{h}{r_t} + \frac{r_t}{2\rho} + \frac{h}{r_r} + \frac{r_r}{2\rho}$$

$$\gamma' \approx \frac{r_t + r_r}{2\rho} + \frac{h}{r_t} + \frac{h}{r_r} = \frac{d}{2\rho} + \frac{h}{r_t} + \frac{h}{r_r} \tag{2-50}$$

To determine when the location does not allow satisfactory illumination of the receiver, consider the limiting case

$$\gamma' - \gamma = \frac{\delta v}{2} = \frac{\lambda}{2ns \cos \phi_r} \approx \frac{\lambda}{2ns} \quad . \tag{2-51}$$

From Equations (2-49), (2-50), and (2-51),

$$\frac{d}{2\rho} + \frac{h}{r_t} + \frac{h}{r_r} - \frac{\lambda}{s} = \frac{\lambda}{2ns} \tag{2-52}$$

$$\frac{d}{2\rho} + \frac{hd}{r_r(d - r_r)} - \frac{\lambda}{s} = \frac{\lambda}{2ns} \tag{2-53}$$

$$hd = \left(\frac{\lambda}{2ns} + \frac{\lambda}{s} - \frac{d}{2\rho}\right)(r_r d - r_r^2) \tag{2-54}$$

$$r_r^2 - dr_r + \frac{hd}{\frac{\lambda}{2ns}(2n + 1) - \frac{d}{2\rho}} = 0 \tag{2-55}$$

$$r_r = \frac{d}{2} \pm \sqrt{\frac{d^2}{4} - \frac{hd}{\frac{\lambda}{2ns}(2n + 1) - \frac{d}{2\rho}}} \quad . \tag{2-56}$$

The limits of the longitudinal range imposed by this conditions are

$$x_2 = 2\sqrt{\frac{d^2}{4} - \frac{hd}{\frac{\lambda}{2ns}(2n + 1) - \frac{d}{2\rho}}} = \sqrt{d^2 - \frac{8hd}{\frac{\lambda}{ns}(2n + 1) - \frac{d}{\rho}}}$$

$$x_2 = \sqrt{d^2 - \frac{8hdns\rho}{\lambda\rho(2n + 1) - nsd}} \quad . \tag{2-57}$$

In all practical cases, the horizon sets the limit.

c. Effect of Positioning of the Scatterer

In many applications, one would like to achieve the longest possible hop which can be obtained. This occurs when the scatterer is placed at the path midpoint at the highest realizable altitude. If, however, the distance between terminals is less than this extreme case, distinct advantages may be

realized, particularly within a regime where free space losses are closely approximated. This assumption is made for the remaining discussion on the effect of positioning of the scatterer.

According to (2-29) the propagation efficiency can be expressed by

$$e = \frac{K}{(r_t r_r)^2} \quad . \tag{2-58}$$

Because of the symmetry in r_t and r_r it is useful to introduce the deviation x of the position of the scatterer from the center at r_m, so that

$$e = \frac{K}{(r_m + x)^2 (r_m - x)^2} = \frac{K}{r_m^2 - x^2)^2} \quad . \tag{2-59}$$

This expression shows that the center position of the scatterer is the least efficient one with the efficiency being

$$e_m = \frac{K}{r_m^4} \quad . \tag{2-60}$$

Thus, a gain in efficiency can be realized by positioning the scatterer unsymmetrically, whereby

$$\frac{e}{e_m} = \left(\frac{r_m^2}{r_m^2 - x^2} \right)^2 \quad . \tag{2-61}$$

A plot of this function is shown in Figure 2-8. It shows that substantial gain can be achieved if the scatterer is positioned near one of the terminals. However, when the slant range deviates appreciably from the ground range, a more rigorous expression must be derived. Also, a correction for the reduction of cross section in the direction of the nearer terminals must be made.

The higher altitude of the scattered when placed off center is expressed according to (B-4) by

$$h_{ro} = h_o = \frac{(r_m + x)^2}{2\rho} \tag{2-62}$$

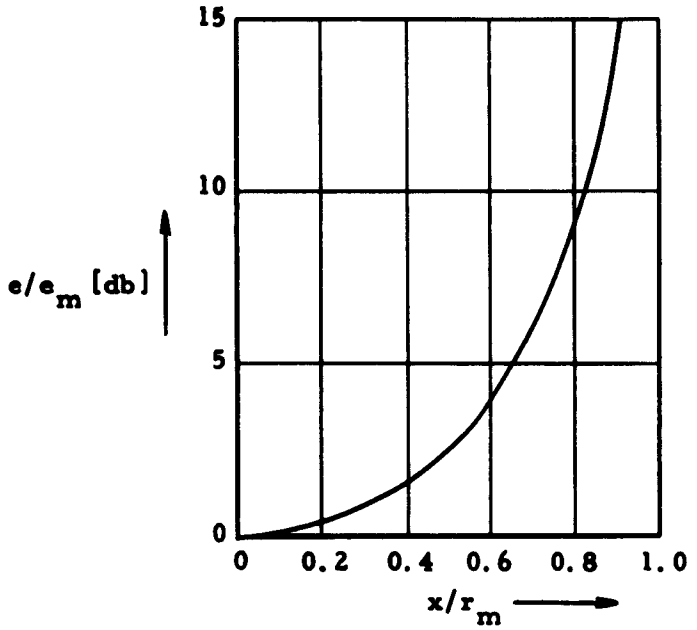

Figure 2-8. Signal Gain Versus Scatterer Position

whereby h_o relates to the line-of-sight with respect to the more distant station being on the horizon. In actual cases, we have to provide angular clearance of the horizon and this depends much on the terrain and the height of the antenna support. A plot of the minimum height is shown in Figure 2-9.

While the elevation angle of the scatterer with respect to the more distant station is always zero under the above assumption, the elevation angle with respect to the nearer station can be determined by means of formula (B-5)

$$\theta = \arctan\left(\frac{h_o}{r_m - x} - \frac{r_m - x}{2\rho}\right) \qquad (2\text{-}63)$$

With h_o as in (2-62)

$$\theta = \arctan\frac{2 r_m x}{\rho(r_m - x)} \quad . \qquad (2\text{-}64)$$

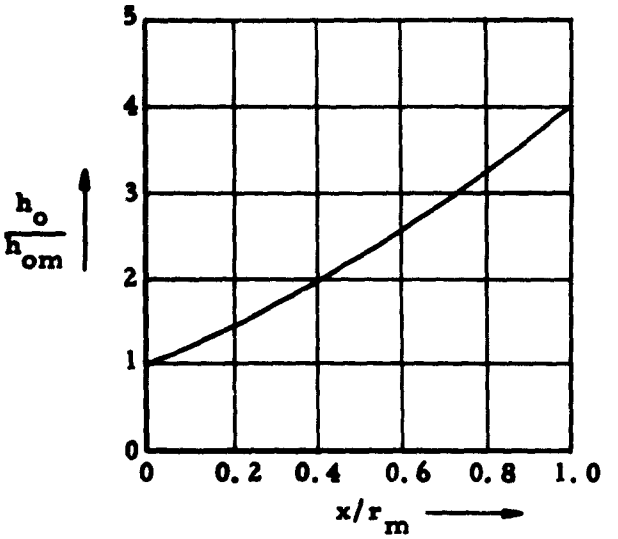

Figure 2-9. Height Factor Versus Scatterer Position

A plot of this angle (2-64) is shown in Figure 2-10.

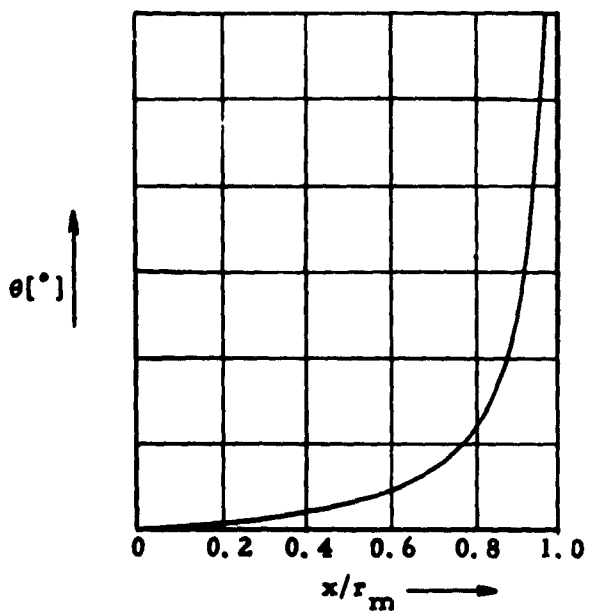

Figure 2-10. Elevation Angle Versus Scatterer Position

A plot of this angle is shown in Figure 2-10 for the r_m value of 218.5 km which was subsequently chosen for the field experiment described in Section II-C of this report. One can conclude from these results that a great advantage regarding signal strength or size of the scatterer can be gained if it is positioned in the vicinity of one terminal. Under certain operational situations it may also be of advantage to keep the scatterer in the vicinity of one terminal or to launch it there.

Greater elevation angles reduce the projection of the physical cross section in the direction of the nearer terminal, thus limiting the gain achievable due to the favorable ranges. However, a position near $x = 0.9\ r_m$ is quite attractive from an integrated point of view. Here, the gain is about 14 db, while the elevation angle is not greater than 25 degrees.

It must also be pointed out that the scatterer in the vicinity of one terminal has a smaller maneuverable space. If, however, the scatterer is reduced in size, the coherent scatter beam will correspondingly widen, thus providing some compensation for the narrowing of the maneuverable space.

C. The "Scatterloon"

A nonresonant grating array supported by a free-floating helium balloon appeared to be an attractive means for field testing the preceding theory. A balloon-supported scatterer of this type has been called a "Scatterloon". The Aerospace Research Department of GMI has had extensive experience in balloon operations, and successfully launched the Scatterloon described in the following sections.

1. Design Parameters of an Experimental Grating

To verify the theory of grating arrays (Gratar) an experiment was conducted which utilized a commercial TV station as the transmitter and laboratory assembled equipment at the receiving terminal. Although the low directivity of the TV antenna pattern and high bandwidth of the signal lead to a large grating area, the TV transmitter was selected because of its high power as well as its economic attractiveness and its location in relationship to our laboratory.

For the final selection of the TV station, the following considerations were applied.

1) The station should operate in one of the high power channels, namely 7 through 13.

2) If possible, the balloon launching facilities of GMI 10 miles north of Minneapolis should be used.

3) The distance between receiver and transmitter should be long enough so that sufficient separation between the scattered signal level and the level due to natural propagation was assured.

4) The receiving site should be in an electromagnetically quiet area.

It was found that only the TV station WKBT, Channel 8 at LaCrosse, Wisconsin met all these requirements. With the balloon launching site halfway between the two terminals, the receiving site fell on Wadena, Minnesota.

The computation of the design parameters of the grating was based on the following data:

Gain x power of the transmitter	$G_t \times P_t = 412 \times 10^3$ w
Gain over isotropic radiator	$G_t = 11.5$ (10.6 db)
Radio frequency (center of Channel 8)	f = 183 mcps
Bandwidth	B = 4 mcps
Gain of receiving antenna	$G_r = 40$ (16 db)
Distance between transmitter and scatterer	$r_t = r = 218.5$ km (136 miles)
Distance between transmitter and receiver	d = 2r - 437 km (272 miles)
Signal-to-noise ratio required	$\eta = 10$ (10 db)

From these basic data we derive the required received power and propagation path efficiency as discussed in the following paragraphs.

a. Required Receiver Power

The limiting power in the VHF band is cosmic noise. According to Hogg and Mumford[1], the average noise temperature of the sky in °K is

$$T_c' = 290\,\lambda^2. \tag{2-65}$$

With $\lambda = 1.64$ meter, we have

$$T_c' = 780°K\ . \tag{2-66}$$

Peak temperatures can reach five times this value:

$$T_c = 3900°K\ . \tag{2-67}$$

Thus, we can determine the received power with the aid of the formula

$$P_r = \eta K T_c B \tag{2-68}$$

where $K = 1.38 \times 10^{-23}$ is Boltzmann's constant. Hence

$$P_r = 10 \times 1.38 \times 10^{-23} \times 3900 \times 4 \times 10^6 = 2.15 \times 10^{-12}\ w\ . \tag{2-69}$$

b. Propagation Path Efficiency

The propagation path efficiency is defined as

$$e = \frac{P_r}{P_t} \tag{2-70}$$

with $P_t = 35.8 \times 10^3$ watts we obtain

$$e = \frac{2.15 \times 10^{-12}}{35.8 \times 10^3} = 0.6 \times 10^{-16}\ (-162.2\ db)\ . \tag{2-71}$$

If we had free space loss between the two terminals, the efficiency would assume the value

$$e_o = \frac{G_t\, G_r\, \lambda^2}{(4\pi d)^2} = 0.409 \times 10^{-10}\ (-103.9\ db)\ . \tag{2-72}$$

From (2-71) and (2-72) we derive the ratio of the gratar propagation efficiency over that of the free space and obtain

$$\frac{e}{e_o} = \frac{0.6 \times 10^{-16}}{0.409 \times 10^{-10}} = 1.47 \times 10^{-6} \quad (-58.3 \text{ db}) \tag{2-73}$$

According to various measured data as reported by Bullington[2] and Rice[3] the intensity ratio for tropospheric propagation over that of the free space ranges between -78 and -63 db for mean values. This means that the artificial scatterer will provide a 5 to 20 db stronger signal than the tropospheric propagation. This appears to be an acceptable separation in view of the fact that only the increase of the scatterer cross section would increase this separation.

The area of the scatterer can now be obtained from (2-31)

$$A_s = \pi^2 \times 437^2 \times 10^6 \times \sqrt{\frac{0.6 \times 10^{-16}}{11.5 \times 40}} = 682 \text{ m}^2. \tag{2-74}$$

For an operational altitude of 3660 meters (12,000 feet) s can be derived from (2-8) whereby $\phi_t = \phi_r = \phi$. From (B-9) we compute

$$\tan \phi = \frac{3660}{218.5 \times 10^3} + \frac{218.5 \times 10^3}{2 \times 8500 \times 10^3} = 0.0296 . \tag{2-75}$$

Hence, since ϕ is very small

$$s = \frac{\lambda}{2 \sin \phi} \approx \frac{\lambda}{2 \tan \phi} \sqrt{1 + \tan^2 \phi} = \frac{1.64}{0.0592} \sqrt{1 + 0.0009} = 27.7 \text{ m} . \tag{2-76}$$

We have now a choice of n to determine the aspect ratio. This ratio has a bearing on the maneuverable space whose cross section is determined by the range to the receiver and the beamwidth of the scatterer. For scatterers in the center we recall from (2-42) and (2-43)

$$\ell_s = \frac{d\lambda}{4a} \quad \text{and} \quad v_s = \frac{d\lambda}{4ns}$$

Table 2-1 shows a selection of parameters around the optimum design.

Table 2-1. Parameters for Three Gratings Having the Required Area

Example Number	n	(n - 1/2) s (m)	a (m)	ns (m)	ℓ_s (km)	v_s (km)
1	3	69.2	8.2	83.1	21.8	2.16
2	4	97	6.15	110.8	29.1	1.62
3	5	124.7	4.93	138.5	36.1	1.29

To clear the horizon the scatterer must be at a minimum height of

$$h_{om} = \frac{r_m^2}{2\rho} = \frac{218.5^2 \times 10^6}{2 \times 8500 \times 10^3} = 2810 \text{ m} . \qquad (2\text{-}77)$$

Therefore, the apparent altitude (above the horizon) is

$$h_d = h - h_{om} = 3660 - 2810 = 850 \text{ m} . \qquad (2\text{-}78)$$

Thus, the cross section of the maneuverable space is clear of the horizon in two of the three examples as shown by Figure 2-11.

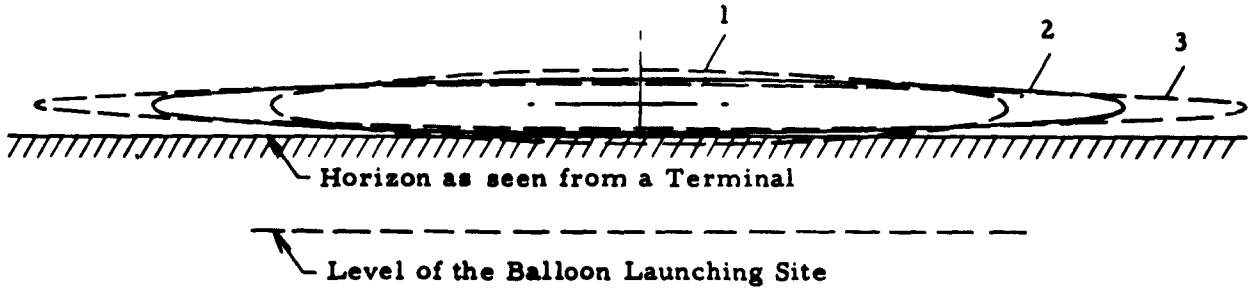

Figure 2-11. Lateral Cross Sections of the Maneuverable Spaces According to Table 2-1

Examining the longitudinal limits, consider the horizon limit indicated by (2-48)

$$x_1 = 2\sqrt{2\rho\, h_{ox}} - d = 62 \text{ km} \qquad (2\text{-}79)$$

Next consider the limit imposed by beam orientation indicated by (2-57)

$$x_2 = \sqrt{d^2 - \frac{8hdns\rho}{\lambda\rho(2n+1) - nsd}} = 186 \text{ km} \qquad (2\text{-}80)$$

2. Fabrication and Launch of the Scatterloon

a. General

For the field experiment of testing the forward scattering technique, it was considered expedient to launch the scattering element in the vicinity of the GMI balloon launch facility at New Brighton, Minnesota with the transmitting and receiving stations at LaCrosse, Wisconsin and Wadena, Minnesota, respectively. The design altitude required to obtain a line-of-sight path (allowing some maneuverability) from the scatterer to the transmitter and receiving terminals is 13,600 $\pm$ 2660 feet above mean sea level. This altitude is greater than the 12,000 feet above smooth earth design value by 1600 feet which represents the median height of the two antennas above msl. The target zone within which the scatterer must be located is essentially a rectangular boundary 18.1 miles wide by approximately 38.6 miles long with the long axis aligned with LaCrosse and Wadena. The center of the target zone is at a point 3 miles east of the GMI balloon launch facility.

Several methods were considered for bringing the scatterer to the required altitude, including airplanes, helicopters, tethered Aerocaps, etc. For reasons of technical feasibility, economy, and short preparation time, the helium-filled free balloon was selected as the transport means. This required, however, optimum meteorological conditions for launching and for wind direction and velocity at float to maximize time in the target zone.

b. Fabrication of the Grating

Figure 2-12 shows the essential dimensions of the scattering element as determined by the grating design. The shaded (blocking) areas are composed of aluminum foil polyethylene (PE) laminate and the clear areas are composed of red PE (the red provides visibility to pilots). The thickness of the

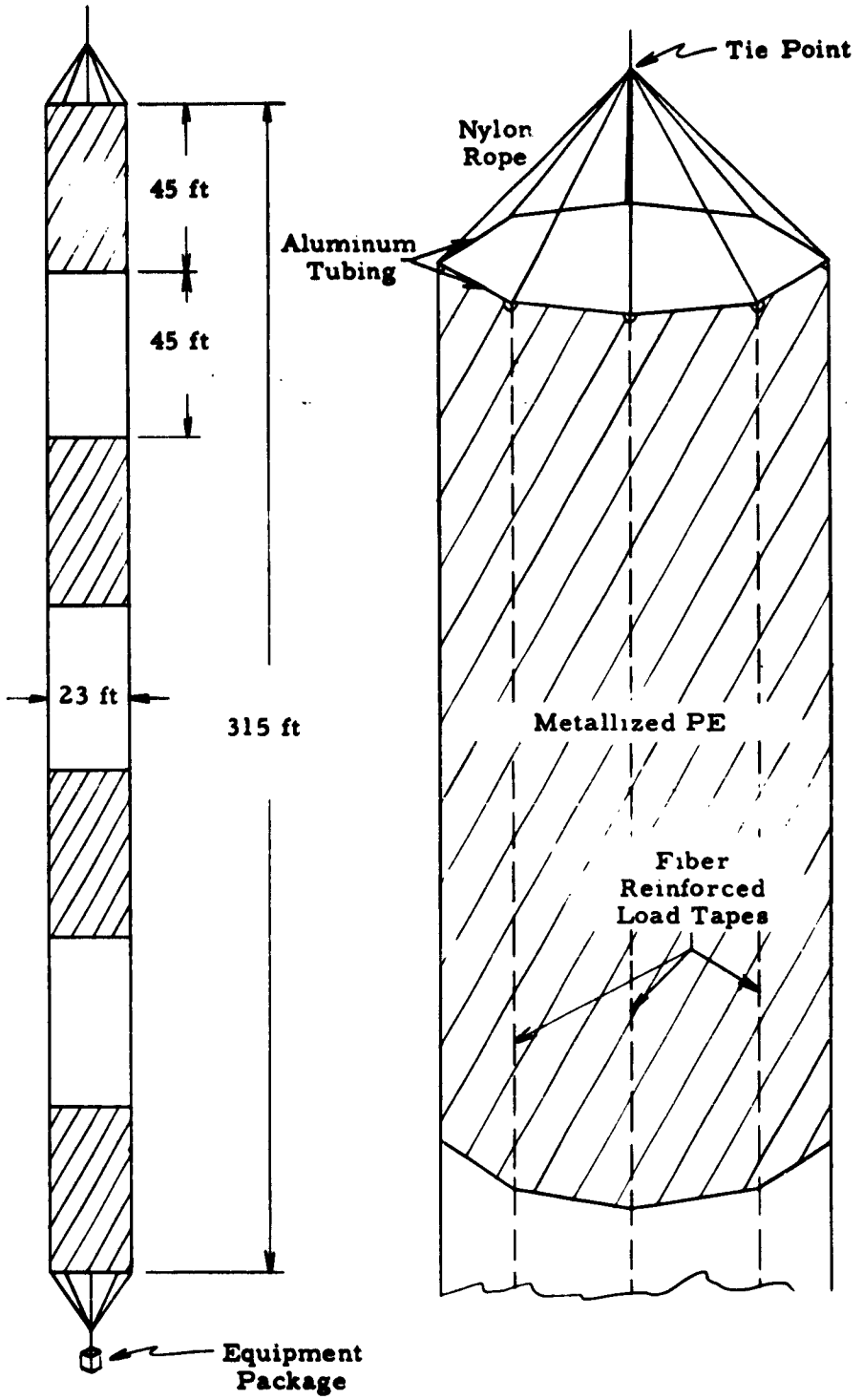

Figure 2-12. The Scatterloon Grated Array

red PE is 3 mil (0.003 in.) and the composition of the laminate is 1.5 mil PE; 0.35 mil aluminum foil; and 1 mil PE. The strips of material (39 in. wide laminate and 108 in. wide red PE) were assembled into gores running horizontally around the cylindrical scatterer. After all the horizontal seals were made the material was refolded in the vertical direction for making the final seal.

Several methods of deploying the scatterer were considered; among them, air inflation, curved pressure beams and rigid metal rings. It was believed the air inflation would have given the best deployment; however, it was considered impractical because of the large volume of air involved (approximately 130,000 ft^3), the extremely low internal pressure which could be tolerated due to the large radius, and the super heat problem which will cause added lift as the air contained within the scatterer heats up and causes a change of altitude. For ease of fabrication, the rings were modified to an octagon shape (23 ft diagonal) rather than the circular shape. This deployment technique was tested by suspending a 1/10 scale model in an elevator shaft. It was found that rings at only the top and bottom were sufficient for satisfactory deployment, providing some agent (such as cornstarch) was used on the PE film to prevent electrostatic attraction of the film to itself.

The scattering element was suspended from a common tie point (at the base of the parachute) by eight nylon cords (1000 lb test) to the eight corners of the top octagonal ring. Also, the cylindrical plastic scatterer was reinforced by load bearing tapes (3M #890) extending vertically from the eight corners of the top ring to the corresponding eight corners of the bottom ring.

The weight of the plastic cylindrical portion of the scatterer was 378 pounds as fabricated and the total weight including suspension lines and rings was 442 pounds.

c. Balloon Design

The parameters of payload and altitude are the basic ones in determining balloon size. In this case the payload suspended from the balloon was 628 pounds and the altitude 13,600 feet msl. The balloon size and gore pattern

was computed on the basis of the "natural" shape using basic equations and tables developed by the University of Minnesota and currently used in all balloon design work. At this low altitude the weight limitation (balloon) is not stringent; therefore, a relatively heavy (2 mil) gauge PE film was selected. The balloon gores were not tailored to lessen cost. The details of the balloon are as follows:

Volume	= 16,200 ft^3
Inflated Diameter	= 34 ft
Deflated Length	= 50 ft
Weight	= 72 lb

d. Launch and Flight

After observing the meteorological conditions for several days, it was decided on Tuesday evening (September 4) that conditions on September 5th would be suitable for launching the balloon-borne scatterer system. Accordingly, the GMI receiving station crew departed for Wadena at midnight. The GMI balloon operations crew was alerted at 1:30 a. m. CST for arrival at the flight center by 2:30 a. m. Flight train layout, component assembly, and other preflight preparations were commenced at approximately 3:00 a. m. Preparations were completed and the launch was effected at 6:43 a. m. CST.

Usual methods of balloon launching (using the dynamic method) were considered unsuitable for this system because of its large size and length. Therefore, the vertical launch technique was used. As the name implies, the system is statically paid out to a vertical position by means of an anchor line attached to the bottom fitting of the balloon. After the entire load train (411 ft long) is vertical and the scatterer properly deployed, the anchor line is released from the balloon and the restraint at the bottom of the load train is released to allow the system to become airborne and rise to float altitude.

The major limitation of the vertical launch method is the requirement for zero (or practically calm) wind conditions from the surface to at least the height of the vertical flight train at launch. During this particular launch it was found that the winds (which were almost clam on the surface) were

blowing at an estimated 5 knots at approximately 200 to 300 feet up. As the system was being paid out the wind gradually caught the reflector as it reached this altitude forming a gigantic sail. This made it necessary for the crew members holding the bottom end of the scatterer and lower instrument bag to move downwind to follow the motion of the upper part of the scatterer as it "sailed out". This required considerable agility on the part of the crew members involved.

It was observed that the angle of the anchor line with the ground shortly before release was approximately 45 degrees. This means that the vertical and horizontal components of forces at the base of the balloon are approximately equal. Knowing that the vertical lift of the balloon was 700 pounds at the bottom fitting implies that the horizontal wind forces were approximately 700 pounds. Knowing the dimensions of the scatter and estimating the drag coefficient, we can compute the wind velocity at approximately 5 knots (5-3/4 mph).

The launch was performed quite smoothly in spite of the wind condition; however, winds of lower magnitude would definitely be more desirable.

The system ascended at a rather slow consistent rate of rise until it reached floating altitude 37 minutes after launch. Winds at the 14,000-foot level were slightly stronger than expected causing the scatterer to cross the southeast boundary leaving the target zone 33 minutes after launch. The trajectory of the balloon system was nearly down the centerline of the target zone in a southeasterly direction.

It was planned to track the Scatterloon by the following means:

1) Visual tracking from launch point using theodolite.

2) Aircraft tracking to locate map position when out of visual range.

3) A B-23 Barocoder for sending pressure information by telemetry to a ground receiver.

4) A HAK-4 recording barograph to obtain the altitude trace after the instrument package is recovered.

An optical theodolite rather than a radio theodolite (such as a GMD-1 system) was chosen as the weather conditions required for the flight would, as a matter of course, include insignificant cloud cover from ground to the balloon altitude. In practice, however, the balloon was lost in haze due to lack of contrast even though its observed azimuth angle was greater than 45 degrees from the sun. The general position of the balloon was reasonably easy to establish from known drift from launch and estimated wind velocity at balloon float altitude derived from a wind velocity profile obtained from a balloon sounding at St. Cloud, Minnesota.

However, it was difficult for the observing aircraft to fly directly to the balloon, and it was spotted near the Minnesota-Wisconsin border beyond the southeast end of the target zone. The observing aircraft was not airborne during the balloon launch. A photographer was on hand to document the launching operation, and also boarded the observing aircraft to record the balloon flight.

Figures 2-13 and 2-14 are a series of photographs showing:

1) Grating laid out on ground on plastic sheets used for protection.

2) Balloon partially inflated.

3) Grating partially airborne.

4) Complete system airborne.

5) First photograph of Scatterloon at altitude.

6) About two minutes later. Grating begins "sagging in" to less than full width. Altitude also shows slight tilt.

7) About two minutes later. Grating has "sagged in" to the greatest extent observed.

8) About five minutes later. Grating is out of target zone, and is satisfactorily deployed.

No telemetry signals were received due to a malfunction of the telemetry transmitter or the antenna release mechanism. Reliable pressure-altitude information was obtained from the recording barograph.

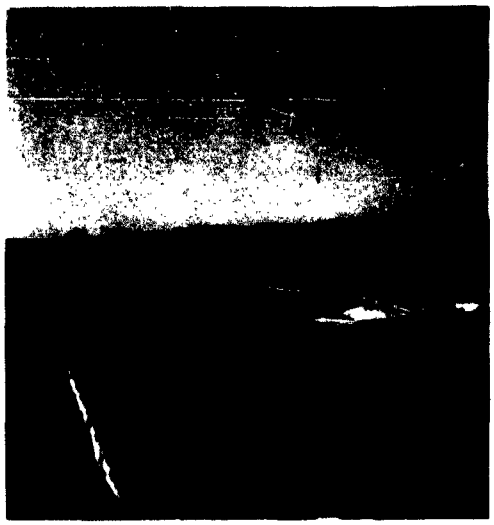

(1)

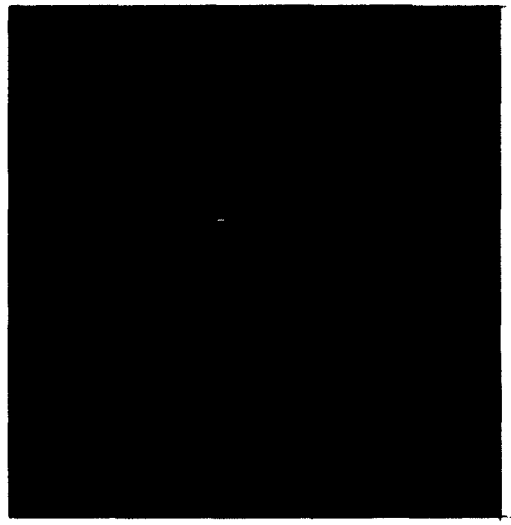

(2)

(3)

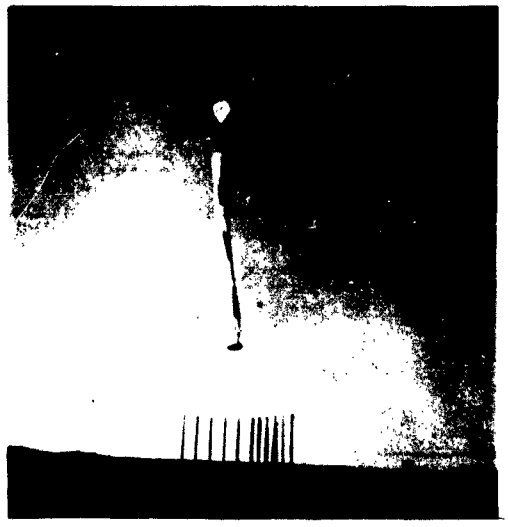

(4)

Figure 2-13. Scatterloon Launch

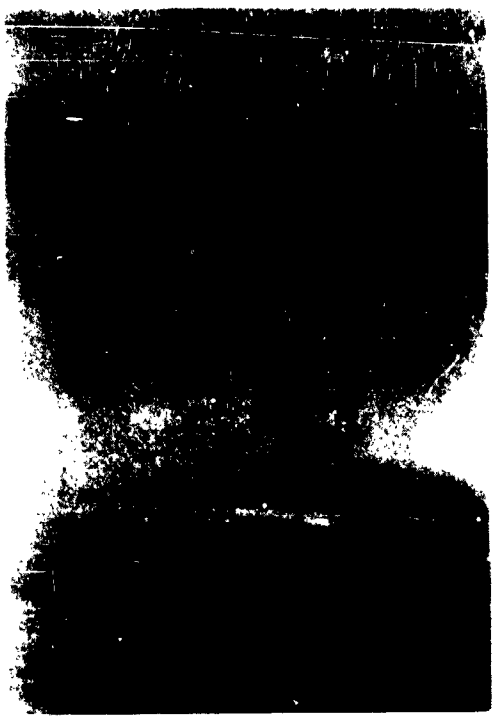

(5)

(6)

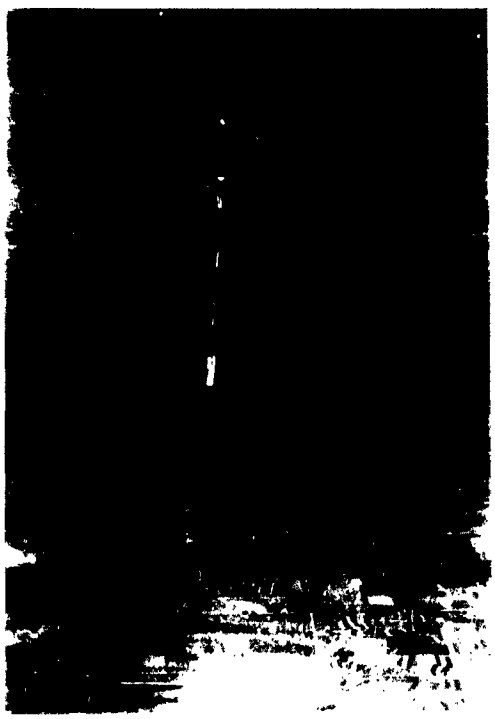

(7)

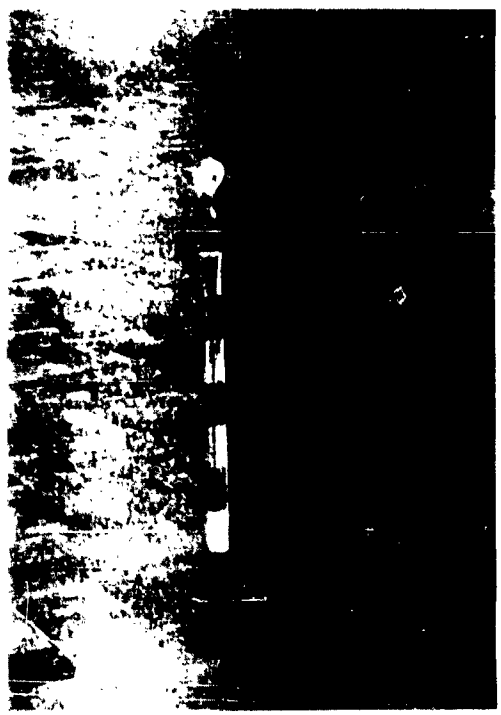

(8)

Figure 2-14. Scatterloon Flight

3071

A trace of the Scatterloon altitude is shown on the profile of Figure 2-15 which is a parabolic 4/3 earth radius path profile. Although the upper winds were known to be about 40 knots, the Scatterloon took more time to reach altitude than expected due to the aerodynamic drag of the grating. The flight was terminated as requested by FAA because of its potential aircraft hazard. It was terminated 52 minutes after leaving the target zone at a point 4 miles southeast of Ellsworth, Wisconsin. Impact was in a clearing in a wooded ravine 4 miles northeast of Bay City, Wisconsin. A track of Scatterloon position versus time in plan view is shown in Figure 2-16. The target zone is determined by computed values of ℓ_s and x_1. A map indicating some salient geographic features is shown in Figure 2-17 to help reference the significant locations used in the experiment.

The balloon and scatterer were not salvageable; however, the parachute and all other instrumentation were retrieved by the recovery crew.

3. The 272-Mile Scatterloon Experiment

a. Description of the Receiving System

Shown in Figure 2-18 is a block diagram of the receiving system at the Wadena site. The antenna was mounted on a boom projecting from a servicing platform 110 feet above ground level on a receiving tower at the Wadena Air Station. The antenna system was comprised of four stacked ten element yagi arrays. Antenna gain was 16 db over an isotropic antenna. The antenna feed system included a balun; the antenna output was unbalanced and at an impedance level of 75 ohms.

Excessive deterioration of the overall receiver noise figure by the tower cable loss (7 db) was prevented by a tower located preamplifier having a gain of 25 db. The preamplifier was a Winegard Model A-400, having a measured noise figure of 4.5 db at 186 mc. The main receiver, a Nems-Clarke Model 1502-A, was located at ground level. This receiver had a noise figure of 6.5 db at 186 mc. The noise figure of the complete receiving system was 5.1 db and the effective bandwidth 300 kc. The receiver output was taken from an envelope detector and fed to a Brush strip chart recorder.

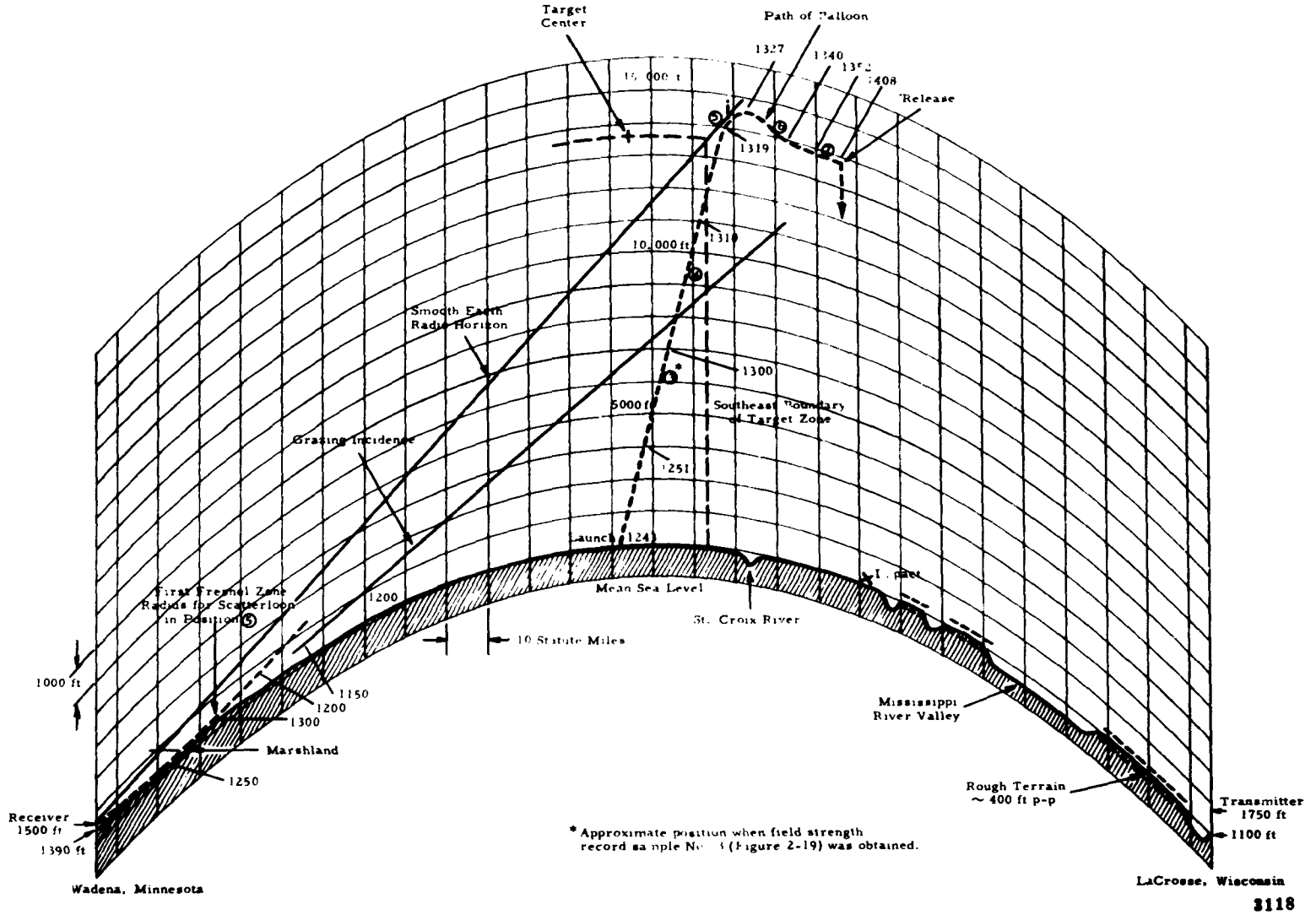

Figure 2-15. Profile of Scatterloon Experiment

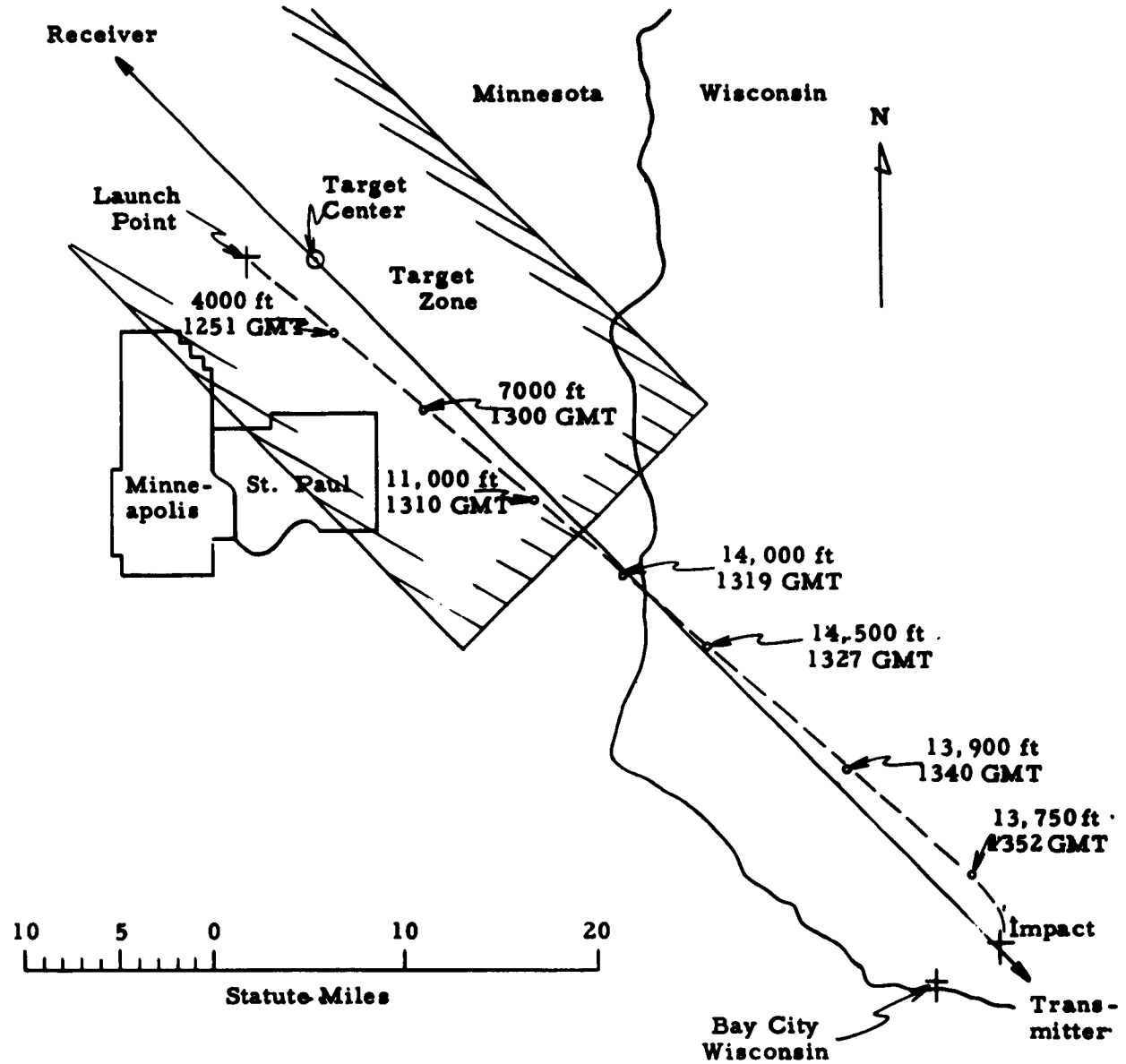

Figure 2-16. Scatterloon Flight Path

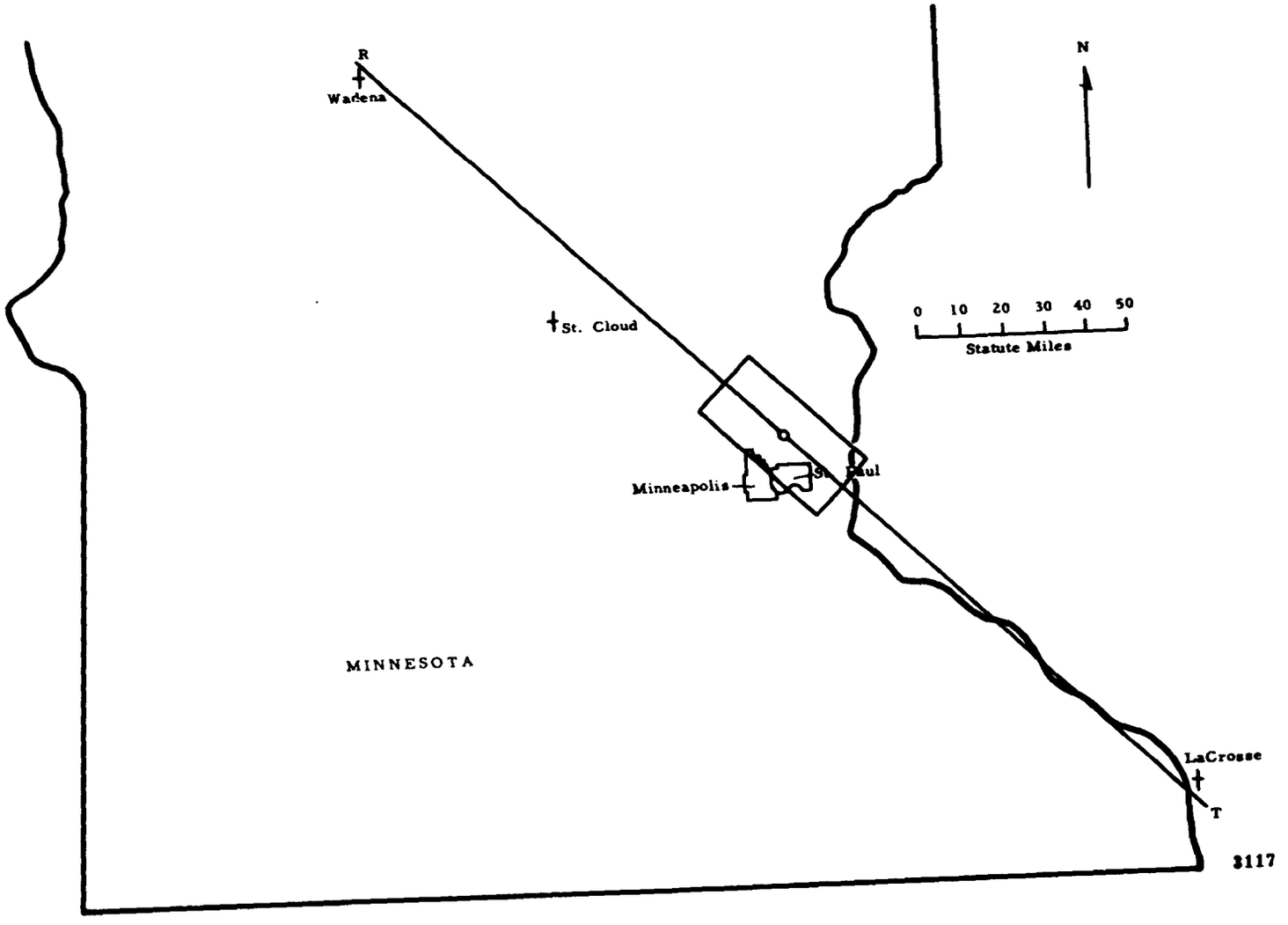

Figure 2-17. Georgraphy of Scatterloon Field Experiment

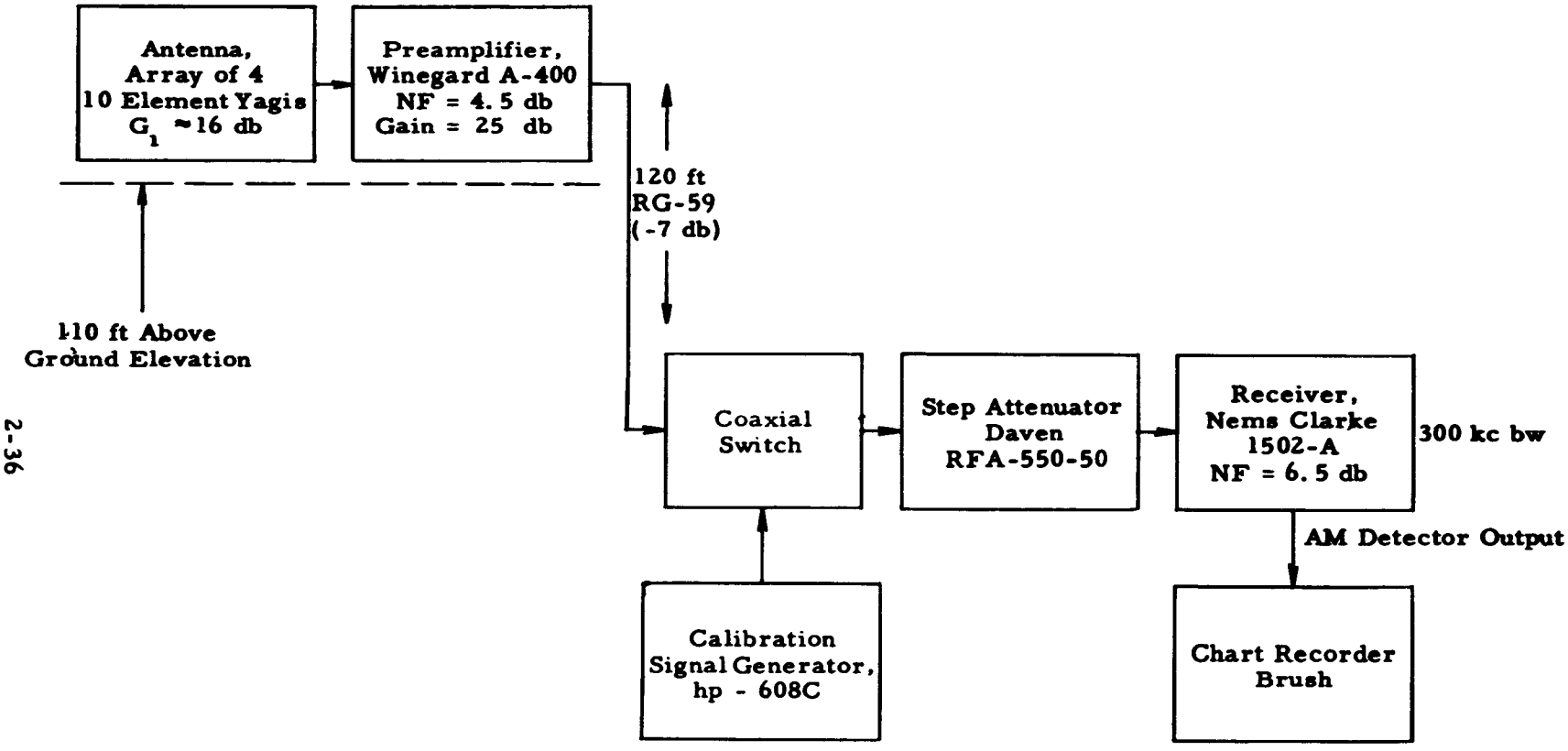

Figure 2-18. Block Diagram of the Receiving Site Equipment

As shown in the block diagram, provision was made to switch into the receiving channel a calibration signal source, an hp 608C signal generator.

A television receiver and preamplifier were also available for observing picture quality.

b. Results Obtained in the Scatterloon Experiment

Figures 2-19 (Charts 1, 2 and 3), 2-20 (Charts 4, 5 and 6), and 2-21 (Charts 7, 8 and 9) show recorded profiles of the field strength during various phases of the Scatterloon experiments. One hour prior to launch field strength measurements at Wadena, Minnesota of the LaCrosse, Wisconsin television station (WKBT) aural carrier (185.75 $\pm$ 0.04 mc) were begun. Chart 1 is a 40-second sample of the recording of the field strength prior to launch. The median of this signal as obtained over a time period of 30 minutes was approximately 0.7 microvolts per meter. This level was approximately as anticipated. According to references 2 and 3, the median tropospheric scattered signal for this situation will be on the order of 73 db below the signal which would be received for free space propagation (79.2 db above 1 microvolt per meter) or around 2 microvolts per meter.

Chart 2 is also a sample record obtained before launch. Here, propagation was evidently accomplished by two mechanisms: tropospheric scatter and aircraft scatter. The aircraft scattered signal is roughly 10 db below the tropospheric scattered signal. The rate of change of the two electrical path lengths with respect to each other is about one wavelength per second.

A path profile of the diffraction grating experiment is given in Figure 2-15. Balloon location with time is shown on this profile. Balloon location for each corresponding chart is also shown. Throughout the test, the balloon remained within a few miles of a vertical plane joining the transmitter and receiver.

The balloon was launched at 1243 GMT. Shown in Chart 3 is a sample record obtained at 1257 GMT. By this time the balloon had reached 6000 feet, still below the horizon with respect to the receiver, but above the

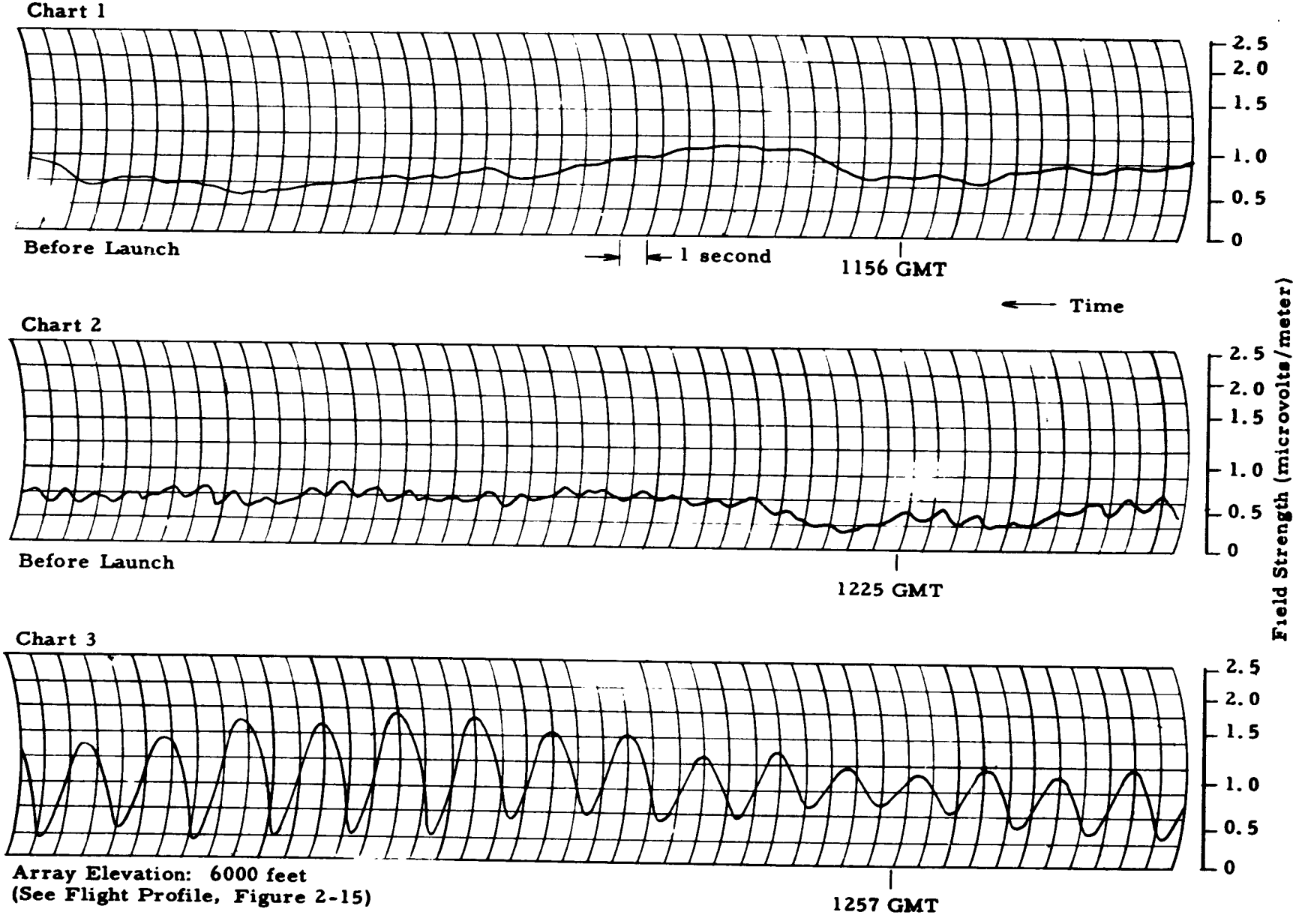
Chart 1
2.5
2.0
1.5
1.0
0.5
0
Before Launch
1 second
1156 GMT
Time
Chart 2
2.5
2.0
1.5
1.0
0.5
0
Before Launch
1225 GMT
Field Strength (microvolts/meter)
Chart 3
2.5
2.0
1.5
1.0
0.5
0
Array Elevation: 6000 feet
(See Flight Profile, Figure 2-15)
1257 GMT

Figure 2-19

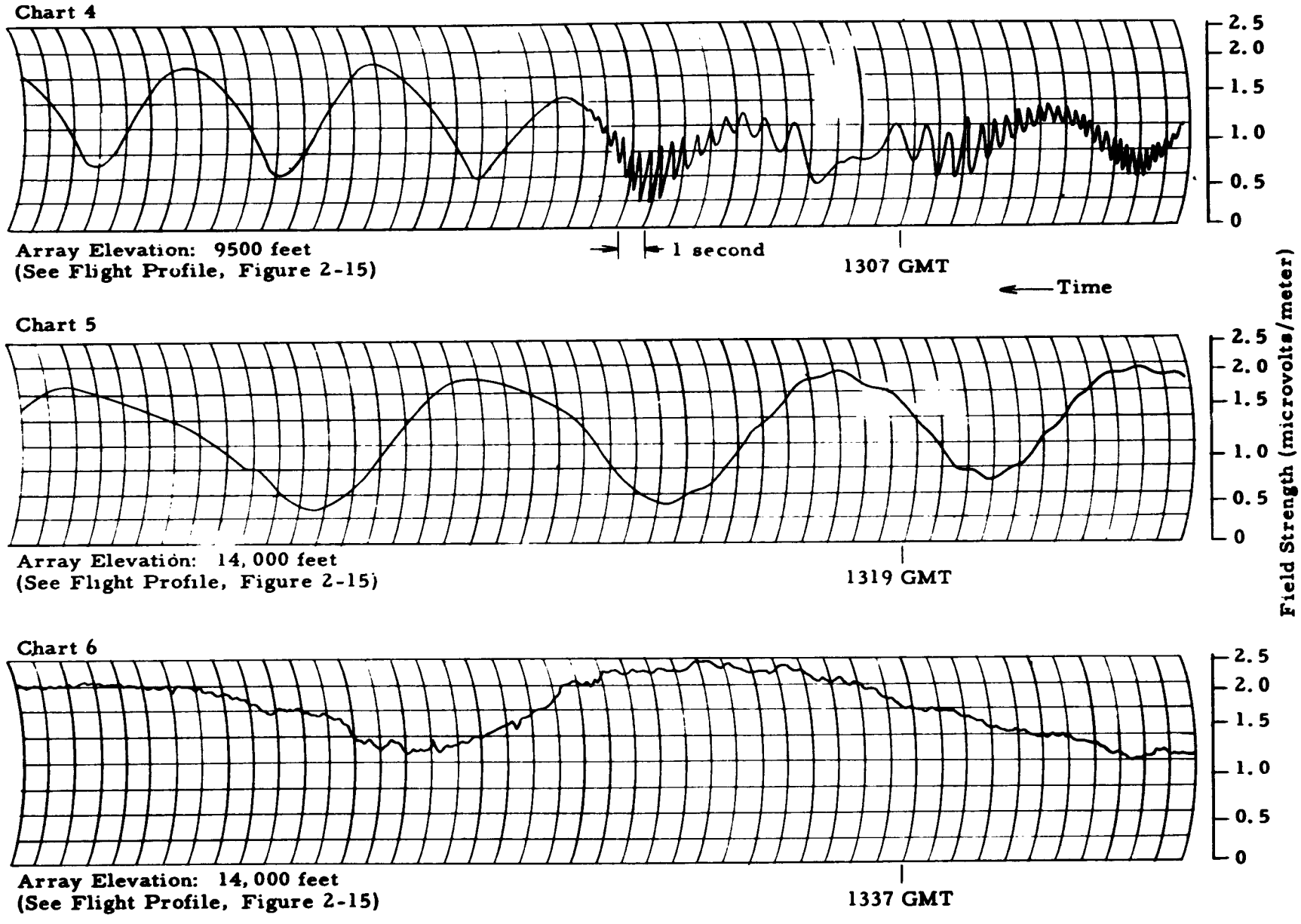
Chart 4
2.5
2.0
1.5
1.0
0.5
0
Array Elevation: 9500 feet
(See Flight Profile, Figure 2-15)
1 second
1307 GMT
Time
Chart 5
2.5
2.0
1.5
1.0
0.5
0
Array Elevation: 14,000 feet
(See Flight Profile, Figure 2-15)
1319 GMT
Field Strength (microvolts/meter)
Chart 6
2.5
2.0
1.5
1.0
0.5
0
Array Elevation: 14,000 feet
(See Flight Profile, Figure 2-15)
1337 GMT

Figure 2-20

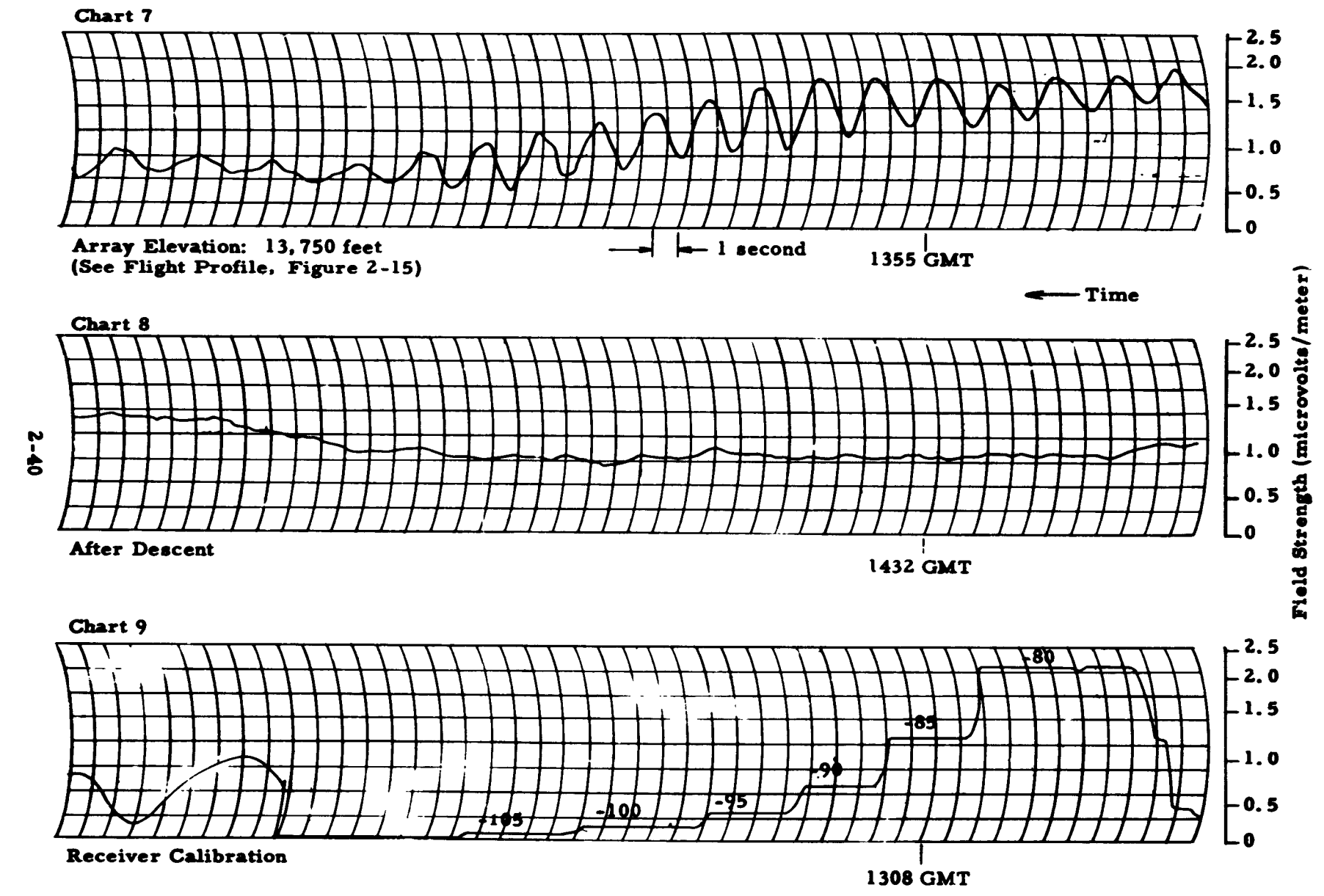
Chart 7
2.5
2.0
1.5
1.0
0.5
0
Array Elevation: 13,750 feet
(See Flight Profile, Figure 2-15)
1 second
1355 GMT
Time
Chart 8
2.5
2.0
1.5
1.0
0.5
0
After Descent
1432 GMT
Field Strength (microvolts/meter)
Chart 9
2.5
2.0
1.5
1.0
0.5
0
-80
-85
-90
-95
-100
-105
Receiver Calibration
1308 GMT

Figure 2-21

horizon with respect to the transmitter (Figure 2-15). A significant feature of all the field strength recordings when the Scatterloon was useful is the interference of received signals arriving by two mechanisms, the gratar scatter propagation and the tropospheric scatter propagation. Constructive and destructive phase additions are readily apparent. The signal amplitudes as received over each of the two scattering mechanisms are comparable. The difference in electrical path length in Chart 3 shows a uniform rate of one wavelength in 3 seconds. It was noted that this rate continued uniformly for five minutes. This rate appears to be greater than the rate caused by the movement of the grating alone by almost an order of magnitude, and indicates that the varying electrical path length difference must be due primarily to other causes.

In Chart 4 we see a third scattering mechanism contributing to the recording, presumably a commercial airliner near the transmitting terminal, as airline traffic is more dense there than in any other part of the path. There was no evidence that our chase plane altered the communication path significantly.

Interference periods of 10 to 15 seconds are shown in Chart 5. The first Fresnel zone radius is shown on the path profile for the scatterer to Wadena path when the scatterer is located as shown in Chart 5. It clears the ground.

In Chart 6 the period is about a half minute and some higher frequency fluctuations appear which may be due to aircraft scattering.

In Chart 7 the average signal level shows a decided dip which could be due to a tropospheric fade.

A recording of a representative tropospheric signal after grating decent is shown in Chart 8. The average level is a few db above that shown prior to launch on Chart 1.

Chart 9 shows a calibration which was made during the flight to verify the gain stability of the receiving equipment. The numbers represent db below 1 mw at the receiver input terminals.

When the amplitude excursions are large due to phase interference, one may deduce that the received signal levels over the two paths are nearly equal. During phase addition, the peak amplitude is about 6 db above the amplitude of a single signal. Throughout the Scatterloon experiment, the received field strength from the grating was near 1 microvolt per meter. The expected field strength when the scatterer is in the design center location would be 7.12 microvolts per meter if free space path loss is assumed (refer to Appendix C). In the following sections, it is noted that for the scatterer location which existed during the experiment, cumulative path losses equivalent to a median value of about 13 db below free space conditions are more realistic. This reduces the expected field strength to 1.59 microvolts per meter when the scatterer was at the more favorable locations encountered in the experiment. Most of the factors that cause deviations from the ideal would cause the actual signal levels to be less than expected. For example, if the grating were not deployed to its full width in the plane perpendicular to the signal path, the energy intercepted and the forward gain would be reduced. If this width were halved, the field strength would be reduced by 6 db. Path losses which occurred during the Scatterloon experiment were probably different than when measured some weeks later.

Measured and expected field strengths agree favorably within the limited accuracy of propagation measurements. There can be no doubt that the effects of the Scatterloon were apparent in the recordings.

c. Propagation Path Loss Measurements

The path loss between terminals where the direct ray passes close to the earth is frequently not predictable with a great deal of accuracy. Some references describe methods for predicting losses and some state expected accuracy limits (which are generally quite broad). The conditions causing a specific path loss to occur between two fixed terminals are affected by varying atmospheric conditions such as the variability of the refractive index which causes the ray paths to be altered. In addition, there are cases wherein the location of a terminal causes the path loss to be a few db

different that it would be if it were relocated a few hundred feet away. This may be due to nearby objects or terrain, or to terrain an appreciable distance away.

To better determine the performance of the Scatterloon during the main field test, two additional field tests were performed. From the results of these two tests, the transmitter grating path loss and the grating receiver path loss were established. The measured transmitter grating path loss was within one or two db of that which would occur for free space conditions. The transmitter grating path profile (Figure 2-15) shows that direct ray horizon clearance is over 2000 feet; also, the region from which most of the ground reflected signal reaches the array positions is rough. These two factors make the near free space loss measurement obtained very plausible. The grating receiver path loss was determined to be, however, significantly greater (12 to 14 db) than that which would occur in free space. Inspection of the profile of this path (Figure 2-15) shows poorer horizon clearance than for the transmitter grating path.

(1) Transmitter Grating Path Loss Measurement. - Field strength measurements of the aural carrier of the LaCrosse station (WKBT) were made from an airplane (Piper Tri-Pacer) flown in the same region as that occupied by the grating during the main field test.

A coaxial half wave dipole antenna was used. This dipole was trailed about 15 feet behind the aircraft. Such an antenna system was used as its gain is predictable, being very near that of an isolated half way dipole.

The receiver used was an Empire Devices Model NF 105 Noise and Field Intensity Meter. The receiver was calibrated periodically throughout the flight. Although the bandwidth of the receiver (10 kc) was less than the allowable aural carrier excursion, it was determined by observing indicated signal strength before and during the presence of audio modulation that this receiver band limiting did not significantly (< 0.2 db) affect the signal strength measurements.

The basic transmission loss between two half wave dipoles in free space is[4],

$$L_{bf} = 32.28 + 20 \log_{10} d_{mi} + 20 \log_{10} f_{mc} .$$

At 185.75 mc and a distance of 130 statute miles,

$$L_{bf} = 32.28 + 42.28 + 45.38 = 120 \text{ db}$$

The effective aural carrier radiated power of the transmitter along the propagation path is +51 dbw.

The power delivered to a receiver matched to a half wave dipole through a transmission line having 1 db loss for free space propagation would be:

$$P_{rec} = P_t - 120 - 1 = 51 - 120 - 1 = -70 \text{ dbw} = -40 \text{ dbm.}$$

Below is a tabulation of the power received at several altitudes in a region about 10 miles from the target center in the direction of LaCrosse (130 miles from the transmitter).

Altitude Above Sea Level (ft)	Received Aural Carrier Power (dbm)
4000	-76
5000	-67
6000	-61
7000	-55
8000	-50
9000	-45
10000	-41
12000	-40
14000	-44

The 12,000 and 14,000-foot values were extrapolated from measurements made closer to the transmitter and at reduced altitude.

In summary, the measurements indicated that the transmitter grating path loss for grating altitudes over 10,000 feet was within one or two db of the free space path loss.

(2) Array Receiver Path Loss Measurement. - For this measurement a low power transmitter was installed in the aircraft used in the previous test. The trailing coaxial half wave dipole antenna was again used.

The receiving antenna at Wadena comprised two stacked 10 element yagi arrays having a gain of about 11 db over a half wave dipole. The remainder of the receiving equipment was the same as that used in the main field test (Figure 2-18). The 110-foot tower was again used.

The aircraft was flown generally toward Wadena. At distances, -10, 0, 10, 20, 40 and 60 miles from the target center in the direction of Wadena, the received signal was measured for several aircraft altitudes. As a voice communication was established between transmitter and receiver, it was possible to insure that the transmitter antenna was properly oriented and that altitude was noted when data were to be taken.

The free space basic transmission loss between a half wave dipole located at the receiving site and a dipole located at a point 10 miles in the direction of LaCrosse from the target center (140 miles from the receiver) is, at 185.75 mc, 120.6 db. The power radiated was -1 dbw. The gain of the receiving antenna was 11 db. Therefore for free space propagation, the power available at the receiving antenna terminals would be,

$$-1 - 120.6 + 11 = -110.6 \text{ dbw} = -80.6 \text{ dbm}.$$

The antenna harness, preamplifier and tower transmission line had an overall gain of 14.5 db. The receiver input power for free space transmission would, therefore, have been -80.6 + 14.5 or about -66 dbm. With the aircraft at an altitude of 10,000 feet over the reference point (10 miles southeast of the target center), the receiver input power was measured as -78 dbm; being 12 db less than the free space value. Tabulated below are the received signal levels observed and referenced to the region 10 miles in the direction of LaCrosse from the target center.

The measurements show then that after the balloon-borne diffraction grating reached 10,000 feet, the grating receiver propagation path loss was 12 to 14 db greater than the free space value.

Altitude Above Sea Level (ft)	Received Signal Power (dbm)	Path Loss Relative to Free Space Value (db)
5,000	-90	24
7,000	-82	16
8,000	-85	14
9,000	-80	14
10,000	-78	12
11,000	-80	14
12,000	-78.5	12.5
14,000	-78.5	12.5

4. Conclusions

Within the limits of instrumentation and experimental accuracy, the Scatterloon did indeed provide the field strength in the desired diffracted beam lobe predicted from theory. The maneuverability conditions were not thoroughly evaluated by the experiment. Path losses on each leg of the scatter path were evaluated on different days, and were found to be greater than anticipated, accounting for the lack of more dramatic results from the Scatterloon. Particularly on the leg from the Scatterloon to the receiving site, path losses were high. This is presumably due to a number of receiving site factors which were less than ideal. Also, the Scatterloon drifted away from the receiving terminal, thereby increasing this path loss.

SECTION III

ACTIVE OCEAN SURFACE SCATTERING

III. ACTIVE OCEAN SURFACE SCATTERING

A. Introduction

The purpose of this type of system is to increase the useful range of a radio communication path. In a standard two-terminal system, the efficiency $e = P_r/P_t$ drops monotonically as range increases. Therefore, theoretically one could maintain communication over any distance provided sufficient power is transmitted. In practice, however, serious range limitations are set. If one would place amplifying scatterers along the propagation path, the total amount of radiated power can be drastically reduced or the range can be markedly extended. If one can control the distribution of active scatterers, a regular distribution would give optimum results. However, this is not easy on the surface of the ocean. Initially, a fairly regular distribution can be achieved, but as time passes, a random distribution will be approached.

Two schemes for implementation of this system have been investigated and are presented in the following paragraphs. One, considers a transponder communication "Chain" system, and the second, an ensemble of coherent repeaters in a relatively small area of the ocean surface "Patch" system.

Because many factors must be assessed to evaluate the practical effectiveness of either active ocean surface system, no recommendations are made. Construction of circuits or other hardware to demonstrate the usefulness of either system was not undertaken. Until a promising communication technique is chosen which appears suitable from a cost, operational, and countermeasures standpoint, etc., a specific circuit approach would seem premature.

B. Transponder Chain Communication System

This system would comprise a relay chain of rf transponders distributed along the communication path. The feasibility of such a system is partially dependent upon the required number, spacing, and complexity of the transponders. A pictorial of such a system is shown in Figure 3-1. As treated in the following discussion, the transponders are represented as deployed at approximately equidistant points between the two terminals.

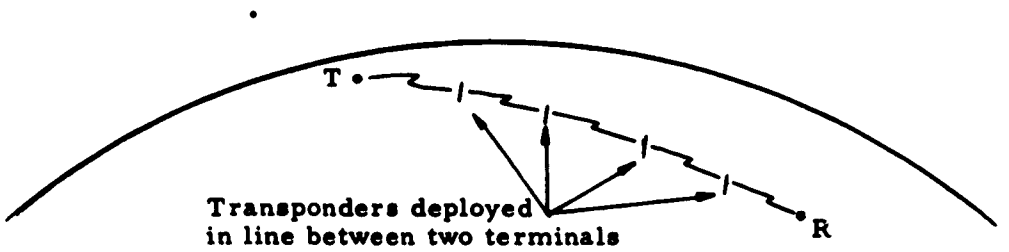

Figure 3-1. Representation of a Transponder Chain System

The transponder spacings possible for operating frequencies in the range of 1 to 50 mc will be estimated. Only the "ground wave" signal is assumed to be present. The communication system is not dependent on ionospheric or tropospheric propagation. In addition, the following parameters are assumed.

Signal Wave Form	Pulsed sinusoid, gaussian envelope, 1 ms to $e^{-1/2}$ amplitude points
Receiver Transmission Characteristic	Gaussian envelope, 1 kc to $e^{-1/2}$ points, approximately linear phase
Transmitter Power	1 watt to antenna circuit
Signal-to-Noise Ratio	A 20 db ratio at each transponder is assumed. Later, system performance to be expected with such a ratio will be described.

The basic transmission loss which can be tolerated between any two transponders[4],

$$L_b^* = P_t - L_{tc} + G_p - R - F - B + 204 \text{ db.} \qquad (3\text{-}1)$$

where:

P_t = the power input to the transmitting antenna circuit in db above 1 watt

L_{tc} = the transmitting antenna circuit losses ($-10 \log_{10}$ antenna circuit efficiency)

G_p = the path antenna gain (the sum of the receiving and transmitting antenna gains relative to an isotropic radiator along the propagation path)

R = the signal-to-noise ratio

F = the effective system noise figure

B = the receiver bandwidth ($10 \log_{10} b$)

The transponders must be easily deployed. The antenna would most likely be erected after deployment. Antenna length is assumed to be limited to 1.5 meters.

An estimate of antenna circuit efficiency may be obtained by considering only tuning inductor losses and radiation resistance. In this case, antenna circuit efficiency becomes, $R_r/(R_r + R_l)$, where R_r is the antenna radiation resistance referred to its base, and R_l is the equivalent series resistance of the tuning coil. For a short monopole of height h and radius a,

$$R_r \approx 40\pi^2 \left(\frac{h}{\lambda}\right)^2 . \qquad (3\text{-}2)$$

Antenna reactance

$$X_a \approx -j60 \ln \frac{2h}{a} \cot 2\pi \frac{h}{\lambda} . \qquad (3\text{-}3)$$

*Capitals indicate decibel ratios.

An inductive reactance of this magnitude must be supplied by the tuning coil. Assuming a coil Q of 200, the series resistance of the coil would then be

$$R_1 = X_a/Q = 0.3 \ln \frac{2h}{a} \cdot \cot 2\pi \frac{h}{\lambda} \quad . \tag{3-4}$$

Antenna fractional efficiency would then be,

$$\eta \approx \frac{40\pi^2 \left(\frac{h}{\lambda}\right)^2}{0.3 \ln \frac{2h}{a} \cot 2\pi \frac{h}{\lambda} + 40\pi^2 \left(\frac{h}{\lambda}\right)^2} \quad . \tag{3-5}$$

In Figure 3-2, antenna circuit loss ($-10 \log_{10} \eta$) is plotted as a function of operating frequency for h = 1.5 meters, a = 2 mm and Q = 200.

The same antenna will be used for both transmitting and receiving. The antenna will have uniform horizontal coverage. With an antenna height of 1.5 meters, antenna gain will be between 1.7ℓ db at low frequencies and 2.15 db at frequencies near 50 mc. Antenna gain will, however, be assumed to be independent of frequency and equal to 2 db. Antenna path gain, G_p, then becomes 4 db.

The effective system noise figure[5] F which appears in the transmission loss relationship equals $10 \log_{10} f$ where

$$f = f_a - 1 + f_c f_t f_r \quad . \tag{3-6}$$

Here:

f_a = the antenna external noise factor

f_c = the antenna circuit noise factor

f_t = the transmission line loss factor

f_r = the receiver noise factor

The antenna external noise factor f_a is dependent on time, frequency, and location. Values of f_a typical for the North Atlantic at night time will be used.

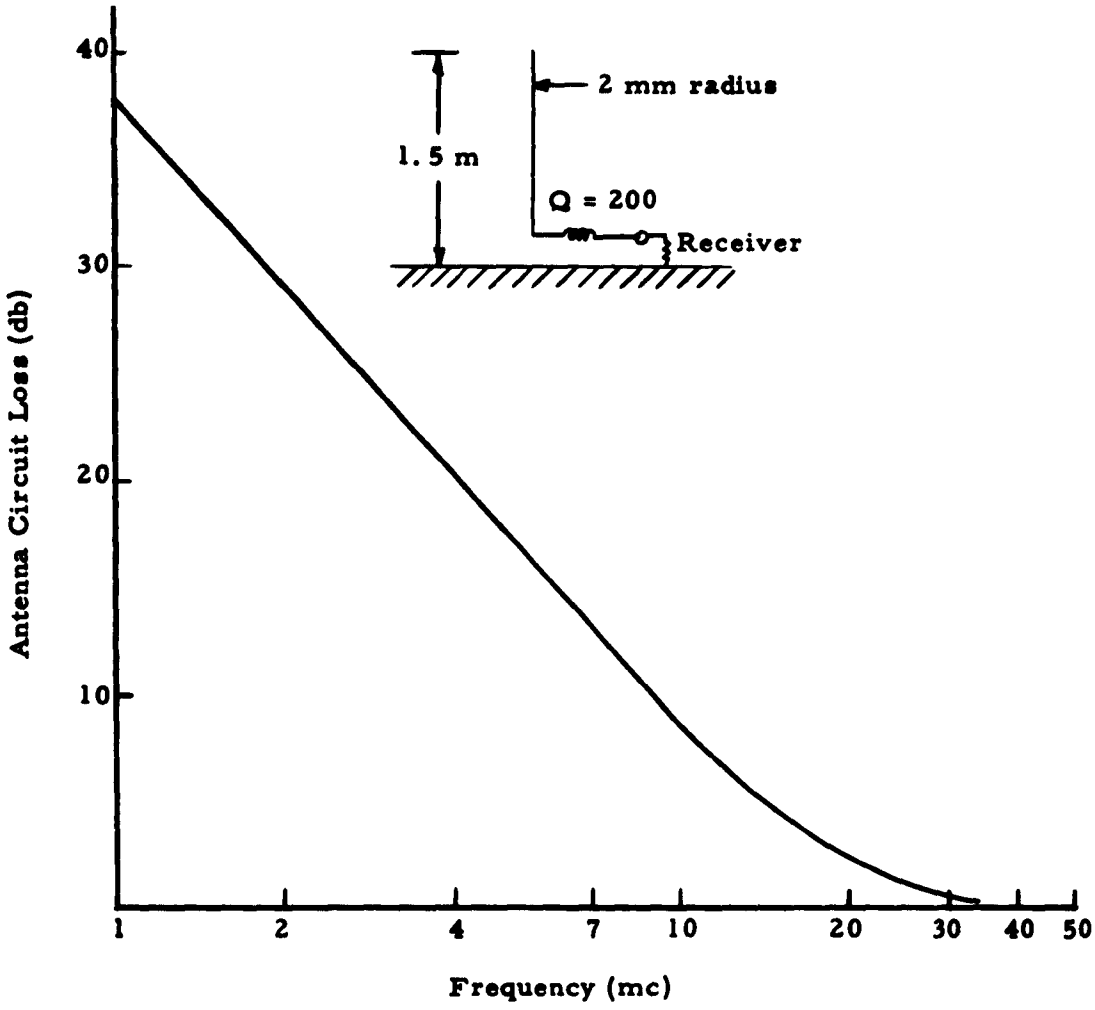

Figure 3-2. Antenna Circuit Loss versus Frequency

The antenna circuit loss factor is equal to the inverse of antenna circuit fractional efficiency. This receiving antenna circuit efficiency is approximately equal to the transmitting antenna efficiency.

f_t, the transmission line loss factor is assumed to be unity as such losses for the transponders should be negligible. The receiver noise factor f_r is taken to be 3.

A tabulation of F for frequencies in the range of 1 to 50 mc, determined in accordance with the foregoing discussion, is given below.

Frequency (mc/s)	Effective Receiver Noise Figure, F (db)
1	50
2	45
4	42
7	40
10	35
20	20
30	11
40	7
50	5

B, the receiver bandwidth term in the transmission loss equation for the assumed 1 kc bandwidth is $10 \log_{10} 1000 = 30$ db. The received signal-to-noise ratio as noted earlier is taken to be 20 db.

At a frequency of 1 mc then,

$$L_b = P_t - L_{tc} + G_p - R - F - B + 204.$$

or

$$L_b = 0 - 38 + 4 - 20 - 50 - 30 + 204 = 70 \text{ db.} \qquad (3\text{-}7)$$

Reference 4 indicates that at 1 mc the basic transmission loss for vertically polarized ground waves over sea water is 70 db for a distance of 64 nautical miles. Therefore, in this case, a transponder spacing of 64 miles would result in a received signal-to-noise ratio of 20 db.

The transponder spacings attainable at other frequencies for the hypothetical transponder chain have been determined in a similar way. These spacings are tabulated below.

Frequency (mc/s)	Transponder Spacing (nautical miles)
1	64
2	113
4	130
7	122
10	140
20	113
30	95
40	71
50	61

The foregoing discussion has assumed a received signal-to-noise ratio of 20 db. At this point it will be of interest to determine the performance of the transponder chain for the 20 db ratio. Figure 3-3 is a schematic diagram of the transponder assumed for the discussion.

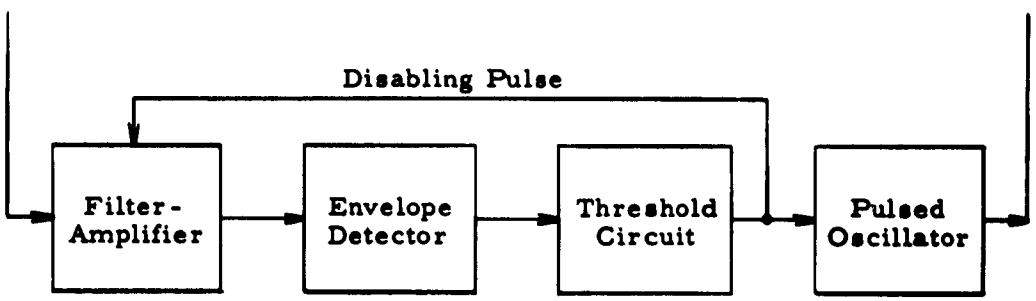

Figure 3-3. Transponder Diagram

The relayed signal and receiver transmission characteristic are as already specified. In addition, the interfering noise (internal plus external) is approximated as being white with a gaussian amplitude density function.

The probability of receiving a pulse in a specified time interval at the receiving terminal of a chain of n transponders when no pulse was sent is

$$P_f = 1 - P_{nf} \quad , \tag{3-8}$$

where P_{nf} is the probability in that time interval that no false signal arrives at the receiving terminal. But,

$$P_{nf} = (1 - p_f)^n \quad , \tag{3-9}$$

where $(1 - p_f)$ is the probability that one of the n transponders is not triggered by noise during the time interval. Therefore,

$$P_{nf} = 1 - (1 - p_f)^n \quad , \tag{3-10}$$

such that for p_f small,

$$P_f \approx np_f \quad . \tag{3-11}$$

This would be exact if there were no possibility for two or more transponders being triggered by noise simultaneously. It is assumed here that a false signal generated by any transponder propagates over the entire chain.

The probability of receiving a pulse at the receiving terminal of the chain when a pulse was sent (the "detection probability" of the chain),

$$P_d = p_d^n \quad , \tag{3-12}$$

where p_d is the detection probability of each transponder. p_d is assumed equal for all of the transponders.

Say that on the average, a false pulse at the receiving terminal per hour can be tolerated. P_f for a millisecond time interval must then be about 0.3×10^{-6}. If there are 20 transponders the probability p_f that any transponder is triggered by noise in a specified 1 ms interval must be

$$\frac{0.3 \times 10^{-6}}{20} = 0.15 \times 10^{-8} \quad .$$

This means that the threshold of each transponder must be set to exceed the rms noise level by about 12.6 db. For a signal-to-noise ratio of 20 db and such a threshold setting, the detection probability for each transponder is greater than 99.9%, and for the chain of 20, greater than 99.8%.

The channel is incapable of relaying a signal pulse whenever a false signal is propagating down the chain toward the transmitter. If the overall delay between transponders is T and the nth transponder is triggered by noise, any signals would encounter the false signal from transponder n on its way toward the transmitter. The noise triggering of a transponder would on the average cause channel blocking for a time of about nT/2 seconds. If T = 1 msec and n = 20, this blocking time would be 10 msec. If the false alarm rate for the chain is about once per hour, this blocking time may not be objectionable.

C. The "Patch"

1. General Theory and Constraints

A system of deploying an ensemble of coherent repeaters in a relatively small area of the ocean surface has been investigated. This ensemble or "patch" has some interesting properties which include the equivalent of obtaining a high powered narrow beam along the line from the illuminating source.

To keep the analysis on a level of limited complexity, it is assumed that the distribution of scatterers in a patch is statistically uniform within the limits of the patch boundary. The forward beam shape of the signal produced by the patch is derived. A description of the maneuverability and the ensemble gain or effective radiated power from the patch is derived. Beamwidths are determined from geometric and diffraction considerations. Earth curvature causing the scatterers to be nonplanar is also considered.

Several mechanisms are involved in the shaping of the coherent forward beam. For the shaping of the horizontal beam, diffraction by the lateral spread of the patch is the determining factor (essentially like the beam

shaping of a cross fire array) provided the patch is small. In this case it is found that the effective radiated power varies nearly as the square of the spread of the scatterers. For wider patches the spherical shape of the incident wave front determines the width of the horizontal beam resulting in no further increase of the effective radiated power as the spread increases. For the shaping of the vertical beam diffraction by the longitudinal spread of the patch becomes the determining factor (end fire array) as long as the patch is small. For longer patches the spherical shape of the illuminating wave front modified by the curvature of the earth determines the beamwidth. Hereby, the limitation of the effective length of the patch by the horizons with respect to the two terminals must be considered.

Another useful way to study the scattering characteristics of ocean surface scatterers is by mapping the outline of Fresnel zones. These are the zones formed by the intersections of a family of isophase ellipsoids similar to those shown in Figure 2-2 of the Phase I report, with the surface of the earth. All scatterers falling on such intersections contribute to a coherent signal build-up, provided they lie within the boundary of the horizons.

a. Horizontal Beamwidth

A plan view of the ocean surface is depicted in Figure 3-4. Halfway between the terminals T and R, i.e., in the vicinity of O, active scatterers or repeaters are deployed in a random array. They are triggered and phased by the waves originating in T so that a wave front arriving in O forms a circular arc of the radius r. In order to build a coherent signal at R, in-phase signals should originate from the arc through O whose center of curvature is at R. Consequently, the spacing s between the arcs determines the phase shift of scattered radiation paths. The largest phase shift before destructive interference will develop is $\pi/2$ corresponding to a spacing s of $\lambda/4$. The range along the y-axis over which scatterers may be deployed to contribute to the signal strength can be derived as follows.

$$(r + \frac{s}{2})^2 = r^2 + (\frac{a}{2})^2 \tag{3-13}$$

or

$$4rs + s^2 = a^2 \approx 4rs = r\lambda \ .$$

Hence

$$a = \sqrt{r\lambda} \ . \tag{3-14}$$

Therefore, the beamwidth can be narrowed down to a limit by spreading scatterers over the width of a. This limiting value is

$$\delta_d = \frac{\lambda}{a} = \frac{\lambda}{\sqrt{r\lambda}} = \sqrt{\frac{\lambda}{r}} \ . \tag{3-15}$$

Spreading scatterers over a wider stretch would result in destructive interference until one would reach another zone of constructive interference. However, no further gain can be achieved.

An example may illustrate the significance of these formulas. If the radiation orginates from an airborne repeater at a distance of 715 km from the path and the wavelength is 4 m, we obtain

$$a = 1692 \text{ m} \tag{3-16}$$

and

$$\delta_d = 0.00237 \text{ rad.} = 0.136^\circ = 8.1' \ . \tag{3-17}$$

Due to the spherical wave front, the energy would spread out within a sector of

$$\delta_g = \frac{a}{r} = \frac{\sqrt{r\lambda}}{r} = \sqrt{\frac{\lambda}{r}} = \delta_d \tag{3-18}$$

with its origin at the energy source. Therefore, geometric optics doubles the beam angle and it appears as if the image of the source were halfway between the real source and the scatterers.

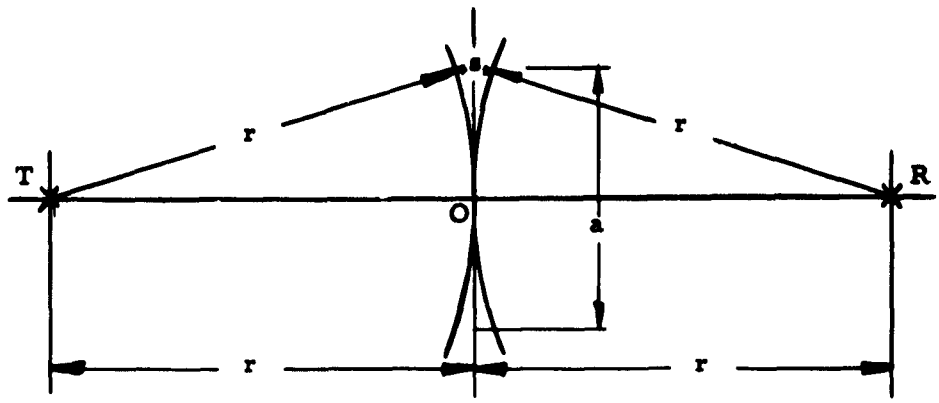

Figure 3-4. Restriction of Patch Width to Preserve Phase Addition

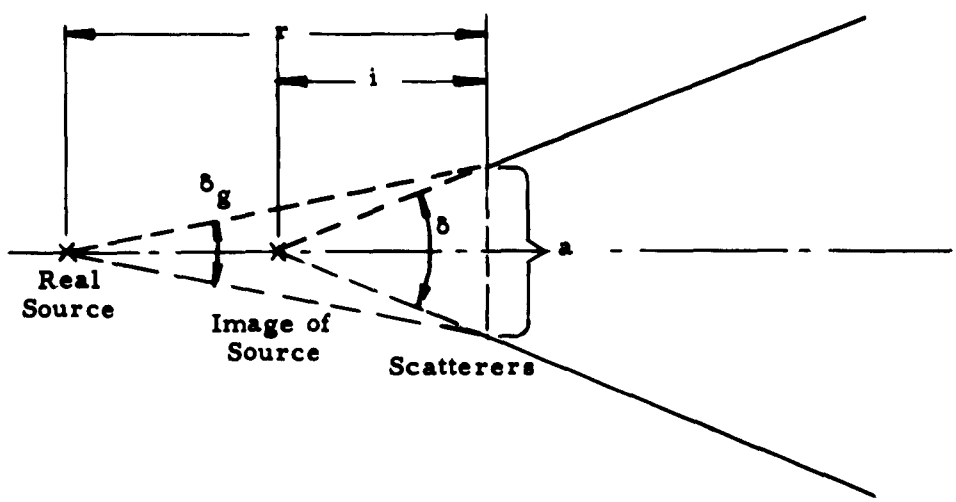

Figure 3-5. Image Position for $a = \sqrt{r\lambda}$

For narrower clusters of scatterers the diffraction beamwidth increases and dominates. This means that the image source moves toward the scatterers. For wider clusters the spherical spread dominates so that the image source moves toward the real source. Tentatively, we assume that the total beamwidth is

$$\delta = \delta_d + \delta_g = \frac{\lambda}{a} + \frac{a}{r} = \frac{\lambda r + a^2}{ar} \tag{3-19}$$

so that the image point is at i with

$$\delta_g = \frac{a}{i} \tag{3-20}$$

$$i = \frac{a}{\delta} = \frac{a}{\delta_d + \delta_s} , \tag{3-21}$$

$$i = \frac{a}{\frac{\lambda}{a} + \frac{a}{r}} = \frac{a^2 r}{\lambda r + a^2} . \tag{3-22}$$

The manner in which the image point is related to the actual source and the patch is shown in Figure 3-6.

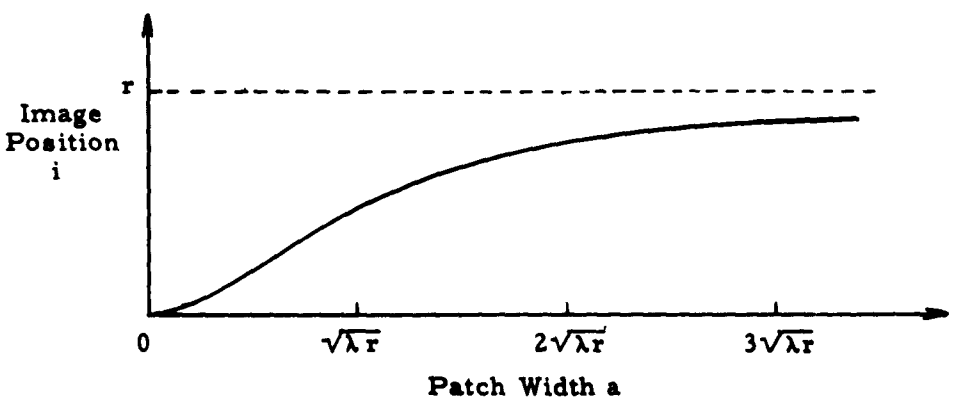

Figure 3-6. Image Position versus Patch Width

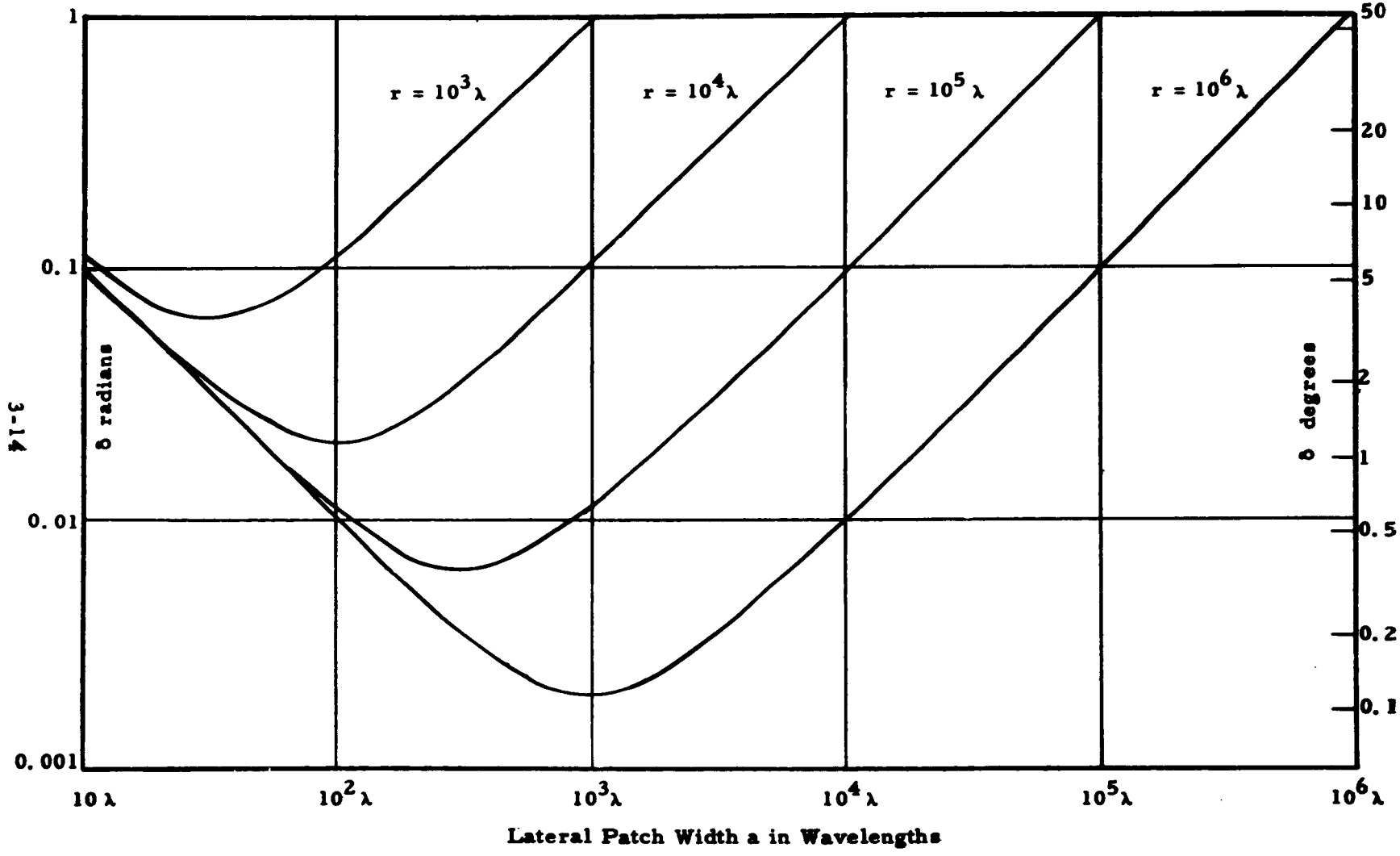

Figure 3-7. Horizontal Beamwidth versus Lateral Patch Width

A plot of total beamwidth based on $\delta = \frac{\lambda r + a^2}{ar}$ is shown in Figure 3-7.

b. Vertical Beamwidth

The vertical beamwidth is analyzed by considering the end array effect. Assume that each scatterer is in a straight line, and the array is excited along this line. The aperture is a function of the length as illustrated by Figure 3-8.

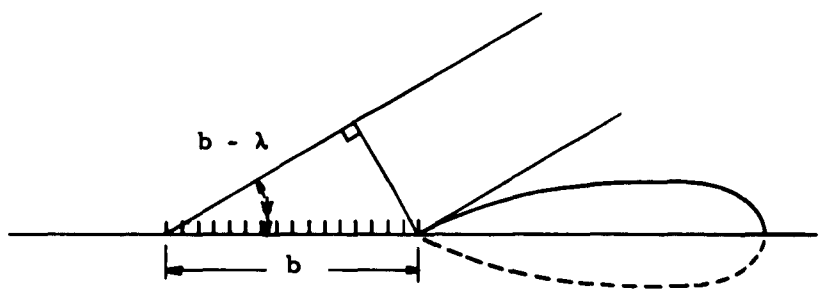

Figure 3-8. Vertical Beamwidth for Flat Earth Case

For a uniform distribution, the first null occurs at x for

$$\cos \psi = \frac{b - \lambda}{b} \; ; \tag{3-23}$$

$$\cos \psi = \sqrt{1 - \sin^2 \psi} \approx \sqrt{1 - \psi^2} = 1 - \frac{\lambda}{b} \; ,$$

$$1 - \psi^2 = \left(1 - \frac{\lambda}{b}\right)^2 = 1 - 2\frac{\lambda}{b} + \frac{\lambda^2}{b^2} \; ,$$

$$\psi^2 = 2\frac{\lambda}{b} - \frac{\lambda^2}{b^2} = \frac{\lambda}{b}\left(2 - \frac{\lambda}{b}\right) \; ,$$

$$\psi = \sqrt{\frac{\lambda}{b}}\sqrt{2 - \frac{\lambda}{b}} \approx \sqrt{\frac{2\lambda}{b}} \; . \tag{3-24}$$

In general, earth curvature limits the effective length of the patch array. This effect is analyzed with reference to Figure 3-9. Here geometric optics are assumed, and β is the geometric beamwidth for which we may write

$$\beta = \gamma + \theta \, . \tag{3-25}$$

Furthermore, we derive from Figure 3-9:

$$\theta = \gamma + \alpha \, , \tag{3-26}$$

so that with Equation (3-25)

$$\beta = 2\gamma + \alpha \, . \tag{3-27}$$

Hereby,

$$\alpha \approx \sin\alpha = \frac{h}{r_n} \, . \tag{3-28}$$

The height of a circular arc can be derived from

$$c = \sqrt{2h\rho - h^2} \approx \sqrt{2h\rho} \tag{3-29}$$

so that

$$h = \frac{c^2}{2\rho} \, . \tag{3-30}$$

Since

$$c \approx \gamma\rho \, , \tag{3-31}$$

$$h = \frac{\gamma^2\rho}{2} \, . \tag{3-32}$$

From Figure 3-9 and Equation (3-31), we derive

$$r_n \approx r_g - c = \sqrt{2H\rho} - \gamma\rho \, , \tag{3-33}$$

$$r_n = \rho\left(\sqrt{\frac{2H}{\rho}} - \gamma\right) = \rho(\zeta - \gamma) \, , \tag{3-34}$$

$$\delta = 2\zeta - \gamma \, . \tag{3-35}$$

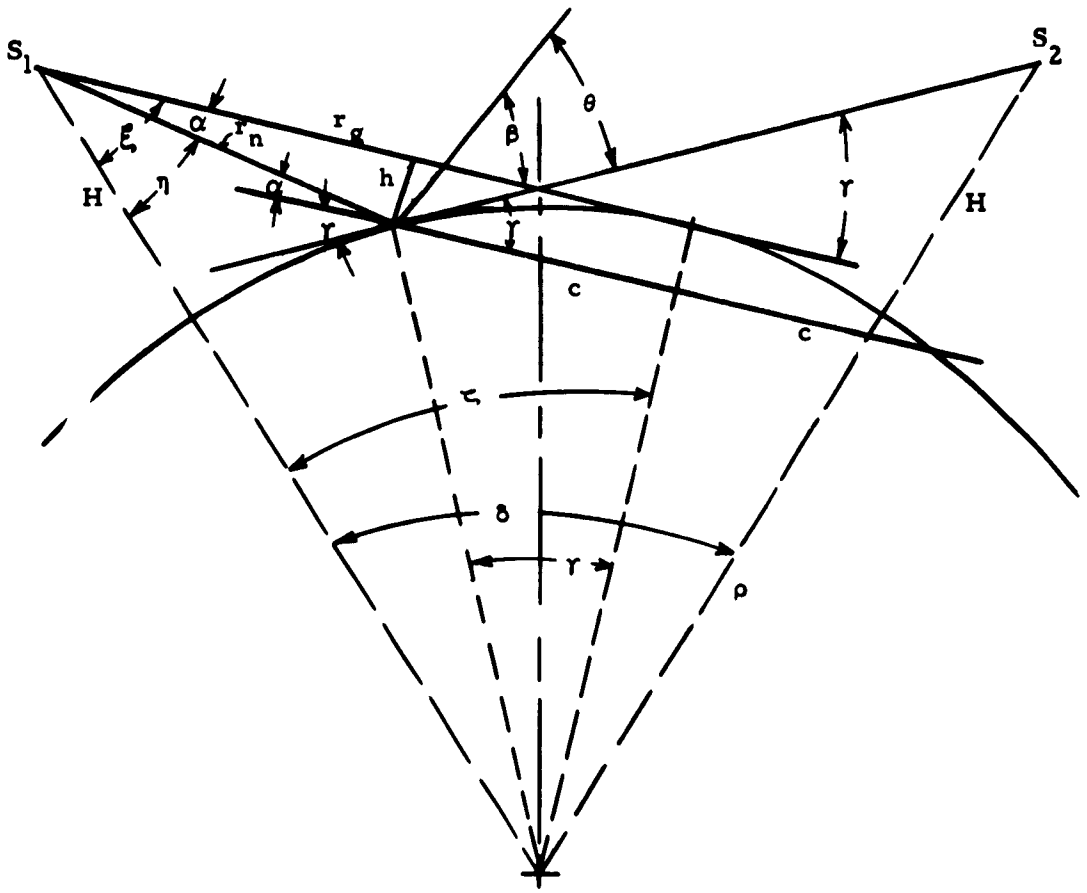

Figure 3-9. Geometry Applicable for Analyzing Vertical Beam due to Earth's Curvature

$$r_n = \rho \frac{\delta - \gamma}{2} \cdot \tag{3-36}$$

Now we express Equation (3-28) by the forms of (3-32) and (3-36) and obtain

$$\alpha = \frac{\gamma^2}{\delta - \gamma} \cdot \tag{3-37}$$

Hence, Equation (3-27) becomes

$$\beta = \beta_g = 2\gamma + \frac{\gamma^2}{\delta - \gamma} = 2\gamma + \frac{\gamma^2}{2(\zeta - \gamma)} \tag{3-38}$$

According to this, the beam is narrowest ($\beta = 0$) if $\gamma = 0$. However, for such short arrays, the diffraction law applies. In this case β would be one half of the beamwidth of the diffraction lobe which is

$$\beta = \beta_d = \frac{\Psi}{\Sigma} = \sqrt{\frac{\lambda}{2b}} , \tag{3-39}$$

with

$$b = \gamma\rho ,$$

$$\beta_d = \sqrt{\frac{\lambda}{2\gamma\rho}} \cdot \tag{3-40}$$

Again, we get the resulting beamwidth

$$\beta = \beta_g + \beta_d = 2\gamma + \frac{\gamma^2}{\delta - \gamma} + \sqrt{\frac{\lambda}{2\gamma\rho}} \tag{3-41}$$

or

$$\beta = 2\gamma + \frac{\gamma^2}{2(\zeta - \gamma)} + \sqrt{\frac{\lambda}{2\gamma\rho}} \cdot \tag{3-42}$$

The minimum value which β can assume as a function of the array length or of γ is where

$$\frac{d\beta}{d\gamma} = 0 .$$

It is found that this computation is tedious, and a suitable description of the parameters are best shown graphically in the curves of Figure 3-10.

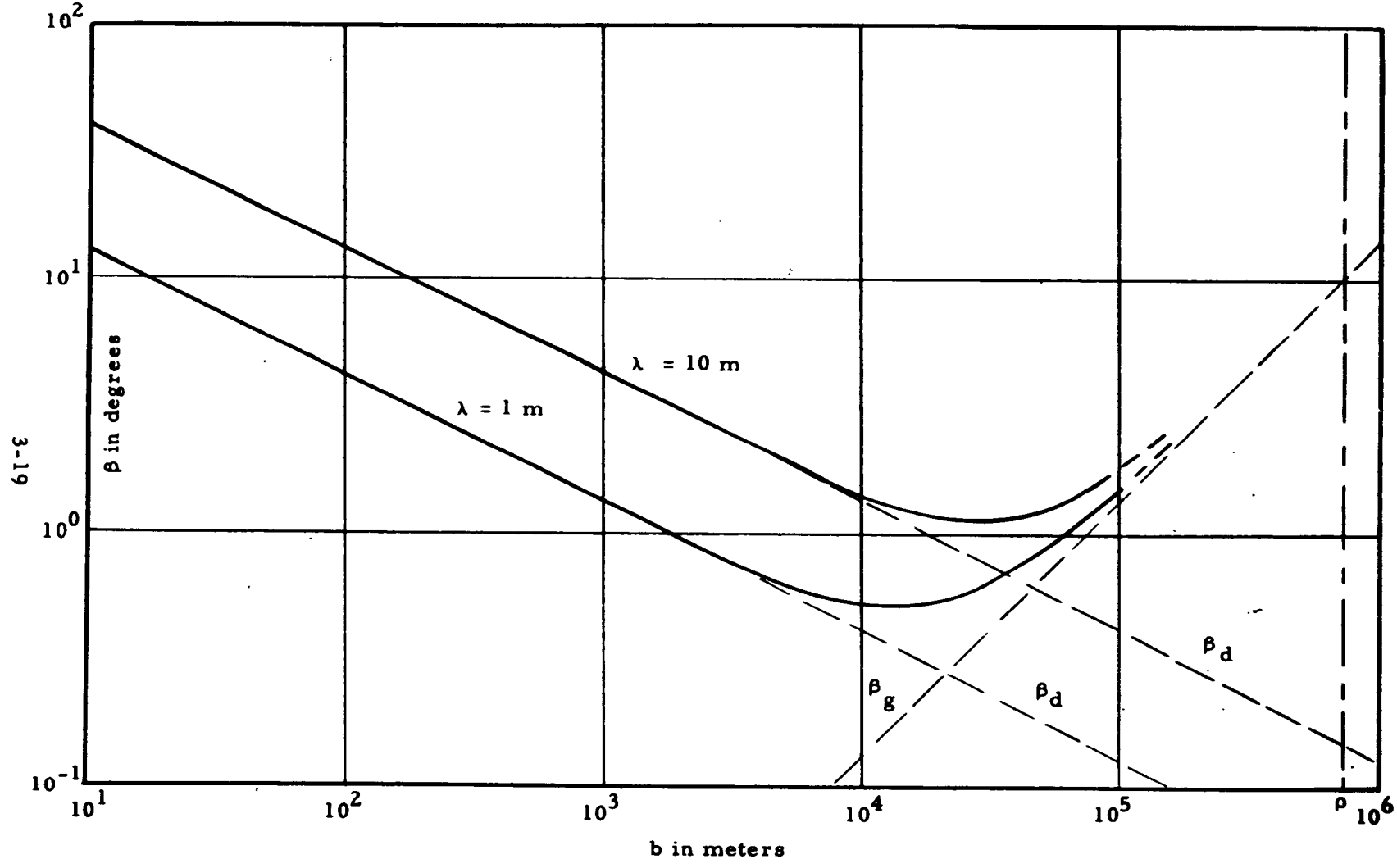

Figure 3-10. Vertical Beamwidth β as a Function of Longitudinal Path Length b

c. Factors Affecting Patch Shape and Location

Although quantitative results are obtained for the beam shape of the patch, other conditions must be considered in practice. For instance, the path length over each scatterer has not been analyzed for the three-dimensional case. For a system bouncing a signal off a patch from two airborne locations, the intersection of the earth with some Fresnel ellipsoids having foci at the airborne locations are studied. This sets a restriction on the size of the patch, particularly on the lateral width of the patch to obtain constructive addition.

Also, the longitudinal length of the patch should be limited because each scatterer in the patch must not be horizon limited from either airborne location or its effectiveness would be reduced.

Preserving the proper path length is illustrated by considering the intersection of isophase ellipsoids with the earth. The geometry is indicated by Figure 3-11.

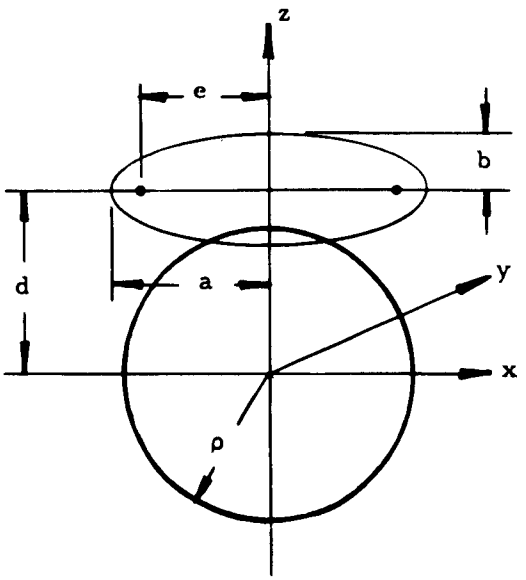

Equation of sphere at origin:

$$\rho^2 = x^2 + y^2 + z^2 . \qquad (3\text{-}43)$$

Equation of ellipse:

$$\frac{x^2}{a^2} + \frac{z^2}{b^2} = 1 . \qquad (3\text{-}44)$$

That of ellipsoid:

$$\frac{x^2}{a^2} + \frac{y^2 + z^2}{b^2} = 1 . \qquad (3\text{-}45)$$

With center at z = d:

$$\frac{x^2}{a^2} + \frac{y^2 + (z - d)^2}{b^2} = 1 . \qquad (3\text{-}46)$$

Figure 3-11. Intersection of Sphere and Ellipsoid

The intersection of the sphere and the ellipsoid forms a three-dimensional curve. For nearly tangent intersections, the z-ordinate varies so little that we may consider this curve a two-dimensional one. This means that we are only interested in its projection upon the x-y plane. To obtain this curve, we substitute z of Equation (3-46) by z as defined by (3-45) and derive the function

$$(b^2 - a^2)^2 x^4 + 2a^2(b^2\rho^2 + b^2d^2 - b^4 - a^2\rho^2 + a^2d^2 + a^2b^2) x^2$$

$$+ 4a^4d^2y^2 + a^4(\rho^4 + d^4 + b^4 - 2\rho^2d^2 - 2\rho^2b^2 - 2d^2b^2) = 0. \qquad (3\text{-}47)$$

This function can be reorganized as a perturbed ellipse; the perturbation being caused by the x^4 term. The unperturbed ellipse obeys the equation

$$2(b^2\rho^2 + b^2d^2 - b^4 - a^2\rho^2 + a^2d^2 + a^2b^2) x^2 + 4a^2d^2y^2$$

$$+ a^2(\rho^4 + d^4 + b^4 - 2\rho^2d^2 - 2\rho^2b^2 - 2d^2b^2) = 0. \qquad (3\text{-}48)$$

The semi-major and semi-minor axes of the unperturbed ellipse are, respectively

$$A = a\left[\frac{2\rho^2d^2 + 2\rho^2b^2 + 2d^2b^2 - \rho^4 - d^4 - b^4}{2(b^2\rho^2 + b^2d^2 - b^4 - a^2\rho^2 + a^2d^2 + a^2b^2)}\right]^{\frac{1}{2}} \qquad (3\text{-}49)$$

and

$$B = \frac{1}{2d}\left[2\rho^2d^2 + 2\rho^2b^2 + 2d^2b^2 - \rho^4 - d^4 - b^4\right]^{\frac{1}{2}} \qquad (3\text{-}50)$$

The perturbed ellipse has the same minor axis as the unperturbed. That means for $x = 0$

$$y_o = B_p = B \quad , \qquad (3\text{-}51)$$

while the major axis differs, and if we set $y = 0$ in Equation (3-47) we obtain a quadrature equation for x_o from which we derive

$$x_o = A_p = \frac{a}{a^2 - b^2}\left\{2bd\left[a^2d - (\rho^2 - a^2)(a^2 - b^2)\right]^{\frac{1}{2}}\right.$$

$$\left. + (\rho^2 - b^2)(a^2 - b^2) - d^2(a^2 + b^2)\right\}^{\frac{1}{2}} \qquad (3\text{-}52)$$

The following approximations are valid for our range of parameters:

$$x_o \approx \frac{1}{a}\left\{2bd\left[b^2\rho^2 + a^2(a^2 + d^2 - \rho^2)\right]^{\frac{1}{2}} - a^2(d^2 - \rho^2) - b^2(a^2 + d^2 + \rho^2)\right\}^{\frac{1}{2}} \quad (3\text{-}53)$$

$$y_o \approx \left[b^2 - (d - \rho)^2\right]^{\frac{1}{2}} \quad (3\text{-}54)$$

For the case of zero line-of-sight clearance, we set $d = \rho$ and obtain

$$x_{oo} \approx \frac{1}{a}\left\{2b\rho\left[b^2\rho^2 + a^4\right]^{\frac{1}{2}} - b^2(2\rho^2 + a^2)\right\}^{\frac{1}{2}} \quad (3\text{-}55)$$

$$y_{oo} \approx b \quad (3\text{-}56)$$

To obtain a more useful form of Equations (3-53) and (3-54), we introduce the clearance $f = d - \rho$ of the line-of-sight with respect to the earth, whereby some insignificant terms are neglected:

$$x_o \approx \frac{1}{a}\left[2b\rho\left(\rho^2b^2 + 2\rho a^2 f + a^4\right)^{\frac{1}{2}} - 2\rho^2b^2 - 2\rho f(a^2 + b^2) - a^2b^2 - a^2f^2\right]^{\frac{1}{2}} \quad (3\text{-}57)$$

$$y_o \approx \left[b^2 - f^2\right]^{\frac{1}{2}} \quad (3\text{-}58)$$

A number of surface Fresnel zones have been computed and are shown in Table 3-1. They were computed for a 1430 km path with line-of-sight grazing the earth's surface. Four wavelengths and five Fresnel zones per wavelength are shown. The geometry for this case is shown in Figures 3-11 and 3-12.

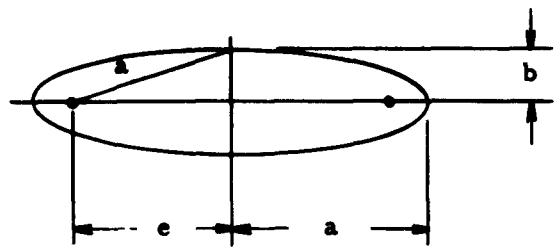

Figure 3-12. Geometry for Computing Fresnel Zones

$$2a_n - 2e = n\frac{\lambda}{2}, \qquad b_n = \sqrt{a_n^2 - e^2} = \sqrt{a_n^2 - (a_n - k_n)^2},$$

$$a_n - e = n\frac{\lambda}{4} = e + k_n, \qquad b_n = \sqrt{a_n^2 - a_n^2 + 2a_n k_n - k_n^2},$$

$$e = a_n - k_n, \qquad b_n = \sqrt{k_n(2a_n - k_n)} \approx \sqrt{2a_n k_n}.$$

The geometry is illustrated for the elevated line-of-sight case by Figure 3-13.

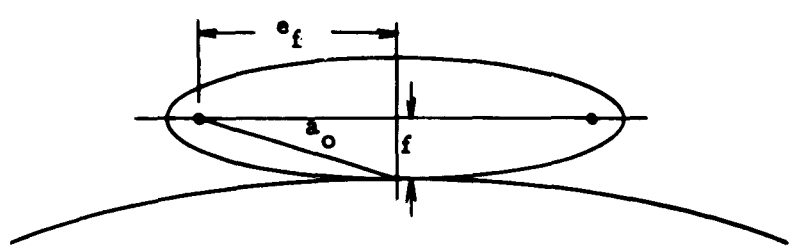

Figure 3-13. Geometry for Elevated Line-of-Sight Case

The shortest half path

$$a_o = \sqrt{e_c^2 + f^2} = e_f + k_o$$

and

$$a_n = e_f + k_o + k_n \cdot$$

where n is the Fresnel zone which is greater by the number n than that corresponding to a_o. Different relations are derived for the width and length of the surface zones for the elevated line-of-sight case.

Data in Table 3-1 are computed for: e = 715 km; d = ρ; λ_i = i (meters); i = 1, 2, 4, 8; $k_n = n\frac{\lambda}{4}$; n = 1, 2, 4, 8, 16 (Fresnel zone number).

Table 3-1. Some Surface Fresnel Zones for Zero Line-of-Sight Clearance

No.	λ_i (meters)	n	y_{on} (meters)	x_{on} (meters)
1	1	1	598	100,300
2	1	2	846	119,400
3	1	4	1196	141,400
4	1	8	1691	167,400
5	1	16	2392	198,800
6	2	1	846	119,400
7	2	2	1196	141,400
8	2	4	1691	167,400
9	2	8	2392	198,800
10	2	16	3382	233,000
11	4	1	1196	141,400
12	4	2	1691	167,400
13	4	4	2392	198,800
14	4	8	3382	233,000
15	4	16	4784	274,300
16	8	1	1691	167,400
17	8	2	2392	198,800
18	8	4	3382	233,000
19	8	8	4784	274,300
20	8	16	6765	319,200

A similar set of values are computed for a path with the same height (30 km), but the terminals brought closer so there is an overlapping region of length q where scatterers are above each terminal horizon.

Data for Table 3-2 are based on the following: e_f = 643.5 km; f = 6 km; k_o = 28 meters. The λ_i and n are as before.

Table 3-2. Some Surface Fresnel Zones for Elevated Line-of-Sight

No.	λ_i (meters)	n	y_{on} (meters)	x_{on} (meters)
1	1	1	568	19,200
2	1	2	803	27,200
3	1	4	1135	38,000
4	1	8	1805	56,000
5	1	16	2270	78,600
6	2	1	803	27,200
7	2	2	1135	38,000
8	2	4	1805	56,000
9	2	8	2270	78,600
10	2	16	3210	109,200
11	4	1	1135	38,000
12	4	2	1805	56,000
13	4	4	2270	78,600
14	4	8	3210	109,200
15	4	16	4540	149,400
16	8	1	1805	56,000
17	8	2	2270	78,600
18	8	4	3210	109,200
19	8	8	4540	149,400
20	8	16	6420	205,600

The visible area of each station forms a circular cap on the earth as shown in Figure 3-14. The slight tilt of ζ = 3.84 degrees has such a small effect on the projection of the boundary that it does not need to be taken into account. Therefore, we have the shape of a patch bounded by two circles of radius r_h, whereby the centers of the circles are $2r_h - q$ apart. The lateral width of this patch is

$$p = 2\sqrt{r_h^2 - (r_h - \tfrac{q}{2})^2} = \sqrt{4r_h q - q^2} \qquad (3\text{-}59)$$

with

$$r_n = 715 \times 10^3 \text{ m} \quad \text{and} \quad q = 0.2 \cdot r_h = 143 \times 10^3 \text{ m}$$

Thus

$$\rho = 624 \times 10^3 \text{ m} \tag{3-60}$$

For all practical cases the lateral patch width is limited by surface Fresnel zones rather than by the horizon limit ρ.

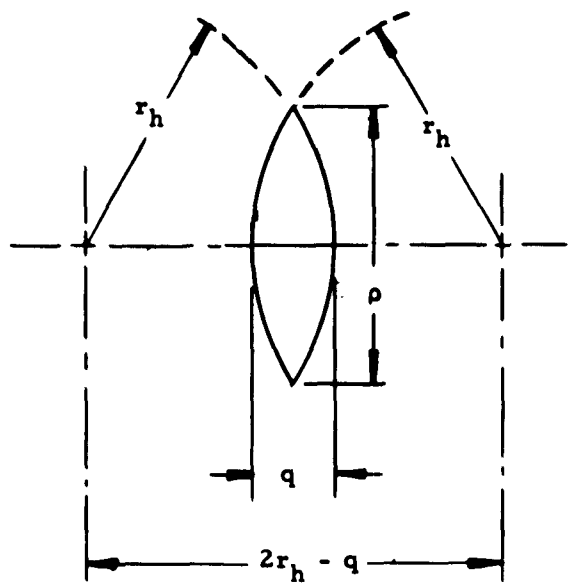

Figure 3-14. Common Visible Area

Figure 3-15 gives a pictorial representation of the areas described in this section in representative relation to each other.

d. Example of a Two-Hop System

An example of a two-hop system will be presented to illustrate factors that will appear in practice. The system is shown in Figure 3-16.

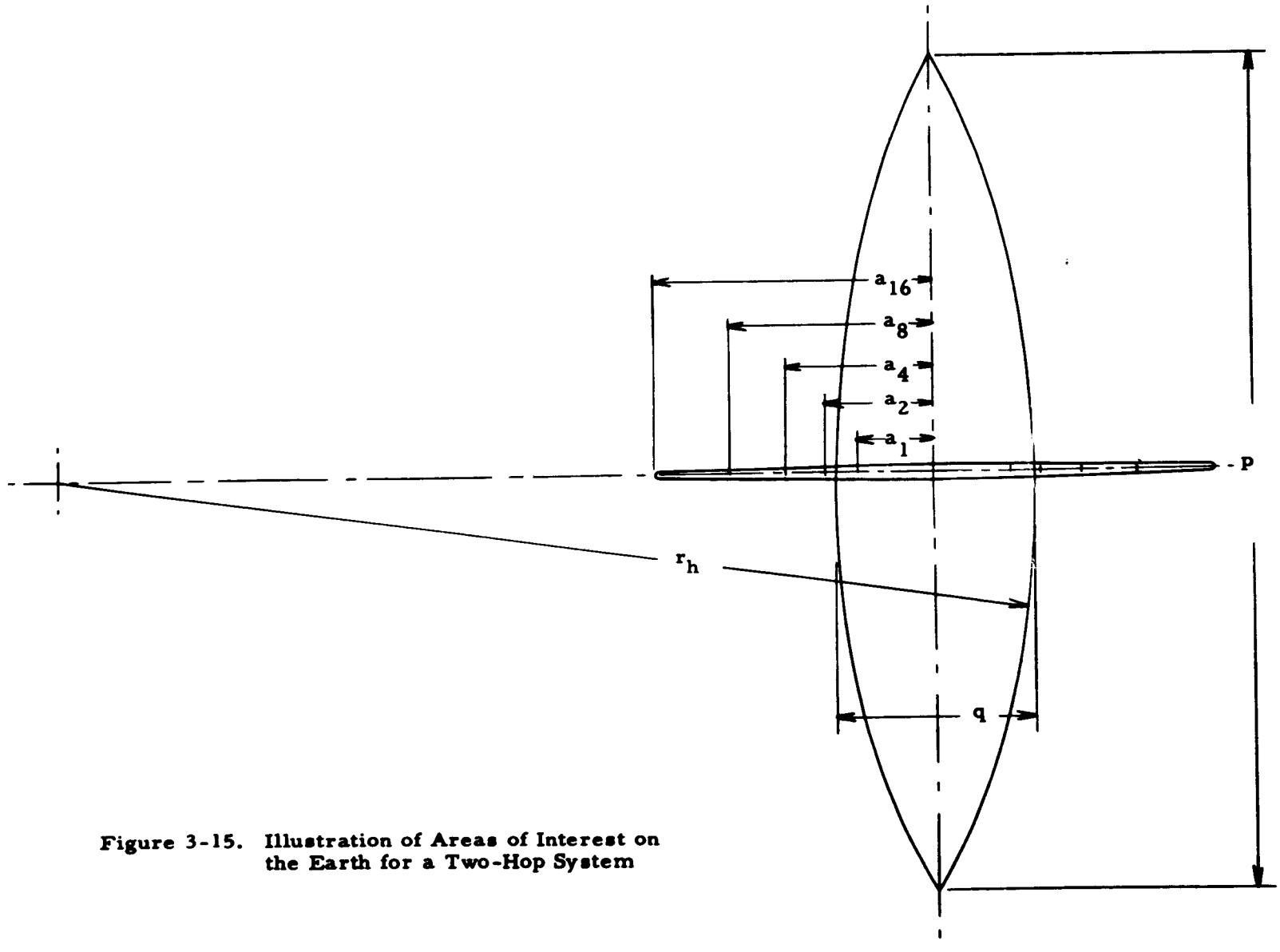

Figure 3-15. Illustration of Areas of Interest on the Earth for a Two-Hop System

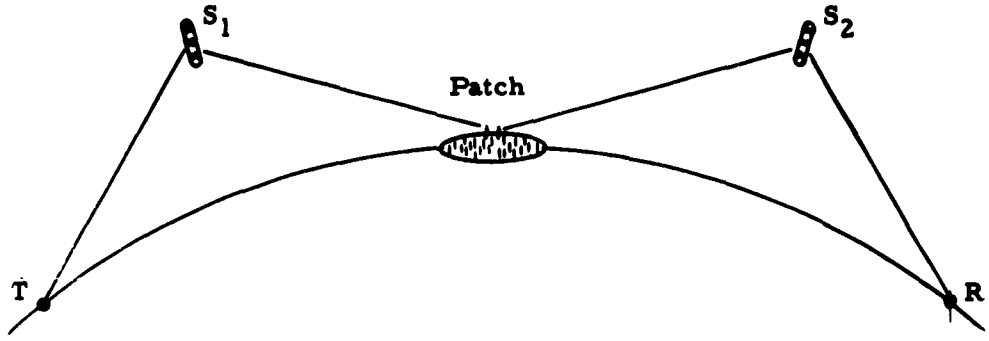

Figure 3-16. Illustration of Two-Hop System

The signal is sent from T to R by first bouncing off balloon scatterer S_1, then the amplifying patch, and finally off balloon scatterer S_2. It will be noted that in some operating conditions, balloon scatterer S_2 could be replaced by an aircraft relay to a fixed station R. Also, if suitable conditions exist, the patch could be located on a stationary surface such as land or ice, avoiding the problem of patch dispersal.

The first hop should give sufficient intensity to trigger scatterers which have nondirectional antennas ($G_r = 1$). Therefore, the average sky noise can be assumed, which is only equivalent to 290°K or room temperature at one meter. Thus, the receiver noise sets the actual noise level, which may be about 5 db higher. For a low false alarm rate the threshold should be set sufficiently high above the noise level. It is tentatively assumed that the signal-to-noise ratio is 10 db. Therefore, a total of 15 db signal strength over thermal noise is required. Thus, the equivalent temperature becomes 9160°K. Hence, the propagation efficiency

$$e = \frac{P_r}{P_t} = \frac{G_t}{4\pi r^2} \cdot \frac{\Sigma}{4\pi r^2} \cdot \frac{G_r \lambda^2}{4\pi} \qquad (3\text{-}61)$$

can be derived. The bandwidth is tentatively assumed to be $10^{-5} f_c = 3000$ cps.

Thus,

$$P_r = KTB = 1.374 \times 10^{-23} \times 9160 \times 3000 = 3.78 \times 10^{-16} \text{ w} . \quad (3\text{-}62)$$

Now we assume a balloon scatterer as described in the Phase I report, page 2-26, with

$$\Sigma = 2.49 \times 10^{4} \text{ m}^2 .$$

Further assume

$$r = 715 \times 10^{3} \text{ m} \quad \text{and} \quad G_t = 250$$

so that

$$e = 1.2 \times 10^{-20} \ (-199.2 \text{ db})$$

Hence, the transmitted power

$$P_t = \frac{P_r}{e} = 31.5 \text{ kw} . \quad (3\text{-}63)$$

The second hop should operate with the same type balloon scatterer, but the gain of the transmission system is that of the active scatterers, while the gain of the receiving antenna is 10 db.

The vertical beamwidth is less than 1 degree for array length of more than 1700 meters. Therefore, we will assume 1 degree. The horizontal beamwidth can go down as low as

$$\delta = \sqrt{\frac{\lambda}{r}} = \sqrt{\frac{1}{715 \times 10^{3}}} = 0.00118 \ (= 0.00675^\circ) \quad (3\text{-}64)$$

when the array extends over

$$a = \sqrt{r\lambda} = \sqrt{715 \times 10^{3}} = 845 \text{ m} . \quad (3\text{-}65)$$

We assume 0.01°.

The solid angle becomes

$$\Omega = 0.0174 \times 0.000174 = 0.00000305 = 3.05 \times 10^{-6} . \quad (3\text{-}66)$$

The gain

$$G_t = \frac{4\pi}{\Omega} = \frac{4\pi}{3.05 \times 10^{-6}} = 4.14 \times 10^{6} . \quad (3\text{-}67)$$

This gain cannot be used in the formula for e because it cannot be realized. One should determine the power requirement for one scatterer alone whose gain is one. Computing, using Equation (3-61) and $G_t = 1$, we have

$$e_1 = 478 \times 10^{-24} = 4.78 \times 10^{-22} . \quad (3\text{-}68)$$

The received power is assumed to be at the noise level due to peak cosmic noise, whose temperature is 1450°K. Thus,

$$P_r = 5.98 \times 10^{-17}$$

and

$$P_t = 125 \text{ kw} . \quad (3\text{-}69)$$

If the individual scatterer generates 1 watt, the required number is

$$n = \sqrt{125000} = 154 \text{ scatterers} . \quad (3\text{-}70)$$

2. Types of Transponders for a "Patch"

Several transponder circuits are considered here as to their suitability for use as active scatterers. Ideally, the active scatterer would reradiate the signal reaching it without distortion or added noise. The first two repeaters to be described are linear and would come closest to this ideal were they not oscillatory. Of the three nonlinear transponders then described, the last is the most promising. In this transponder the transmitted signal is separated in frequency from the incoming signal by one octave. An oscillatory loop is avoided, yet coherency between input and output signals is maintained.

a. Two Terminal, Linear Circuit

The simplest possible active scatterer seems to be that shown in Figure 3-17. Power is furnished to the circuit by the resistance, -R. In the equivalent circuit, R_r represents the radiation resistance of the dipole referred to its center (losses are assumed negligible), L and C are in resonance at the frequency of operation, E is the field strength of the incident wave, and h is the equivalent height of the dipole.

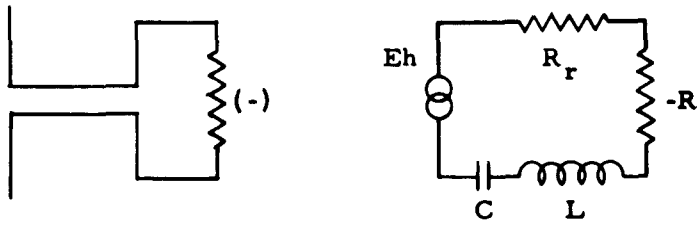

Figure 3-17. Two Terminal Active Scatterer

Now if the scatterer were merely a shorted dipole, the reradiated power would be equal to $\frac{(Eh)^2}{R_r}$. With the short removed and the resistance, -R, inserted, the reradiated power becomes $\frac{(Eh)^2}{R_r - R}$. This power is thus $\frac{R_r}{R_r - R}$ times that which would be reradiated by a shorted dipole.

The two terminal active scatterer will become oscillatory when the difference, $R_r - R$, is negative. However, in order to provide adequate gain the difference, $R_r - R$, must be very small. If a gain of 120 db is to be attained, $R_r - R$ must be equal to $10^{-6} R_r$. The radiation resistance, R_r, is however dependent somehwat on the position of the antenna relative to (for this case) the surface of the water. The radiation resistance variation would be not much less than 10 percent. In order to avoid oscillation, transponder gain must then be less than 10. This amount of gain would be inadequate in the application considered here.

The Q of a shorted dipole may be defined[6] as $\frac{\omega}{2R_r}\left(\frac{dX}{d\omega}\right)_{res.}$ $\left(\frac{dX}{d\omega}\right)_{res.}$ is the derivative with respect to frequency of antenna reactance at resonance. The Q of the antennas under consideration here when shorted[6] should be between 5 and 10. The Q of a negative resistance terminated dipole would be $\frac{R_r}{R_r - R}$ times that of a shorted dipole. Addition of the negative resistance thus causes a circuit bandwidth reduction equal to the gain increase. Were it not for the gain limitation arising from instability, this bandwidth reduction would be an important gain limiting factor.

b. Four Terminal, Linear Circuit

In Figure 3-18 is shown a repeater circuit comprising a receiving antenna, amplifier, and transmitting antenna. There is an unavoidable coupling between the antennas. This coupling would be on the order of -30 db. (This assumes that the antennas are colinear half wave dipoles with a center spacing of one wavelength.) It is desired that the amplifier gain be on the order of 120 db. Loop transmission would in this case be about 90 db. As the amplifier is selective, having several poles, it would be extremely difficult to avoid oscillation.

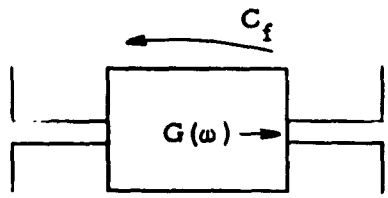

Figure 3-18. Four Terminal Repeater

c. Variable Gain Transponder

It is seen that neither the two terminal nor the four terminal linear repeaters can provide adequate gain due to their tendency to oscillate. Several nonlinear transponders can be thought of which overcome this oscillation difficulty. Being nonlinear, however, these transponders must be designed for a specific signal time structure.

Since the received waveform is not preserved, it is appropriate to call these nonlinear circuits transponders rather than repeaters.

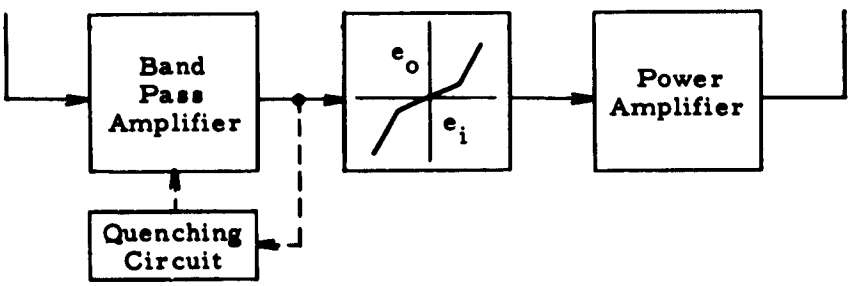

Figure 3-19. Variable Gain Transponder

The transponder shown in Figure 3-19 is very similar to the four terminal linear repeater just described. In the transponder now, however, there is inserted a nonlinear element which has a transfer characteristic as shown in the diagram. For small signals, the gain of this element is low and there is insufficient overall loop gain for the transponder circuit to oscillate. For large signals, the nonlinear element incremental gain is more than enough to provide a loop gain sufficient for oscillation. Therefore, a received signal which exceeds some threshold level is capable of initiating a sustained loop oscillation. The starting phase of this oscillation is governed by the received signal. The frequency of oscillation is established by the loop transmission of the complete circuit. (Practically, the loop transmission pass

band characteristic could be formed largely by a single crystal filter. Loop oscillation frequency would then have a stability comparable to that of a crystal oscillator.) The quenching circuit shown in the block diagram limits the duration of oscillation to a fixed value, for otherwise once started, the circuit would oscillate continuously.

The frequency of oscillation of a particular transponder in the array must be close to that of the incident signal as well as the oscillation frequencies of the other transponders. This frequency accuracy is necessary to insure that the signals transmitted from all transponders add nearly in-phase at a distant point from the scatterers in the direction of the incident wave and for the duration of the signal.

Assume that the patch of active scatterers extends a distance, $c(t_2 - t_1)$, in the direction of the incident wave (Figure 3-20). At time $t = t_2$, the phase difference between the signals arriving at X_2 over path "a" and path "b" is equal to

$$\omega_i t_1 + \omega_1 (t_2 - t_1) - \omega_i t_2 = (\omega_1 - \omega_i)(t_2 - t_1) \ . \qquad (3\text{-}71)$$

This would also be the phase difference between the signals from the scatterers, S_1 and S_2, at a large distance from the patch in the direction of the incident wave and at the time when the signal first arrives. If the signal duration is τ seconds, toward the end of the pulse the phase difference between the signals from S_1 and S_2 at this same distant point would change an additional amount, $(\omega_1 - \omega_2)\tau$. Therefore, if there is to be in-phase addition of the signals from all of the scatterers at a distant point in the direction of the incident wave throughout the entire pulse, the magnitude of the quantities, $(\omega_1 - \omega_i)(t_2 - t_1)$ and $(\omega_1 - \omega_2)\tau$ should each be less than say $\pi/8$. The more severe requirement is that $|\omega_1 - \omega_2|\tau < \pi/8$, as τ might be on the order of 100 microseconds, whereas $(t_2 - t_1)$ would be on the order of 10 microseconds. If it is assumed that the pulse duration is 100 microseconds and the nominal operating frequency is 100 mc,

for

$$|\omega_1 - \omega_2|\tau < \frac{\pi}{8} \quad ,$$

or

$$f_{nom}\left|\frac{\Delta\omega}{\omega_{nom}}\right|\tau < \frac{\pi}{8}$$

it is required that

$$\frac{\Delta\omega}{\omega_{nom}} < \frac{1}{16} \cdot \frac{1}{\tau} \cdot \frac{1}{f_{nom}} = 0.625 \times 10^{-5} \qquad (3\text{-}72)$$

The scatterers must therefore be tuned initially to have resonant frequencies within better than 10 ppm of one another, and retain this tolerance throughout their life.

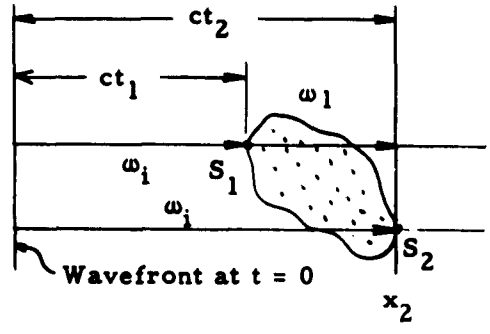

Figure 3-20. Timing Diagram

d. Phase Locked Transponder

In Figure 3-21 is shown a scheme whereby the oscillation frequency of the transponders is controlled by the incident signal. In this way the necessity for precise and stable tuning is avoided. Circuit complexity is increased, however. Also, the signal carrier must be present even though a signal is not being transmitted (Figure 3-21).

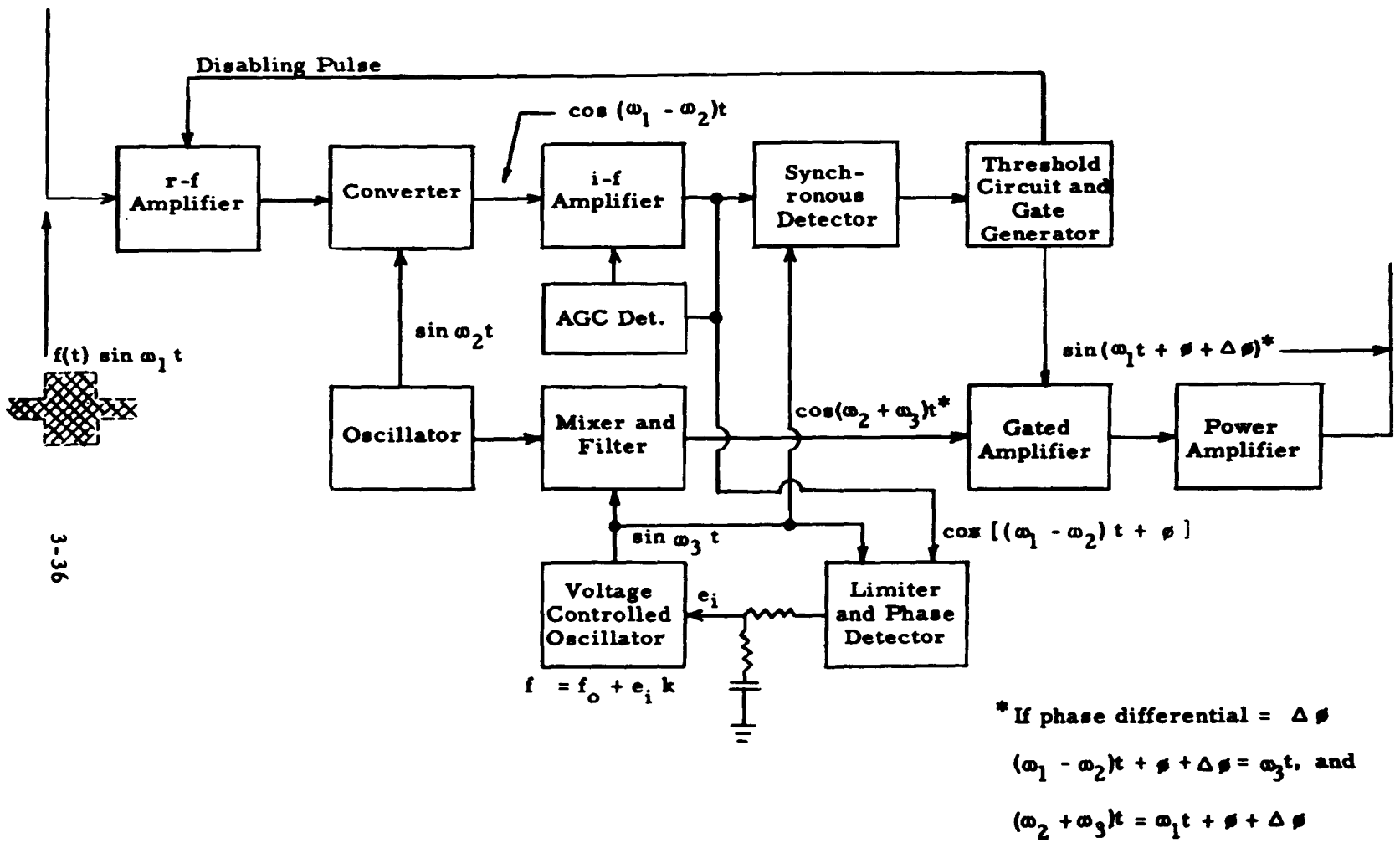

Figure 3-21. Phase Locked Transponder

The incoming signal is mixed with a locally generated sinusoid, $\sin \omega_2 t$, the first difference frequency component in the mixer output ($\omega_1 - \omega_2$) is amplified. This i-f signal is used to control a phase locked oscillator, ω_3. When locked, $\omega_3 = \omega_1 - \omega_2$, and the synthesized signal, $\omega_2 + \omega_3$, thus equals ω_1, the frequency of the received signal. The i-f signal is also detected and compared to a reference threshold. If this threshold is exceeded, a gate of fixed duration is generated. It is this gate which causes the locally generated sinusoid ($\omega_2 + \omega_3 = \omega_1$) to be amplified and transmitted.

As shown in the block diagram, the transmitted signal will have a phase shift relative to the received signal equal to the phase shift of the receiving channel at the signal frequency plus the error signal of the phase locked oscillator circuit. This total phase shift must be nearly equal for all of the transponders.

This transponder overcomes some of the main difficulties encountered with those circuits described earlier. The phase locked transponder is, however, not simple enough for the application under consideration here.

e. Frequency Doubling Transponder

This transponder is basically as shown in Figure 3-22. Here the received signal is applied to a nonlinear element. The output of this element is filtered such that only its second harmonic component is delivered to the output amplifier. Since the frequency of the signal transmitted is separated from that of the incoming signal by one octave, it is possible to provide filtering in the transponder such that loop gain for signals at either of the two frequencies is insufficient to cause oscillation.

The process performed by the transponder does not destroy coherency. The signals from each transponder will still add nearly in-phase at a distant point beyond the patch of transponders along the axis of illumination.

Figure 3-23 is a more detailed block diagram of the frequency doubling transponder. A common receiving and transmitting antenna is used. Input and output circuits are isolated by means of transmission line filters.

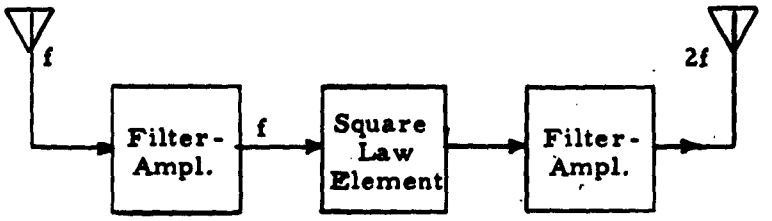

Figure 3-22. Simplified Block Diagram of Frequency Doubling Transponder

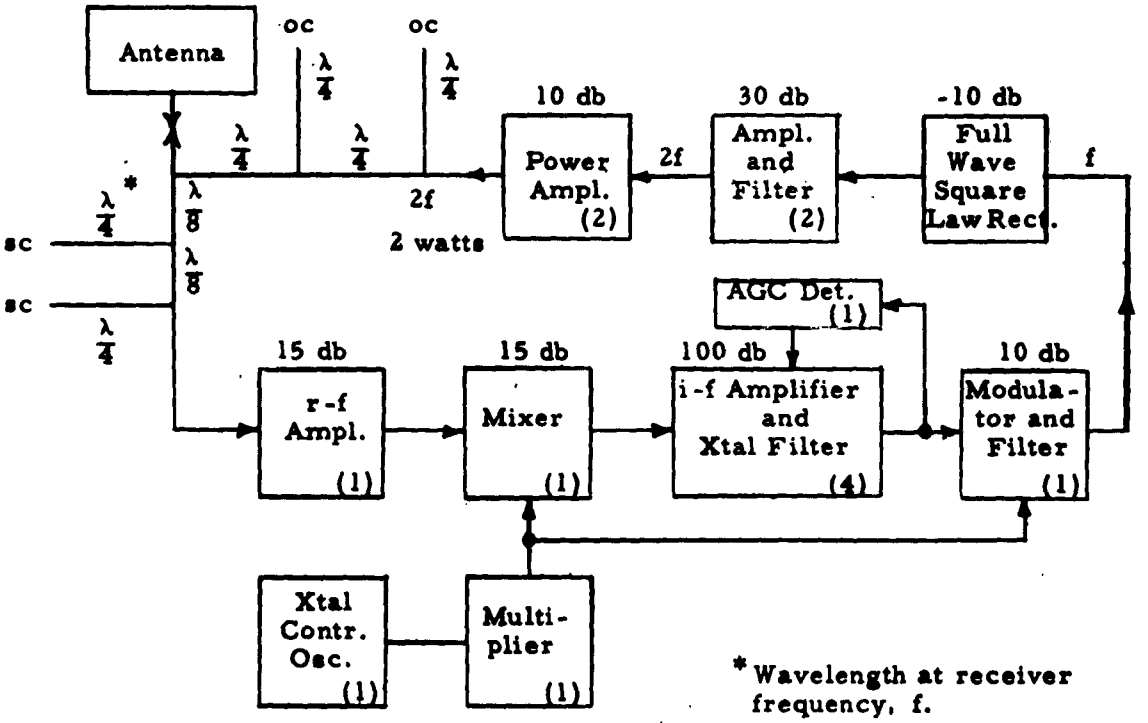

Figure 3-23. Frequency Doubling Transponder

The attenuation of the receiving filter would be about 75 db for the transmitted frequency, 2f (if constructed of coaxial cable such as RG-58), whereas attenuation at the receiving frequency, f, would be only slight. Performance of the transmitting filter would be comparable.

It would be fortunate if the received signal could be amplified without frequency conversion. Economical transistors are now available which make possible stage gains over 15 db in the 100 mc region. Frequency conversion seems necessary here, however, in order to attain a stable, narrow band frequency response. After amplification the signal is passed through a nonlinear element. In order to preserve signal-to-noise ratio as much as is possible in the frequency doubling transponder, this nonlinear element must be preceded by a filter whose pass band is just wide enough to accommodate the signal. With the filter absent, some noise components present outside the signal band would beat together in the nonlinear element and enter the signal band. If the signal has a 1 kc bandwidth and 100 mc center frequency, attainment of the required filtering seems to require frequency conversion. The transponder shown in Figure 3-23 employs frequency conversion. A stable, low percent bandwidth frequency response is obtained through the use of a crystal controlled local oscillator and a crystal i-f filter.

A transponder such as that shown would require about 14 transistors. When not transmitting, power consumption would be about 1/2 watt; during transmission about 5 watts would be required.

The output signal-to-noise ratio for this frequency doubling transponder is poorer than would be obtained using a linear amplifier-repeater. Because of the nonlinear element, for low S/N ratios, the S/N ratio at the transponder output is approximately the square of the input S/N ratio. Thus, for an input ratio of -10 db, the output S/N ratio would be about -20 db. For high input S/N ratios, however, the output ratio is almost equal to the input ratio; in this case, degradation in S/N ratio caused by the nonlinear element is only slight.

SECTION IV

ARTIFICIAL RANDOMLY ORIENTED SCATTERERS

TABLE OF SYMBOLS - SECTION IV

a	dipole radius
A_{eff}	effective pressure area of dipole
A_t	effective area of transmitting antenna
b	dipole length
B	bandwidth
c	velocity of light
d	distance from transmitter to receiver
ϵ	permittivity
E	electric field
f	noise factor
F	noise figure in db
F_r	force due radiation field
g	acceleration of gravity
G_r	gain of receiving antenna (relative to isotropic)
G_t	gain of transmitting antenna (relative to isotropic)
h	altitude of cloud center above smooth earth
I_s	radiant intensity from scatterer cloud
K	Boltzmann's constant
λ	wavelength
m	mass
μ	permeability
η	efficiency factor for aperture antenna
N	number of scatterers
p	power density or irradiance
P_n	noise power referred to receiver input
P_r	signal power available to receiver
P_t	signal power delivered to transmitting antenna
Q_l	Q of scatterer with lossy loading coil
Q_{ll}	Q of scatterer with lossless loading coil
Q_x	Q of loading coil
r	range from one terminal to cloud
ρ	modified (4/3) earth radius--taken as 8500 km
Σ	integrated bistatic cross section
SNR	signal-to-noise ratio
T_a	antenna noise temperature
T_o	reference noise temperature, 290°K
T_s	source noise temperature
$\bar{v}_m$	mean exit velocity

IV. ARTIFICIAL RANDOMLY ORIENTED SCATTERERS

A. Introduction

The use of chaff dispersed at an intermediate point above the horizon for each of two communication terminals has been discussed in the literature[7, 8]. The basic problem in this technique is to obtain the required bistatic cross-section for the required period of time that will establish a satisfactory communication channel for the chosen geography and wavelength.

Field experiments to establish artificial communication paths and to measure their characteristics have been performed for short ranges with low altitude chaff dispersal. There have also been many high altitude experiments performed for meteorological purposes which include chaff dispersal from rockets. It does not appear, however, that these high altitude experiments involved the investigation of possible artificial communication paths.

This section describes feasibility studies on the use of chaff and other individual scatterers for long range communication. Various types of scattering elements are studied, and the short conductive dipole is shown to be the most effective. A broad optimum for the communication frequency falls in the UHF band. The settling rate of scatterers at high altitude is discussed, along with some observations on lift mechanisms which appear to be very weak compared to gravity.

B. System Considerations

Parameter selection for a scatterer communication system will be described. The scatterers are assumed to be in a cluster and randomly oriented. The number of scatterers and their aggregate bistatic cross-section required for a hypothetical system will be determined with operating frequency a variable. It will be seen that a broad optimum frequency range exists in the UHF band.

1. Path Geometry

For a specified scatterer cloud height, the maximum communication path length is attained by placing the cloud at the path midpoints. Placement of the scatterers above either system terminal, however, minimizes path loss and also may be tactically more feasible. For this a prescribed scatterer placement communication path length is half that attainable with mid-path scatterer placement.

With the scatterers at the path midpoint, the radio horizon limited path length, d (Figure 4-1) is given closely as $2\sqrt{2h\rho}$, where ρ is the modified earth's radius and will be taken here as 8500 km. The surface distance d and the path distance 2r differ by a fractional amount which is approximately equal to $\frac{2h}{3\rho}$. With h = 100 km, this fractional difference is 0.0078 and is thus typically negligible.

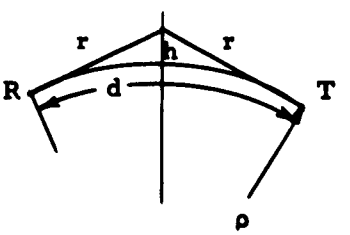

Figure 4-1. Scatter Path Geometry

A solid propellant sounding rocket such as the Arcas (Atlantic Research Corporation) will carry a payload of 20 pounds to an altitude of about 63 km. Scatterers deployed at such an altitude could create a scatter propagation path 2060 km (1275 miles) in length. This rocket has a weight less payload of 65.5 pounds. The 63 km altitude will be used in some calculations to follow as being typical of altitudes attainable with a small rocket and payload of less than 20 pounds.

2. Antennas

The system considered here will be assumed to have one terminal at a location where an antenna of large aperture may be employed and the other terminal mobile and of very limited aperture.

The fixed antenna is assumed to have an aperture of 100 square meters at frequencies less than 755 mc and a gain of 36 db (2.5° pencil beam) at frequencies greater than 755 mc. The gain limit is used at the higher frequencies in order that the required antenna pointing and fabrication accuracies are not extreme. At 755 mc, antenna gain for an aperture of 100 square meters and 50 percent efficiency is 36 db.

For the mobile terminal of the communication system, an antenna aperture of 0.5 square meters or 0.5 λ^2 (whichever is greater) is assumed. Below 300 mc a linear-type antenna could provide the 0.5 λ^2 aperture; at higher frequencies an aperture-type antenna of 0.5 square meters could be employed.

3. Noise

Noise from three sources will be considered, Galactic noise, noise due to atmospheric absorption, and receiver noise.

The output noise of the receiver is given by

$$P_n = KT_oB\left(f - 1 + \frac{T_s}{T_o}\right) ,$$

where:

P_n = noise power referred to receiver input

f = noise factor

K = Boltzmann's constant

T_o = reference noise temperature (290°K)

B = effective bandwidth

T_s = source temperature in degrees Kelvin

Here, the source is the antenna whose temperature is the same as that of the sky which it is observing. Transmission line losses and side lobe effects are considered to be negligible here.

Receiver noise figure F is assumed to be 0 db at 100 mc, 3 db at 1 gc/s, and 6 db at 10 gc/s.

A 3 kc receiver bandwidth is assumed. This would be sufficient for a single sideband commercial voice channel. For keyed telegraphy, 100 cps would be sufficient.

Figure 4-2 shows the effective sky noise temperatures expected as a function of frequency for the worst case of looking at the horizon[1]. Figure 4-3, receiver equivalent input noise temperature versus frequency, was calculated using the expression for P_n given above. The values for T_s of Figure 4-2 were used in this calculation. Receiver bandwidth and noise figure are as described earlier.

4. Ionospheric Absorption

Below 100 mc, ionospheric absorption would be significant. Other considerations, primarily galactic noise, force the choice here of frequencies greater than 100 mc where ionospheric absorption is negligible.

5. Scatter Cross-Section Required

The bistatic cross-section of the scatterer cloud and the number of scatterers within the cloud required to create a suitable propagation path for the system will be now determined. The scatterers are assumed to be midway between transmitter and receiver and at an altitude of 63 km. The horizon limited total path length d is 1275 miles. The number of scatterers required for other path lengths is easily determined since this number varies directly with the fourth power of path length for central placement of the cloud.

Received signal-to-noise is unity. Noise values are taken from Figure 3-4. Effective channel bandwidth is 3 kc. Transmitter power is assumed to be 10 kw at all frequencies.

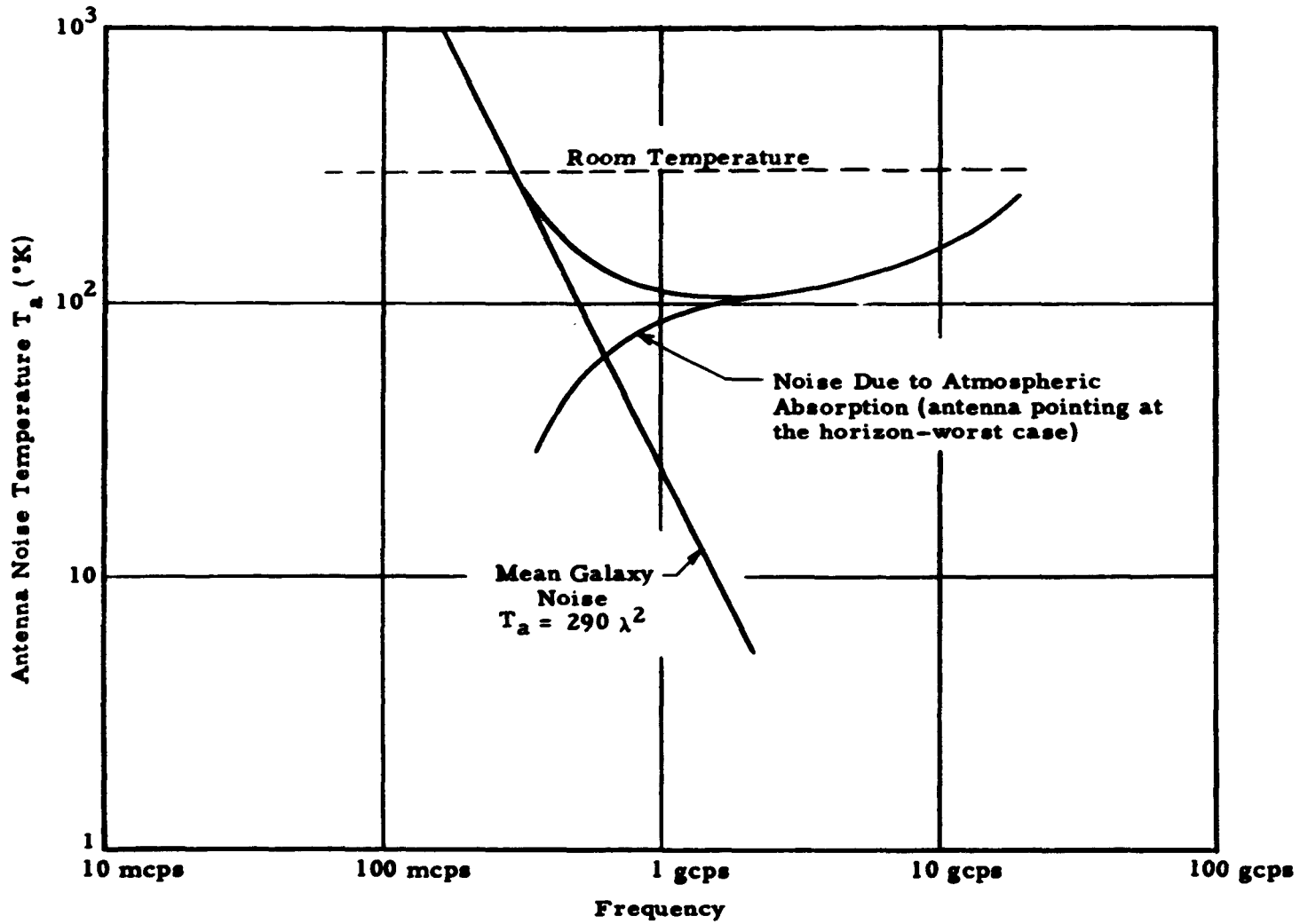

Figure 4-2. Sky Noise Temperature versus Frequency When Looking at Horizon

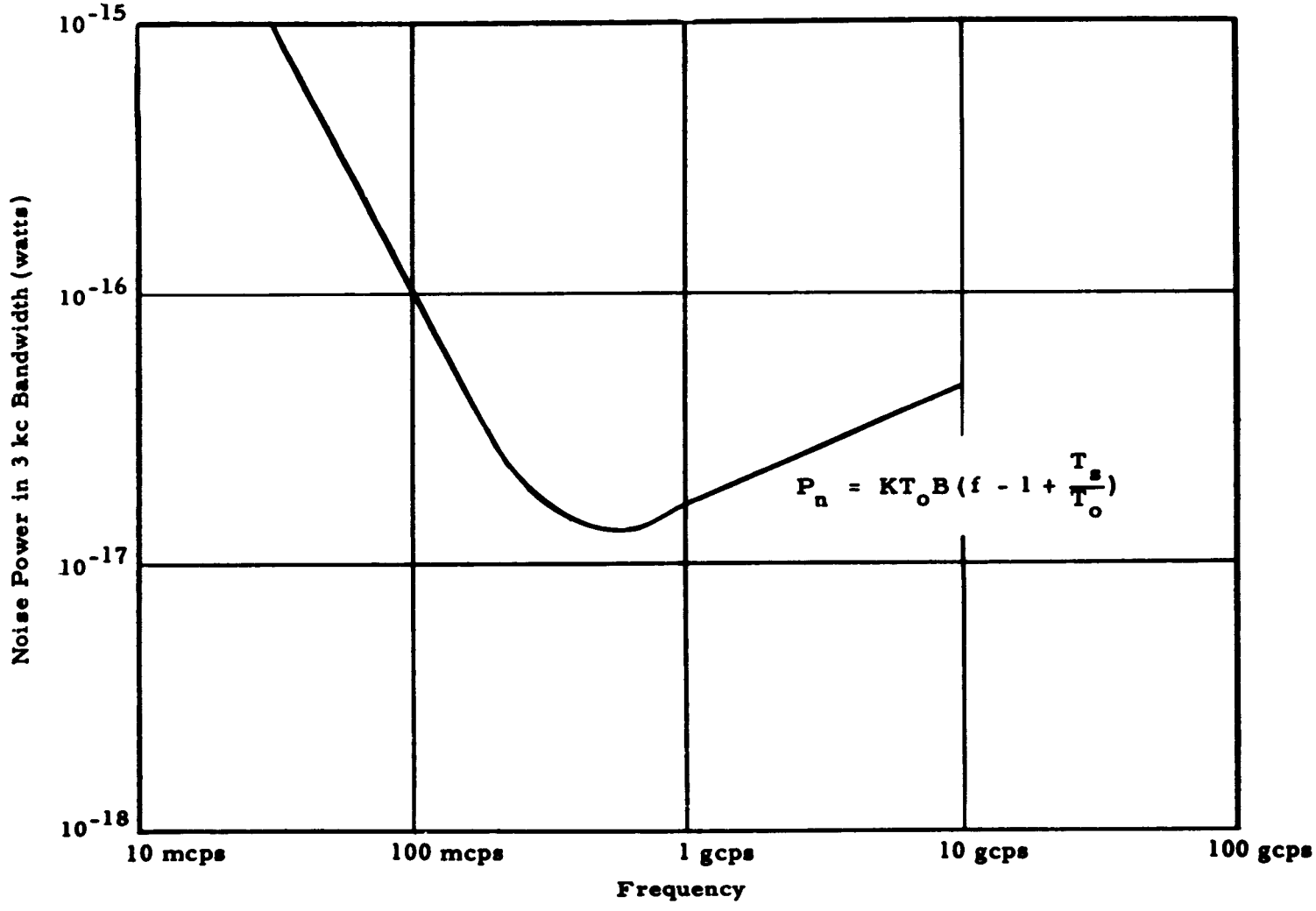

Figure 4-3. Noise Power in 3 kc Band Referred to Receiver Input

It is convenient here to divide the frequency range into three regions on the basis of antenna configuration. Below 300 mc the fixed terminal antenna aperture is 100 square meters and the mobile antenna aperture is $0.5\ \lambda^2$. Between 300 mc and 755 mc the fixed antenna aperture is still 100 square meters but the mobile antenna aperture is 0.5 square meters. Between 755 mc and 17 gc the fixed antenna has a gain of 36 db and the mobile antenna aperture is 0.5 square meters.

The following symbols will be used in the calculation of scatterer cross-section.

P_t = transmitter power

I_s = radiant intensity from scatterers

P_r = signal power intercepted by the receiver antenna

G_t = gain of transmitter antenna

G_r = gain of receiver antenna

A_t = effective area of transmitting antenna

η = efficiency factor for aperture antenna

Σ = effective bistatic scatterer cross-section of scatterers

$N = \frac{5\Sigma}{\lambda^2}$ = number of tuned dipoles required to supply Σ.

The scattering cross-section of a thin half wave dipole averaged over all orientations is taken to be $\sigma = 0.2\ \lambda^2$.[6]

Values of N are determined for optimum dispersal conditions. That is, each scatterer is assumed not be influenced by any other scatterer. The effect of one scatterer in a large ensemble is that it exhibits its full scatterer cross-section.

Calculation of Σ for frequencies less than 300 mc.

$$I_s = P_t G_t \frac{\Sigma}{(4\pi r)^2} \qquad G_t = \frac{4\pi A_t}{\lambda^2} = 2\pi$$

$$P_r = \frac{I_i A_r}{r^2}$$

$$P_r = \frac{P_t A_t A_r}{4\pi \lambda^2 r^4}$$

$$P_r = \frac{(10^4)(10^2)(0.5\lambda^2)(\Sigma)(0.5)}{4\pi \lambda^2 (1.038 \times 10^6)^4}$$

$$P_r = 1.72 \times 10^{-20}$$

$P_t = 10^4$ w

$A_t = 0.5 \lambda^2$

$A_r = \eta \times 100\ m^2 = 50\ m^2$

$\eta = 0.5$

$r = 1.038 \times 10^6$ m

For unity SNR,

$$P_r = P_n \quad \text{and} \quad \Sigma = 0.582 \times 10^{20} P_n$$

f = 100 mc	f = 200 mc	f = 300 mc
*$P_n = 1.08 \times 10^{-16}$ w	$P_n = 3 \times 10^{-17}$ w	$P_n = 1.68 \times 10^{-17}$ w
$\Sigma = 6280\ m^2$	$\Sigma = 1745\ m^2$	$\Sigma = 977\ m^2$

$$N = \frac{5\Sigma}{\lambda^2}$$

N = 3490	N = 3890	N = 4900

Calculation of Σ for frequencies between 300 mc and 755 mc.

$$P_r = \frac{P_t A_t A_r}{4\pi \lambda^2 r^4} \Sigma$$

$A_t = 0.5\ m^2$ $\quad A_r = 50\ m^2$

P_t, A_t, A_r, n and r as above.

$$P_r = \frac{(10^4)(10^2)(0.5)(2)(0.5)}{4\pi \lambda^2 (1.038 \times 10^6)^4} = 1.72 \times 10^{-20} \frac{\Sigma}{\lambda^2}$$

For unity SNR,

$$\Sigma = 0.582 \times 10^{20} \lambda^2 P_n$$

*From the receiver noise curve, Figure 4-3.

$f = 300$ mc	$f = 400$ mc
$P_n = 1.68 \times 10^{-17}$ w	$P_n = 1.4 \times 10^{-17}$ w
$\Sigma = 977$ m^2	$\Sigma = 458$ m^2
$N = 4900$	$N = 4070$

$f = 600$ mc	$f = 755$ mc
$P_n = 1.35 \times 10^{-17}$ w	$P_n = 1.4 \times 10^{-17}$ w
$\Sigma = 197$ m^2	$\Sigma = 129$ m^2
$N = 3940$	$N = 4210$

Calculation of Σ for frequencies between 755 mc and 17 gc.

$$P_r = P_t A_t \frac{G_r}{16 \pi^2 r^4} \Sigma \qquad G_r = 4 \times 10^3$$

P_t, A_r, n and r as above.

$$P_r = \frac{(10^4)(4 \times 10^3)(\Sigma)(0.5)}{16 \pi^2 (1.038 \times 10^6)^4} = 1.093 \times 10^{-19} \Sigma$$

For unity SNR,

$$\Sigma = 0.927 \times 10^{19} P_n$$

$f = 775$ mc	$f = 1$ gc
$P_n = 1.4 \times 10^{-17}$ w	$P_n = 1.65 \times 10^{-17}$ w
$\Sigma = 129$ m^2	$\Sigma = 151$ m^2
$N = 4210$	$N = 8400$

$f = 2$ gc	$f = 4$ gc	$f = 10$ gc
$P_n = 2.23 \times 10^{-17}$ w	$P_n = 2.95 \times 10^{-17}$ w	$P_n = 4.3 \times 10^{-17}$ w
$\Sigma = 204$ m^2	$\Sigma = 270$ m^2	$\Sigma = 393$ m^2
$N = 45300$	$N = 2.41 \times 10^5$	$N = 2.19 \times 10^6$

It is of interest to determine the number of scatterers required when placed above either terminal rather than midway between them. However, attainment of the 1275 mile path length now requires a scatterer cloud height four times that required with midpath scatterer placement or 252 km. Since the variation of scatter cross-section with frequency will be the same regardless of path geometry (assuming identical antenna considerations), the total cross-section Σ will be determined at only one frequency, 1 gc.

$$I_i = P_t G_t \frac{\Sigma}{(4\pi h)^2}$$

$$P_r = P_t A_t \frac{G_r \Sigma}{(4\pi rh)^2} = \frac{(10^4)(4 \times 10^3)(\Sigma)(0.5)}{(4\pi \times 2.076 \times 252 \times 10^4)^2} = 4.65 \times 10^{-19}\ \Sigma$$

For $P_r = P_n$,

$$\Sigma = \frac{1.65 \times 10^{-17}}{4.65 \times 10^{-19}} = 33.5 \text{ m}^2 \quad .$$

Whereas for midpath scatterer placement, the required cross-section was 151 m^2. For midpath placement, Σ varies as the fourth power of path length d. For scatterer placement over one terminal, Σ varies as d^2h^2. Since the required height $h = d^2/2\rho$, the required cross-section Σ varies as the sixth power of path length. For a path length of 2550 miles rather than 1275 miles, Σ for midpath placement would be $2^4 \times 151 = 2420$ m^2; for terminal placement, $\Sigma = 2^6 \times 33.5 = 2120$ m^2. One notes that when the path length approaches this value, the advantage of scatterer placement over one terminal is not great.

6. Summary

Figure 4-4 shows the total effective scatter cross-section required as a function of frequency for the hypothetical communication system. The shape of this curve is, in general, that of the received noise power (Figure 4-3) as modified by antenna restrictions. The optimum frequency range is from 600 mc to 3 gc. Below 600 mc galactic noise increases rapidly and above 3 gc atmospheric absorption noise is quite high and becomes dependent on weather conditions. Another factor which discourages the use of higher frequencies is the large number of tuned dipoles required to achieve the required scatter cross-section.

On the basis of the example system considered here, it seems likely that small (50-pound weight) rockets capable of deploying a few pounds of scatterers at altitudes of 50 to 200 km could create usable forward scatter propagation paths.

C. Resonant Scatterers

An important criterion of scatterer suitability here is the ratio of scatter cross-section to mass. As shown in the Phase I report, this ratio is unfavorable for nonresonant scatterers whose dimensions are less than approximately one wavelength. For resonant scatterers, the ratio is much more favorable. Of interest then are these resonant scatterers. Two types will be considered here, radiating tuned circuits (or loaded dipoles) and piezoelectric crystals.

1. Reradiating Tuned Circuits

The power scattered by a small resonant electric dipole is proportional to the square of dipole current and length. Also, for a loss-free resonant dipole, the scattered power is independent of physical size. In this loss-free case, a reduction in dipole length is just compensated for by a proportionate increase in current. As dipole size is reduced, however, increased

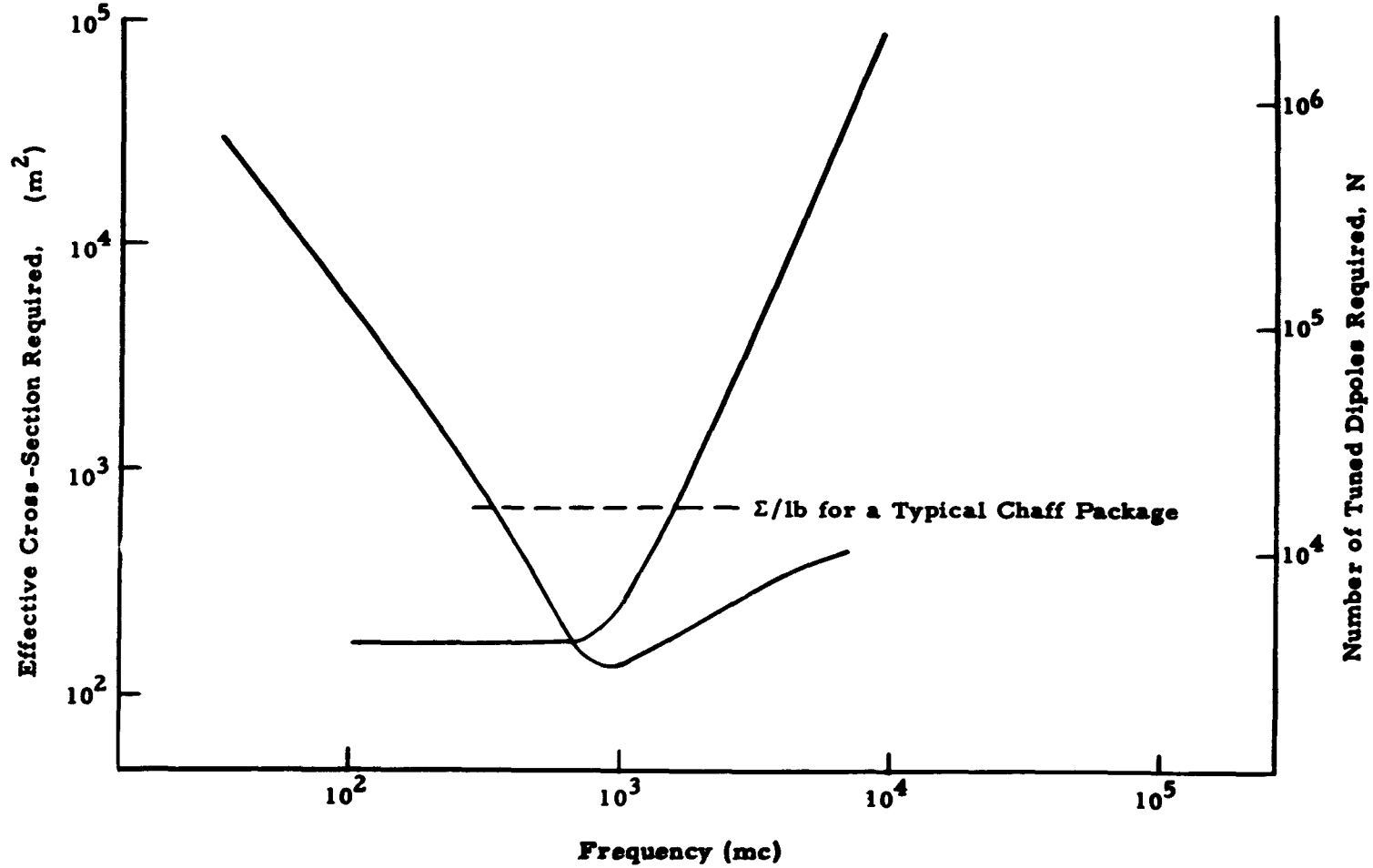

Figure 4-4. Scatter Cross-Section Σ, and Number of Half-Wave Dipoles N, Required to Obtain Unity SNR for a Path Length of 1275 Miles

tuning reactance is required to maintain resonance. The resonator is unavoidably lossy, and in practice it is this loss which seriously limits the degree of scatter size reduction which may be attained without a significant decrease in scatter cross-section.

Suppose that the scatterer is an electrically short cylindrical dipole resonated by means of a center loading inductor. If the loading inductor losses as well as the ohmic dipole losses were zero, the Q of the lossless scatterer would be,

$$Q_{11} = 12 \left[3 \ln (2\, b/a) - 7 \right] \left(\frac{2\pi b}{\lambda}\right)^{-3} , \qquad (9)$$

where b is the dipole length, and a its radius. For b/a = 100 and b = $\lambda/20$ (that is, a fairly thin dipole one-tenth the length of a half-wave dipole), Q = 3440.

If, however, the loading coil is lossy, having a Q of Q_x, the Q of the lossy scatterer is $Q_1 \approx (Q_{11} + Q_x)$. The lossy circuit has a scatter cross-section which is in a ratio, $(Q_1/Q_{11})^2$, to the scatter cross-section of the lossless dipole. If the lossy dipole is to have a cross-section not less than one-half that of a lossless dipole, $Q_x > Q_{11}/(\sqrt{2} - 1) = 2.42\, Q_{11}$. For the above example, a resonator Q of 2.42 x 3440 = 8300 is required. One may thus conclude that to shrink a half-wave dipole by a factor of 10, a resonator Q on the order of 8000 is required if scattering cross-section is not to be reduced significantly. At, say, 300 mc a coil of this Q would be extremely difficult, if not impossible, to construct. Also, the conductive surface of the inductor would exceed that of the original half-wave dipole whose cross-section to mass ratio was to be increased. Since the minimum scatterer weight possible would be proportional to this surface area, even though some dimension shrinkage is possible, weight reduction is not.

Similar problems are encountered if a magnetic dipole (loop) dimension reduction is sought.

A helical scatterer was considered. The helix may be thought of a continuously loaded electric and magnetic dipole. Suppose one starts twisting a hollow conductor, initially resonant and about one-half wavelength long, into a helix, attempting to reduce length yet maintain resonance as well as scatter cross-section. To obtain the required Q, the conductor surface area, and hence tube diameter, must be increased as more turns are made. Again it is found that as length is reduced, required conductor surface area, and hence weight, is increased. Also, it develops that before a length reduction on the order of 10 is attained, adjacent turns become close and the helix acts more as a nonresonant cylinder.

L. J. Chu[10] shows that the minimum Q, gain, and physical size of an electrically small antenna are interrelated. His treatment is very general; the exact antenna form need not be specified. If the antenna can be placed within a sphere of given radius, a statement may be made concerning its Q and gain (or for our purposes scatter cross-section). The minimum Q which the antenna must have for a specific cross-section to be realized is a function of the sphere radius. As the sphere radius becomes less than say, $\lambda/40$, for a scatter cross-section comparable to that of a short lossless dipole, the minimum Q increases very rapidly. This was demonstrated earlier for the specific antenna configuration of a center-loaded dipole.

2. Piezoelectric Scatterers

The use of low-loss piezoelectric resonators as scatterers was considered. For quartz the length of the crystal if it is to be resonant in the extensional mode would be about $10^{-5}\lambda$ where λ is the electrical wavelength. The Q restrictions stated above are still applicable although the antenna here is unusual. For the quartz crystal scatterer to have a scatter cross-section comparable to that of a short lossless dipole, its Q must be on the order of 10^{15}. The crystal, isolated, and in vacuum might have a Q considerably better than the usual mounted crystal. However, even if the required Q is attained other serious difficulties arise. At 100 mc such a Q represents a

bandwidth of 10^{-7} cps and an impulse response time measured in months. If the crystal were damped to have a 1 cps bandwidth, its scatter cross-section would decrease by a factor 10^{14} and it would be an extremely poor scatterer. Even with a 1 cps bandwidth, motion of the scatterers would create doppler shifts greater than 1 cps.

3. Conclusions

The half-wave dipole is easily produced, packed and dispersed in comparison to any of the three loaded dipoles mentioned above. Furthermore, although the maximum dimension of a loaded dipole may be made smaller than one-half wavelength, weight reduction does not appear possible.

D. The Settling Rate of Tuned Scatterers at High Altitudes

In Phase I of this program, two "lift" mechanisms for tuned scatterers were investigated. These were balloons and the radiometer effect.

Balloons are generally limited to altitudes of 30 km and below. At their upper operational limits, balloons must be quite large to be self-supporting. As a consequence, it is more reasonable to use a single balloon bearing a complex system, such as a diffraction grating, than to use a large number of slightly smaller balloons just barely able to lift their own weight.

The force due to the radiometer effect measured in the experimental study conducted in Phase I was disappointingly small. By careful design the radiometer effect may be made a factor in settling rate retardation, but it is highly unlikely that radiometer effect alone can support practical scatterers. The radiometer force is basically a molecular effect and, as such, would ultimately be altitude limited as are balloons but at a much higher altitude.

Radiation pressure and reaction due to subliming are examined briefly as sources of lift at extreme altitudes where buoyancy and perhaps radiometer effect are useless. These prove to be of little use pitted against gravity.

This section is concluded with some data on settling rates for ordinary chaff at extreme altitudes. There is apparently considerable atmospheric drag even at 70 km altitude. A method of combining radiometer effect with the drag experienced by chaff is mentioned.

1. Radiation Pressure on Half-Wave Dipoles

To determine whether the large effective scatter cross-section of a tuned dipole would help make suspension by radiation pressure feasible, the field strength required to sustain a chaff dipole against the force of gravity will be calculated.

The radiation pressure of a plane wave is given by, $P_r = \epsilon E^2$, where ϵ is the permittivity of the medium and E is the field strength.

To determine the radiation force exerted on a half-wave dipole, effective electromagnetic cross-section is used and is taken here as $0.5\,\lambda^2$. (The dipole is assumed to be parallel to the E vector.) Therefore, this radiation force,

$$F_r = A_{eff} P_r = 0.5\,\lambda^2\,\epsilon E^2 ,$$

If the magnitude of the radiation force is to equal that of gravitation, $0.5\,\lambda^2\,\epsilon E^2 = mg$, where m is the mass of the dipole and g is the acceleration of gravity. The required power density of irradiance,

$$p = E^2\sqrt{\frac{\epsilon}{\mu}} = \frac{mg}{0.5\,\lambda^2\,\epsilon}\sqrt{\frac{\epsilon}{\mu}} = \frac{2\,mgc}{\lambda^2} .$$

The dipole mass might be on the order of 10^{-5} kg. For a wavelength of 0.3 meters,

$$p = \frac{2 \times 10^{-5} \times 9.8 \times 3 \times 10^8}{(0.3)^2} = 6.5 \times 10^5 \text{ w/m}^2 .$$

The irradiance required to support a dipole even when optimumly oriented is thus many orders of magnitude greater than would be feasible to supply.

2. Reaction Due to Subliming

Suppose subliming takes place at the surface of the scatterer oriented toward the earth. At high altitudes many materials would sublime rapidly. There would be a reaction on the scatterer due to this escape of molecules. In a way, the scatterer would be a reaction motor.

The reaction force upwards is equal to the mass flow rate times the mean velocity component of the escaping molecules downwards. If the net vertical force on the scatterer is to be zero,

$$mg = -\frac{dm}{dt}\,\bar{v}_m \quad ,$$

where:

m = mass of the scatterer

g = acceleration of gravity

$\bar{v}_m$ = mean departure velocity component downward.

Therefore, $m/m_o = \exp(-gt/\bar{v}_m)$, where m_o is the initial mass of the scatterer. If it were possible to construct a scatterer which sublimed in this way and if initially 95 percent of the scatterer was material which sublimed, after a time, $t = (\bar{v}_m/g)\ln 20$, the "fuel" would be consumed.

An idea of the velocity, $\bar{v}_m$ may be obtained if temperature is known from the relationship, $KT = m\,\bar{v}^2$ Here, K is Boltzmann's constant, T is the temperature, m is the molecular mass, and $\bar{v}$ is the mean molecular velocity. For hydrogen at 300°K, $\bar{v}$ is about 10^3 m/sec; other molecules would be slower. The time constant, $\bar{v}_m/g$ would thus most certainly be less than $(10^3\ \text{m/sec})/(9.8\ \text{m/sec}^2)$ or about 100 seconds. Scatterer sustaining time as given above by $(\bar{v}_m/g)\ln 20$ would therefore be 300 seconds.

Reaction due to subliming does not appear to be a suitable mechanism for sustaining scatterers at altitude. At the most, sustaining times on the order of minutes might be realized.

3. Natural Settling of Chaff

For several years the U. S. Army Signal Missile Support Agency, White Sands Missile Range, New Mexico, has been collecting information on winds at extreme altitudes using rocket-borne chaff tracked by radar[11]. The curves of Figure 4-5 were plotted from eight representative rocket tests performed in the summer of 1960 which indicate typical settling rates for foil chaff.

One notes that settling rates vary little with altitude from 70 to 30 km. Chaff released at 70 km would take roughly 45 minutes to reach 30 km. This is a significant time period when compared with the one to six hours of useful life of a balloon-borne system at 30 km altitude (estimated from the data of the Phase I report).

The launching sites used were in Florida, New Mexico, and Nevada, and the frequencies employed were roughly 3, 6, and 10 gc/s. No significant trend in settling rates due to geography or frequency was obvious. The curves are identified by the page number of the reference from which the data were taken. Also indicated are the firing locations, (CC) Cape Canaveral, (WS) White Sands, and (Nev.) Nevada. Radar wavelength is indicated by the band designations X, C, and S. One parachute descent is shown which indicates that its settling rate changes significantly in the 60 to 30 km region.

Figure 4-6 shows a similar type of plot for three firings of nylon (Suchy) chaff. In each case the chaff was 0.012 inch diameter and cut for S band. These curves are replotted from Figure 16 of the SMSA Special Report 41[12].

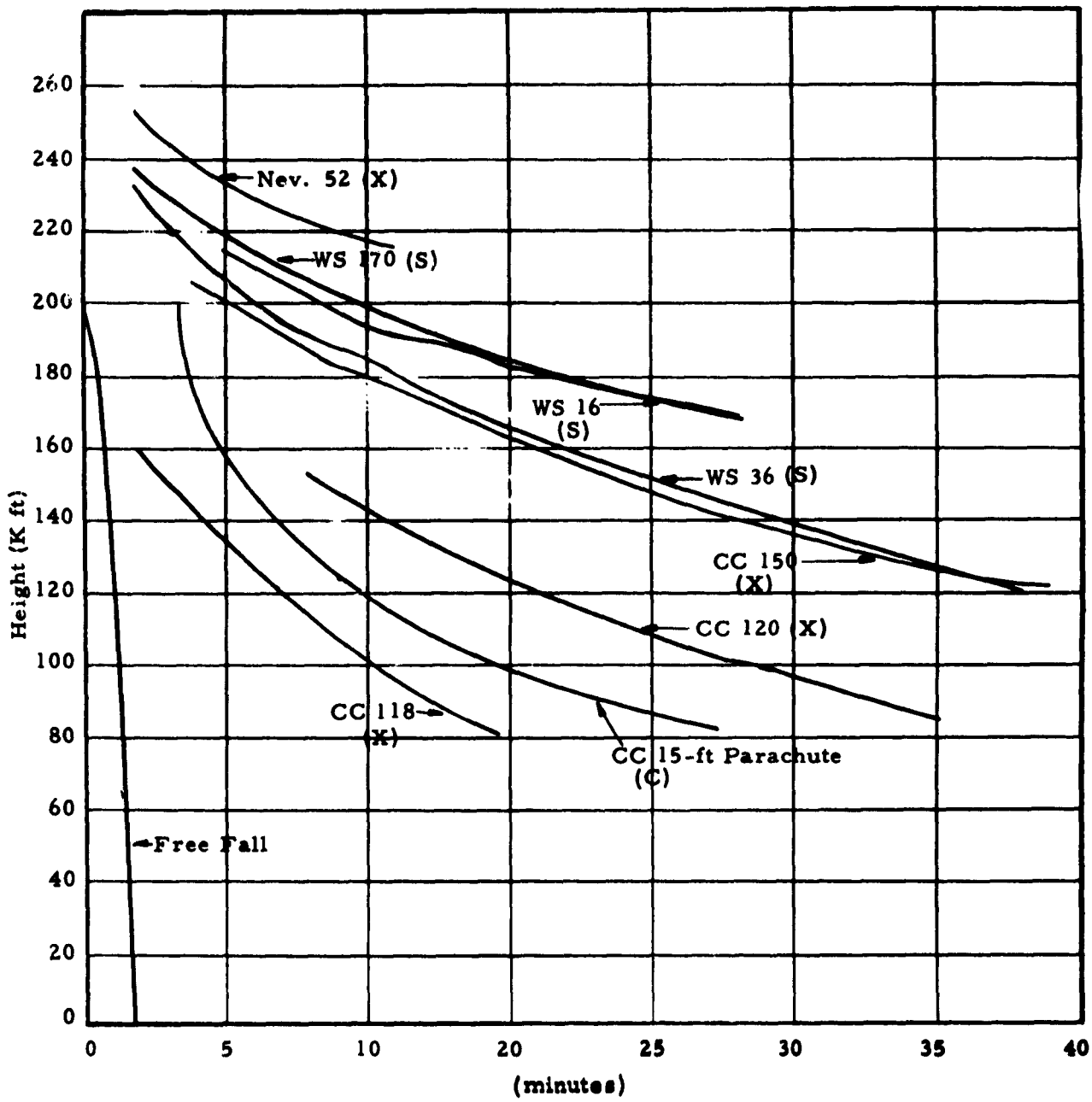

Figure 4-5. Typical Settling of Foil Chaff Delivered by Rocket to High Altitude

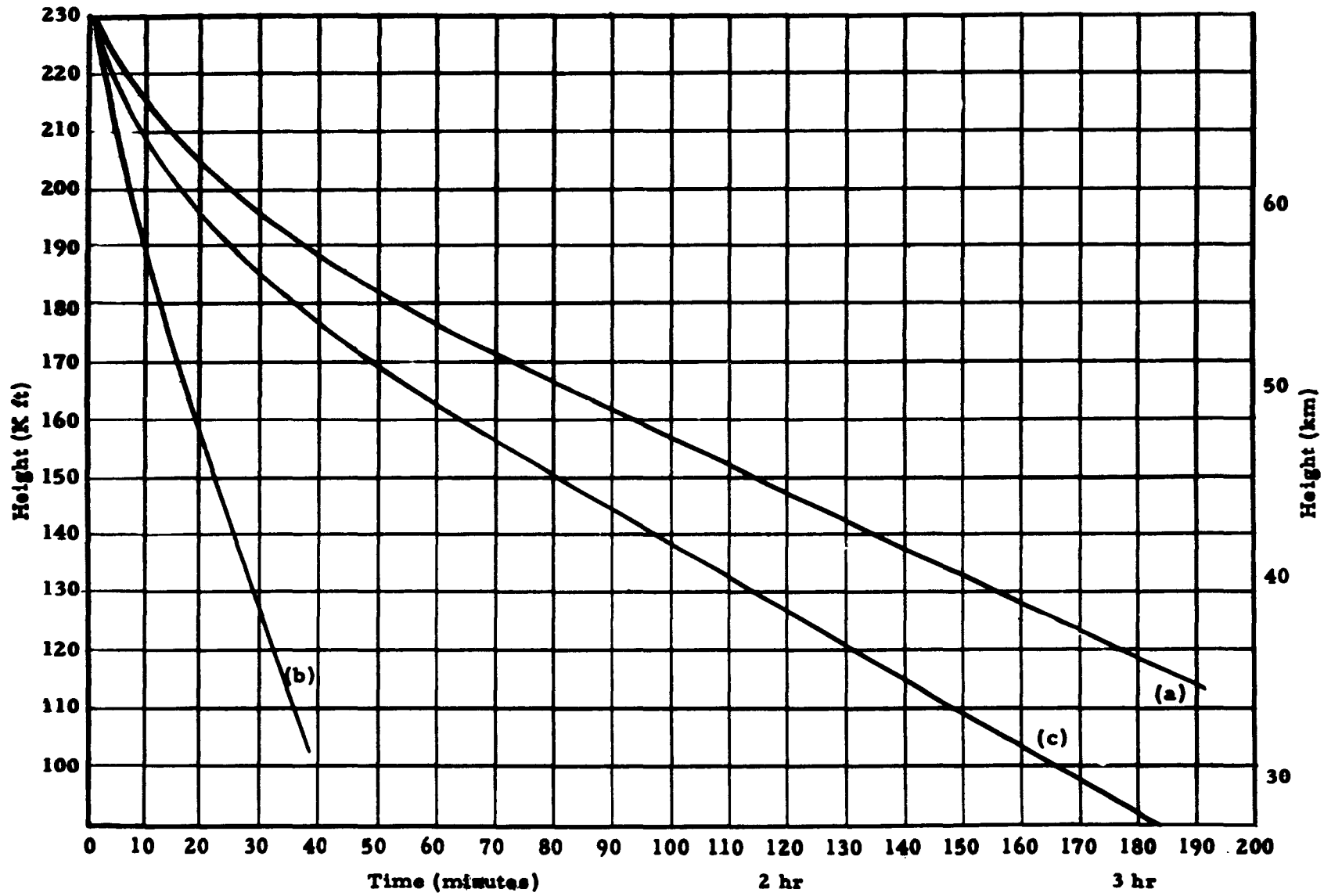

Figure 4-6. Typical Settling of 12-mil S Band Nylon Chaff

E. Potential Exploitation of Radiometer Effect for Scatterer Suspension—Material Aspects

The Phase I final report included theoretical discussion of potential application of the radiometer effect to this program, as well as presenting information on experimental verifications made.

During the present reporting period, an attempt was made to determine whether material processing techniques were sufficiently advanced to enable production of materials which could be used to exploit the radiometer effect for purposes of this program. Achievement of a 4 mm diameter sphere with wall thickness of 1 micron was considered impractical, since the thinnest known unsupported film at the commencement of this investigation was DuPont's 0.15-mil (3.81 micron) Mylar. Although complete suspension through use of this technique was not considered encouraging, it was considered desirable to explore the possibility that materials might exist which would permit application of the radiometer effect to substantially reduce the rate of settling.

Attention turned to cylindrical-shaped tubes as opposed to spheres, since these appeared more manufacturable. In addition, they offered greater reflecting surface per unit weight. In other words, a long cylinder offers more useful scattering cross-section for its weight and packing volume than a number of spheres of the same diameter, equalling the cylinder length by the sum of their diameters.

1. Approaches

The three approaches are:

1) Extruded thin-wall tubing, which could then be metallized by vapor deposition, sealed, and cut into appropriate lengths. These would be inflated (perhaps through use of residual air) in order to achieve some rigidity.

2) Thin-wall tubing formed by sealing two thin sheets, one of which was premetallized in an appropriate striped pattern.

3) Strips of material which would maintain a degree of rigidity along the longitudinal axis through curling about that axis. This material would also be premetallized in stripes prior to cutting into strips.

These approaches are illustrated in Figure 4-7.

The desired electrical performance required a heavier deposit of conductive metal than is commonly applied to plastic films. For this reason, it was considered desirable to include a survey of firms possessing metallizing capability in order to determine whether the desired deposit was feasible. Capability of depositing metal in stripes rather than over the entire web width was also investigated.

2. Investigation

The investigation was carried out through three inquiries:

1) One form letter was sent to all 4A firms listed in Thomas' Register under the headings Plastic Tubing, Extruded and Tubing, Plastic Extruded. Questions were:

   a) Thinnest wall tubing produced

   b) Smallest diameter tubing produced

   c) Could the combination smallest diameter and thinnest wall be produced

   d) Best material for ultra-thin wall tubing

   Of the 61 firms contacted, 37 responded. Achieving small diameter appears not to be a problem. The Danielson Manufacturing Company and U. S. Stoneware Company reported capability of 0.03-inch OD. Unfortunately, their minimum wall thicknesses were 12 and 5 mils, respectively.

   The thinnest wall tubing was reported by Chippewa Plastics Company at 1/2-mil polyethylene in 1/2-inch layflat.

2) A second form letter was sent to all 4A firms listed in Thomas' Register under headings Film, Plastic, and Plastic Films, Flexible. Questions included:

   a) Thinnest film, hopefully considerably less less than 0.15-mil (known to exist)

   b) Density, low desired

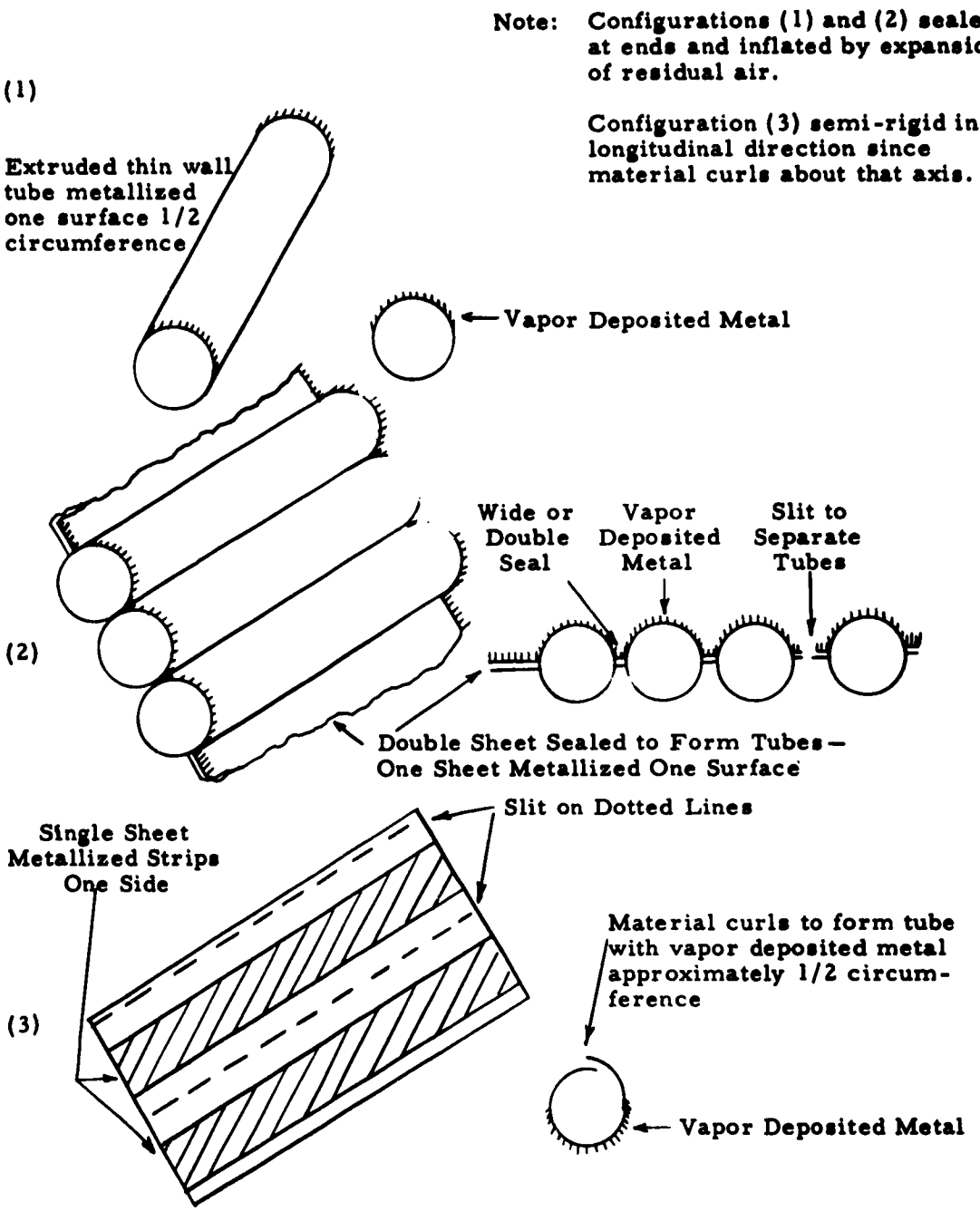

Figure 4-7. Fabrication Approaches for Thin Walled Dipoles Utilizing a Modified Bubble Concept

c) Sealability, heat sealable preferred

d) Curling tendency (for the possible noninflated approach)

e) Metallizability of the film

f) Gas retention properties (for the inflated approach)

Of 57 firms contacted, 30 responded. American Machine and Foundry Company reported the thinnest film (0.06-mil Teflon in experimental stage), and submitted a sample of 0.2-mil Teflon (Amflon UTF-20). They also submitted a sample of curling Fiberfilm T-10G-6N. Thickness of the latter was not reported. The Teflon was reportedly metallizable.

Other thin films reported were Western Electric 0.13-mil acetate, sample submitted was metallized. Pollock Paper Company indicated capability to cast a film 0.15-mil, type undisclosed. Dow Chemical Company reported 0.17-mil polypropylene in experimental stage. DuPont reported their 0.15-mil Mylar (previously known). General Tire and Rubber Company made some mention of films in the 0.15 to 0.0015-mil range. There appears to have been some confusion in the units, however, as they did not respond to our follow-up attempt at clarification.

3) A third form letter was sent to all firms listed in Thomas' Register under the classifications Vacuum Metallizing and Plastic Metallizing. Questions included:

a) Does capability extend to 10,000 Å or more

b) Maximum deposit of aluminum and copper

c) Data on resistivity and weight addition per unit area

d) Capability to deposit in strips

e) Capability to deposit on blackened film

f) Thinnest film which can be handled

g) Capability to metallize half a cylinder (one side of a layflat tube)

h) Degree of vacuum used in deposition

Both National Research Corporation and Joclin Manufacturing Company indicated capability to apply coatings as thick as 10,000 A. Both can deposit in stripes if desired. Bee Chemical Company advised that their inks can be used as vacuum metallizing base coats. Pressures of 0.5 to 0.1-micron are apparently common among metallizers.

Wrinkling of material may be a problem with thin films, although 1/4-mil Mylar is sucessfully metallized. Heat degradation may also be a problem with the thin films, although multiple passes help avoid this. Metallizing lay-flat tubing is a problem and puncturing at intervals would almost surely be necessary in order to eliminate residual air.

3. Summary

General Mills, because of its balloon fabrication activities, is keeping abreast of new plastic film developments. No new film discovered as a result of this investigation offered any substantial hope that it could be used with the radiometer effect to reduce the rate of settling. The films unearthed that were thinner than 0.15-mil Mylar were experimental in nature and very expensive ($25/lb) when compared to thicker film ($1.50 to $3.50/lb).

Prior to the investigation, GMI had not been quite so well informed as to the state-of-the-art in thin-wall, small-diameter tubing. It was disappointing that none were discovered which offered more potential than what we already had.

Hopes for the curled approach were never high, and the investigation did nothing to change this.

Adequate metallization appears to be less of a problem than thin films, although problems with thin films and especially in tubular form, are more severe than in run-of-the-mill metallizing. This is unfortunate since the economic feasibility of an approach employing the radiometer effect would be greatly enhanced should suitable ultra-thin wall tubes become available.

SECTION V

REFERENCES

V. REFERENCES

1) Hogg, D. C. and W. W. Mumford. The effective noise temperature of the sky. Microwave J. 3, 3: 80-84 (March 1960).

2) Bullington, K. Radio transmission beyond the horizon in the 40- to 4,000-mc band. Proc. I.R.E. 41: 132-35 (1953).

3) Rice, P. L. Tropospheric fields and their long-term variability as reported by TASO. Proc. I.R.E. 48: 1021-29 (1960).

4) U. S. National Bureau of Standards. Report 5092. Transmission loss in radio propagation, II, by K. A. Norton (1957).

5) Norton, K. A. Transmission loss in radio propagation. Proc. I.R.E. 41: 146-52 (1953).

6) King, R. W. P. The theory of linear antennas. Cambridge, Harvard Univ. Press, 1956.

7) Hessemer, R. A. Scatter communications with radar chaff. IRE Trans. Antennas Propagation AP-9, no. 2: 211-17 (1961).

8) Blom, B. V. Communications by re-radiation from chaff. I.R.E. Professional Group on Military Electronics. Proceedings, Fourth National Conference on Military Electronics, 1960. pp. 542-46.

9) Harrington, R. F. Small resonant scatterers and their use for field measurements. I.R.E. Trans. on Microwave Theory and Techniques, Vol. MTT-10, May 1962.

10) Chu, L. J. Physical limitations of omni-directional antennas. Jour. of Applied Physics, Vol. 19, Dec. 1948.

11) U. S. Army. Signal Missile Support Agency. Data report of the meteorological rocket network summer 1960 firings. IRIG-MWG, No. 3-60.

12) U. S. Army. Signal Missile Support Agency. Special Report no. 41. Meteorological rocket wind sensors, by N. J. Beyers and O. W. Thiele (Aug. 1960).

APPENDICES

TABLE OF SYMBOLS - APPENDICES

a	lateral width of equivalent grating window
α	general angle in horizontal plane
A	general value of illuminating amplitude on aperture
A_o	constant value of illuminating amplitude on aperture
A_r	effective area of receiving antenna
b	height of rectangular aperture
β	general angle in vertical plane
d	distance from transmitter to receiver
d_s	distance between horizon limited points
E_o	field strength due to free space loss
E_r	field strength at receiver
E_s	field strength at scatterer
$E(50)$	a field strength value that is exceeded 50% of the time
ERP	effective radiated power - in this case related to the field in a horizontal plane which would be created by a half-wave dipole having uniform azimuth coverage and supplied by the stated amount of r-f power
G_t	gain of transmitting antenna (relative to isotropic)
h	altitude of scatterer above smooth earth
h_{om}	height of scatterer at midpoint to appear at radio horizon
h_r	effective height of receiving antenna
h_{ro}	that altitude for scatterer to be at the radio horizon for the nearer (receiving) terminal
h_t	effective height of transmitting antenna
i_{s0}	peak value of radiant intensity from grating
k	wave number
λ	wavelength
m	phase constant
n	number of equivalent grating windows
P_r	signal power density or irradiance at receiver
P_{ro}	irradiance at receiver due to free space propagation
P_{rx}	irradiance at receiver due to tropospheric scatter propagation
P_s	irradiance at scatterer
ϕ_{om}	depression angle of either terminal when positioned at h_{om}
ϕ_r	depression angle of peak of first order diffraction lobe
ϕ_{ro}	depression angle of direct ray to receiver when positioned at h_{ro}
ϕ_t	depression angle of direct ray from transmitter
P_{rf}	available received signal power due to free space propagation
P_{rx}	available received signal power due to tropospheric scatter propagation
P_{rx1}	same as P_{rx} for an ERP of 1 kw
P_{ta}	aural signal power delivered to transmitting antenna
r_m	range from either terminal to scatterer when at midpoint
r_r	range from receiver to scatterer
r_t	range from transmitter to scatterer
ρ	modified (4/3) earth radius - taken as 8500 km
s	spacing between corresponding points on adjacent windows
sinc x	$\frac{\sin x}{x}$
θ_r	apparent elevation angle above the horizon of scatterer when viewed from nearer (receiving) terminal
θ_t	apparent elevation angle above the horizon of scatterer when viewed from remote (transmitting) terminal
ψ	phase of illuminating amplitude across aperture

APPENDIX A

PATTERN OF A RECTANGULAR WINDOW

The illumination function of a rectangular window in a screen in the x-y plane results from an incident plane wave system propagating toward the window at an inclination ϕ_t, which is confined to the y-z plane. The window is oriented parallel with respect to the coordinate system, so that b is the aperture in the direction of y. Figure A-1 illustrates this case. It also shows the amplitude distribution $|A(y)|$ and the phase distribution $\Psi(y)$ across the window.

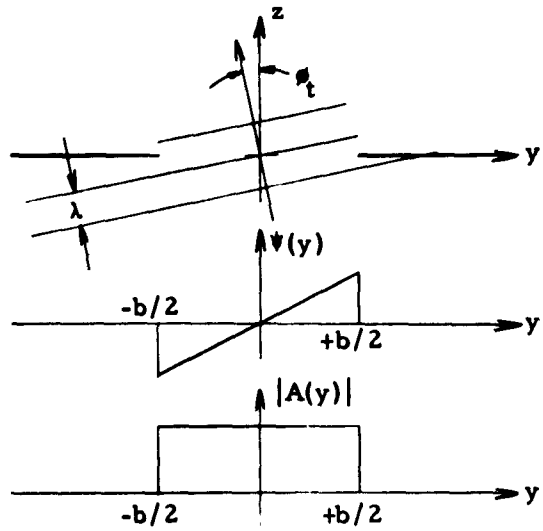

Figure A-1. Illumination Function of a Window

Accordingly, the amplitude is

$$|A(y)| = A_o, \; |y| \leq \frac{b}{2} \quad \text{and} \quad |A(y)| = 0, \; |y| > \frac{b}{2} \tag{A-1}$$

while the phase is defined by

$$\Psi(y) = \frac{2\pi y \sin \phi_t}{\lambda} = my \,. \tag{A-2}$$

Hence, the aperture illumination function becomes

$$A(y) = A_o e^{j\Psi(y)}, \quad |y| \leq \frac{b}{2} \tag{A-3}$$

and the normalized field strength pattern according to the Huygens-Kirchhoff law

$$E(\beta) = \int_{-\infty}^{+\infty} A(y)\, e^{jky \sin \beta}\, dy, \quad k = \frac{2\pi}{\lambda} \,. \tag{A-4}$$

With (A-2) and (A-3) we obtain

$$E(\beta) = \int_{-\frac{b}{2}}^{+\frac{b}{2}} A_o\, e^{jmy}\, e^{jky \sin \beta}\, dy \tag{A-5}$$

or

$$E(\beta) = A_o \int_{-\frac{b}{2}}^{+\frac{b}{2}} e^{jy(m + k \sin \beta)}\, dy \,. \tag{A-6}$$

Integration of (A-6) leads to

$$E(\beta) = \frac{2A_o}{m + k \sin \beta} \sin\left[\frac{b}{2}(m + k \sin \beta)\right] \tag{A-7}$$

or

$$E(\beta) = b A_o \operatorname{sinc}\left[\frac{b}{2}(m + k \sin \beta)\right] \tag{A-8}$$

With m as in (A-2) and k as in (A-4) we get

$$E(\beta) = b A_o \operatorname{sinc}\left[\frac{b\pi}{\lambda}(\sin \phi_t + \sin \beta)\right] \,. \tag{A-9}$$

If we set $\phi_t = 0$, the pattern takes the familiar shape of a symmetrical sinc beam. For small ϕ_t the pattern can be considered as a symmetrical sinc beam slightly tilted by the angle ϕ_t. For larger angles the maximum will still point in the direction of ϕ_t but the beam will assume an unsymmetrical shape.

In any plane, including the x axis, we will have a pattern cross section of the symmetrical sinc shape, so that the two-dimensional pattern function becomes

$$E(\alpha,\beta) = E_o \operatorname{sinc}\left[\frac{a\pi}{\lambda}\sin\alpha\right] \cdot \operatorname{sinc}\left[\frac{b\pi}{\lambda}(\sin\beta + \sin\phi_t)\right] . \qquad \text{(A-10)}$$

APPENDIX B

GEOMETRY OF THE SCATTER RADIATION

The simplest case of a scatterer positioned halfway between the two terminals at the minimum altitude has been analyzed before and led to the simple relations

$$h_{om} = \frac{r_m^2}{2\rho} \tag{B-1}$$

and

$$\phi_{om} = \frac{r_m}{\rho} = \frac{2\,h_{om}}{r_m} \tag{B-2}$$

The symbols are readily explained in Figure B-1. If, however, the scatterer is at an arbitrary position, defined by r_t and h, the depression angles of the two terminals ϕ_t and ϕ_r must be determined as functions of r_t and h. Hereby we restrict ourselves to the condition of minimum altitude, namely that the angle to the more distant terminal is not much larger than ϕ_{om}. Since the terminal assignment, transmitting or receiving, can be exchanged without affecting the quality of the signal transmission, we are not restrictive if we always refer to the more distant station as the transmitter. This means that the elevation angle of the scatterer as seen from the receiving station can assume larger values and therefore, a more rigorous expression must be derived for the geometry of the receiving side than for the transmitting side.

The altitude of the scatterer consists of two parts, the part below the horizon as seen from the receiving terminal h_{ro} and the part above the horizon $h_o - h_{ro}$. The latter forms a nearly right-angled triangle with the line-of-sight to the scatterer and the tangent through the receiving terminal. Thus we have

$$\tan \theta_r = \frac{h - h_{ro}}{r_r} \quad . \tag{B-3}$$

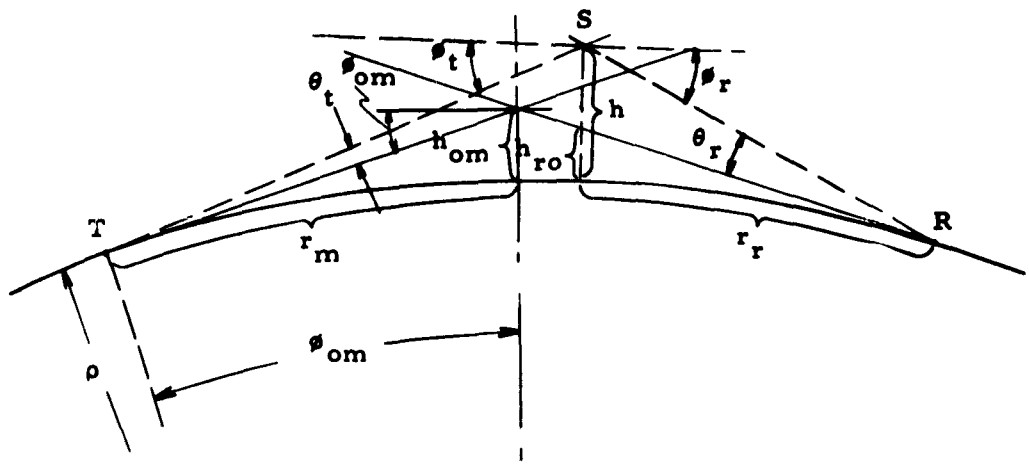

Figure B-1. Geometry of the Scatter Radiation

Here we express h_{ro} according to (B-1)

$$h_{ro} = \frac{r_r^2}{2\rho} \tag{B-4}$$

and obtain

$$\tan \theta_r = \frac{h}{r_r} - \frac{r_r}{2\rho} \quad . \tag{B-5}$$

The depression angle ϕ_r of the receiving terminal as seen from the scatterer is

$$\phi_r = \phi_{ro} + \theta_r \quad . \tag{B-6}$$

The tangent takes the form

$$\tan \phi_r = \tan (\phi_{ro} + \theta_r) = \frac{\tan \phi_{ro} + \tan \theta_r}{1 - \tan \phi_{ro} \cdot \tan \theta_r} \quad . \tag{B-7}$$

Since $\phi_{ro} \ll \theta_r \ll 1$ is a very small angle, we may use the approximation

$$\tan \phi_r = \phi_{ro} + \tan \theta_r \tag{B-8}$$

With ϕ_{ro} expressed like (B-2) and tan θ_r as in (B-5) we obtain

$$\tan \phi_r = \frac{h}{r_r} + \frac{r_r}{2\rho} \cdot \tag{B-9}$$

For the transmitting side we have analogous expressions, however, since the angles θ_t and ϕ_t are very small we can use the simpler form

$$\theta_t = \frac{h}{r_t} - \frac{r_t}{2\rho} \tag{B-10}$$

and

$$\phi_t = \frac{h}{r_t} - \frac{r_t}{2\rho} \cdot \tag{B-11}$$

To derive the sine function from the tangent expression, the following formula may be used.

$$\sin \phi_r = \frac{\tan \phi_r}{\sqrt{1 + \tan^2 \phi_r}} \cdot \tag{B-12}$$

APPENDIX C

FIELD STRENGTH AT WADENA DUE TO SCATTERER

Field strength due to gratar scattering is computed for the television aural signal, for the Scatterloon located at the design altitude and for the path midpoint. The irradiance at the scatterer is given by

$$p_s = \frac{P_{ta}\, G_t}{4\pi\, r_t^2} \,. \tag{C-1}$$

Then the field strength at the scatterer is

$$E_s = \sqrt{120\pi\, p_s} = \sqrt{\frac{30\, P_{ta}\, G_t}{r_t^2}} = \frac{1}{r_t}\, \sqrt{30\, P_{ta}\, G_t} \,. \tag{C-2}$$

Since the field strength recordings were of the aural signal, the transmitted power related to the aural signal P_{ta} and the stated value $P_{ta} \times G_t = 206$ kw are used.

$$E_s = \frac{1}{218.5 \times 10^3}\, \sqrt{30 \times 206 \times 10^3} = 11.37 \text{ mv/m} \,. \tag{C-3}$$

The irradiance at the receiver

$$p_r = \frac{i_{s0}}{r_r^2} = p_s \left(\frac{nas}{\pi\lambda r_r}\right)^2 = \frac{P_{ta}\, G_t}{\pi} \left(\frac{nas}{2\pi\lambda\, r_r\, r_t}\right)^2 . \tag{C-4}$$

And the received field strength

$$E_r = \sqrt{120\pi\, p_r} = \frac{nas}{2\pi\lambda\, r_r\, r_t}\, \sqrt{120\pi\, \frac{P_{ta}\, G_t}{\pi}} = \frac{nas}{\pi\lambda\, r_r\, r_t}\, \sqrt{30\, P_{ta}\, G_t} \,. \tag{C-5}$$

From (C-2), (C-5), and (C-3),

$$E_r = \frac{nas}{\pi \lambda r_r} E_s = \frac{4 \times 7 \times 27.7}{\pi \times 1.64 \times 218.5 \times 10^3} E_s$$

$$E_r = 0.689 \times 10^{-3} E_s = 7.83 \ \mu v/m \qquad \text{(C-6)}$$

APPENDIX D

TROPOSPHERIC PROPAGATION EFFICIENCY BETWEEN LACROSSE, WISCONSIN AND WADENA, MINNESOTA

An estimate is made of the average field strength at the receiving terminal due to tropospheric scatter propagation to evaluate its magnitude compared with the field strength due to gratar scattering. Estimates of field strengths due to tropospheric scattering are based on empirical path loss data from Rice[3], and from Bullington[2].

The first estimates based on data from Rice proceed as follows:

$$d_s = d - \sqrt{2h_t} - \sqrt{2h_r}$$

Values of $h_t = 500$ ft and $h_r = 30$ ft are considered to be sufficiently representative to be used here. Thus

$$d_s = 272 - 32 - 8 = 232 \text{ miles}$$

From Figure 1(d) of the Rice reference,

$$E(50) + 10 \log_{10} d_{mi} \text{ is 14 db above } 1 \frac{\mu v}{m} \text{ for 1 kw ERP}$$

$$10 \log_{10} d_{mi} = 10 \log_{10} 272 = 24.35$$

The irradiance for a field strength $E_o = 1 \frac{\mu v}{m}$ is

$$p_{ro} = \frac{E_o^2}{120\pi} = \frac{10^{-12}}{120\pi} = 0.265 \times 10^{-14} \frac{w}{m^2}$$

Since the actual irradiance for E(50) is 14 - 24.35 = -9.65 db above p_{ro}, we have

$$p_{rx} = 0.0287 \times 10^{-14} \frac{w}{m^2}$$

With an intercepting area of the receiving antenna of

$$A_r = \frac{\lambda^2 G_r}{4\pi} = \frac{1.64^2 \times 40}{4\pi} = 8.56 \text{ m}^2$$

the received power for 1 kw ERP becomes

$$P_{rx1} = p_{rx} A_r = 0.245 \times 10^{-14} \text{ w} .$$

With an actual effective power of $P_{ta} \times G_t = 206$ kw, we have

$$P_{rx} = 206 \times 0.245 \times 10^{-14} = 0.505 \times 10^{-12} \text{ w} .$$

Due to free space propagation, the received power would be

$$P_{rf} = \frac{P_{ta} G_t A_r}{4\pi d^2} = \frac{206 \times 10^3 \times 8.56}{4\pi \times (437)^2 \times 10^6} = 0.733 \times 10^{-6} \text{ w} .$$

Hence

$$\frac{P_{rx}}{P_{rf}} = \frac{0.505 \times 10^{-12}}{0.733 \times 10^{-6}} = 0.680 \times 10^{-6} \text{ (-61.7 db)} .$$

A direct reading of the intensity ratio can be obtained from Figures 3, 7, and 11(a) of the same reference. These readings are:

Figure 3: $10 \log_{10} \left(\frac{P_{rx}}{P_{rf}} \right) = -70$ db,

Figure 7: $10 \log_{10} \left(\frac{P_{rx}}{P_{rf}} \right) = -68$ db,

and

Figure 11(a): $10 \log_{10} \left(\frac{P_{rx}}{P_{rf}} \right) = -76$ db.

According to Figure 5 of the reference by Bullington,

$$10 \log_{10} \left(\frac{P_{rx}}{P_{rf}} \right) = -75 \text{ db.}$$

With free space loss, the field strength at the receiver would be

$$E_{rf} = \frac{\sqrt{30 \times P_{ts} \times G_t}}{d^2} = \frac{\sqrt{30 \times 206 \times 10^3}}{437 \times 10^3} = 5.68 \frac{mv}{m}$$

Assuming a ratio of 10 log $\left(\frac{P_{rx}}{P_{rf}} \right)$ = -73 db, E(50) = 1.27 $\frac{\mu v}{m}$. This is almost 16 db below that due to gratar scattering.